THERMOMECHANICAL TRAINING AND CHARACTERIZATION OF SHAPE MEMORY ALLOY AXIAL ACTUATORS

by

Marcus Patrick Becker

A thesis submitted in partial fulfillment
of the requirements for the degree

of

Master of Science

in

Mechanical Engineering

MONTANA STATE UNIVERSITY
Bozeman, Montana

April 2010

APPROVAL

of a thesis submitted by

Marcus Patrick Becker

This thesis has been read by each member of the thesis committee and has been found to be satisfactory regarding content, English usage, format, citation, bibliographic style, and consistency, and is ready for submission to the Division of Graduate Education.

Dr. David A. Miller

Approved for the Department of Mechanical and Industrial Engineering

Dr. Christopher H. M. Jenkins

Approved for the Division of Graduate Education

Dr. Carl A. Fox

STATEMENT OF PERMISSION TO USE

In presenting this thesis in partial fulfillment of the requirements for a master's degree at Montana State University, I agree that the Library shall make it available to borrowers under rules of the Library.

If I have indicated my intention to copyright this thesis by including a copyright notice page, copying is allowable only for scholarly purposes, consistent with "fair use" as prescribed in the U.S. Copyright Law. Requests for permission for extended quotation from or reproduction of this thesis in whole or in parts may be granted only by the copyright holder.

Marcus Patrick Becker

April 2010

DEDICATION

I dedicate this work to my parents who have been there for me from the beginning. They have always pushed me to strive to do my best and succeed. I will never forget how they have helped me get to where I am today. Thank You!

ACKNOWLEDGEMENTS

I would like to thank Dr. David Miller, who served as the chairman of my thesis committee and as my advisor for the last two years. Dr. Miller has been there for me through thick and thin; we have had long conversations about school, research, and even hunting and fishing. I consider him a great advisor, an excellent teacher, and a caring friend. I also want to thank Dr. Stephen Sofie and Dr. Edward Adams for serving on my committee and for offering their knowledge through classes and words of encouragement throughout my time at Montana State University.

Thanks to all the people who have helped me complete my degree and helped me throughout the process. I would like to thank the office staff for always knowing the proper steps I needed to take. I thank my fellow graduate students and research group members for always offering to lend a hand and also helping to make my college career a little less stressful.

Special thanks go out to my parents, Dale and Marilyn Becker, who have always praised me when I was doing well and offered support and motivation when I was down. I must also thank my fiancée, Jossolyn Sattler, for always standing by my side and keeping me focused during times of stress and distraction

Funding Acknowledgement

The work herein was supported in part by the Montana NASA EPSCoR Grant with NASA Glenn Research Center and the 2009 Montana NASA EPSCoR Summer Graduate Research Assistantship.

TABLE OF CONTENTS

TABLE OF CONTENTS - CONTINUED

LIST OF TABLES

Table Page

LIST OF FIGURES

Figure Page

LIST OF FIGURES - CONTINUED

Figure Page

LIST OF FIGURES - CONTINUED

Figure Page

LIST OF FIGURES - CONTINUED

Figure Page

LIST OF EQUATIONS

Equation Page

ABSTRACT

Although considerable work has been performed to understand the key mechanisms of Shape Memory Alloy (SMA) behavior, little of this work follows a standard testing protocol, quantifies a conditioning methodology, or develops data appropriate for design of SMA actuators. One major issue that limits the ability of the material from being used directly as an actuator is the large, non-recoverable strains likely to accrue in the material during each training cycle, mechanical or thermal. When mechanical or thermal cycling is performed, a hysteresis curve develops and reaches a steady state strain recovery response. At the point where permanent plastic strain stops growing, or saturates, the SMA has been successfully trained.

The focus of this work is oriented toward SMAs in general, but all testing and experimentation was carried out on Nickel-Titanium (NiTi) alloys. The experimentation and testing was performed on a combination of 4 different sizes and 3 different NiTi alloy compositions. Thermomechanical testing was performed to determine critical values to describe the stress-temperature phase space of the materials and parameters to model the applied stress and transformation strain relationship. All material size and alloy combinations were tested in the as-received, or as-machined, and fully annealed state. The results of the training and actuation strain characterization process developed in this work shows that the samples that experienced Transformation Induced Plasticity (TRIP), greater than 2% during the training process and exhibit Two-Way Shape Memory (TWSM) after being fully trained, share a very similar applied stress versus transformation strain curve. This curve is modeled by the Back Stress formulation derived from the Gibbs Free Energy constitutive model by Bo & Lagoudas. The design space created by the Back Stress formulation, recrystallization temperature, and training stress allows SMA materials to be characterized and implemented as stable 1-D actuators. This research formalized a thermomechanical training and characterization method for uniaxial SMA actuators by addressing the interaction between processing, recoverable and non-recoverable deformation. Using various sizes and NiTi alloy combinations, this research develops and evaluates a method to train and characterize a diverse range of SMAs through a set of thermomechanical and physical property measurements.

INTRODUCTION AND BACKGROUND

Introduction to Study

Shape Memory Alloys (SMAs) are a special class of metals which have been identified as having high energy densities compared to other active materials. They have the ability to replace large systems as robust, lightweight, and compact actuators. Due to the lack of understanding and knowledge of how the material works and standard testing methods, acceptance of the material for design usage has been slow over the past 60 years.

SMAs undergo a diffusionless or displacive, solid-to-solid thermoelastic phase transformation between a low-temperature martensite phase and a high-temperature austenite phase. Several complex alloys, including CuAlNi, CuZn, InTi, AuCd, NiTi, and many other metallic alloys[1], exhibit the solid-solid phase transformation. The most common and currently the most widely-utilized is near equiatomic Nickel Titanium (NiTi) and copper based alloys. Intermetallic alloys, such as NiTi, have very specific atom locations in the lattice structure; whereas, normal metal alloys have atoms that occupy random lattice structure positions. These specific atom locations in the lattice structure resist change, causing a defined thermoelastic transformation between phases. Typical NiTi alloys that exhibit the shape memory phenomena range between 49.5-57% nickel by atomic percent, but maintain equiatomic basis with possible solution mixtures of Ti_2Ni or $TiNi_3$ as shown in Figure 1. The focus of this research is oriented toward SMAs in general, but all testing and experimentation was carried out on NiTi alloys.

NiTi offers greater ductility, has corrosion resistance comparable to stainless steels, stable transformation temperatures, high biocompatibility, and larger recoverable strains.

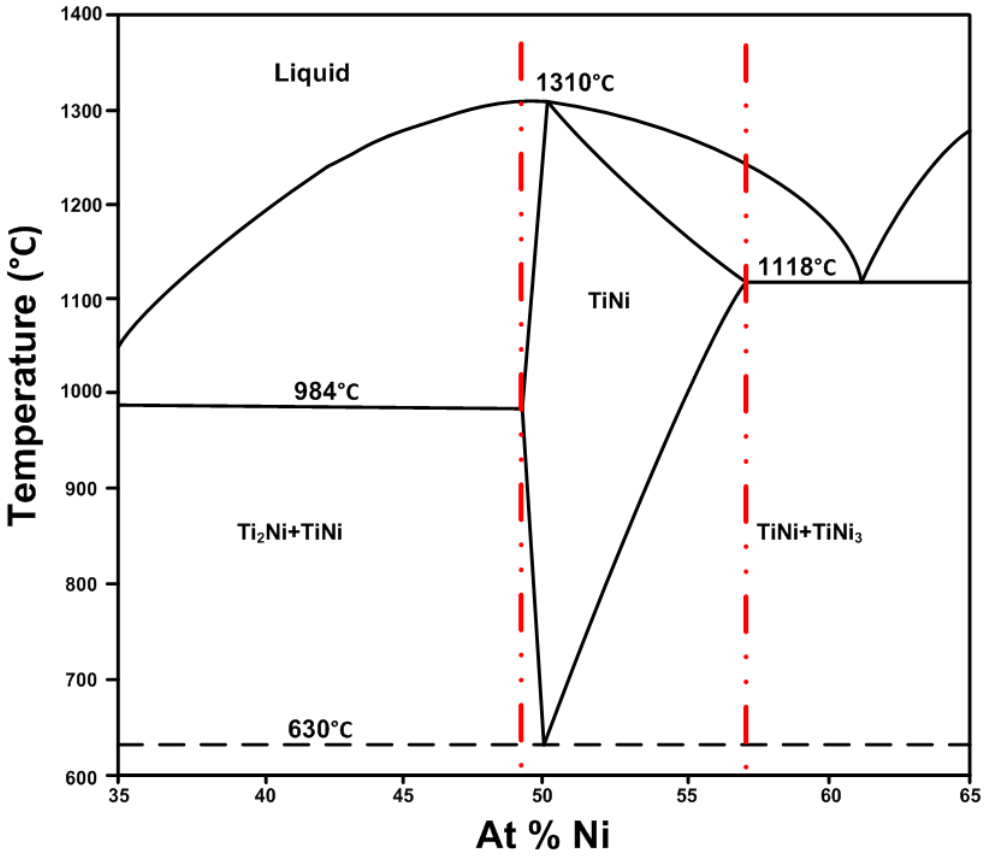

Figure 1: Reduced alloy phase diagram for NiTi alloys, showing where shape memory can occur (based from Massalski, T.B., Binary Alloy Phase Diagrams)

For the remained of this work, NiTi will refer to a near equiatomic form of the alloy composition. A thermoelastic phase transformation is induced through either temperature or stress and is commonly referred to as the shape memory effect (SME) and superelastic effect, respectively. Training is a vital role in the design and use of SMAs. By training, the material can memorize specific configurations through transformation by activating a temperature change, inducing a stress state, or a combination of the two.

This transformation is particularly significant in SMAs because it is accompanied by high stresses (up to 500 MPa) over large displacements or strain (4-8% strain) and in addition, the ability to recover these large strains even when a stress is still being supplied[2].

The temperatures at which the phase transformation occurs can be altered significantly by very small changes in the composition of the material. As the nickel percent is slightly increased in NiTi materials, the transition temperatures decrease significantly[3].

Initial Discovery

Another commonly associated name for equiatomic NiTi is NITINOL, which corresponds to Nickel-Titanium-Naval-Ordinance-Lab. The discovery of this material came from William Buehler while doing research at the Naval Ordinance Lab in late 1950's. Buehler was testing intermetallic compounds to find a material suitable for the nose cone of the Navy's below-the-surface launch missle. Buehler and his assistant cast NITINOL bars in their arc-melting furnace and laid them out to cool. Buehler dropped one of the cool bars on the floor to find that it made a dull thud, whereas the warm bars rang like a bell when dropped. The acoustic change made from dropping the bars signaled a change in atomic structure[4].

The changing structure Buehler noticed was the change from high temperature austenite to lower temperature martensite. This reversible, solid-solid phase transition from one form of crystalline structure to another is known as the martensitic transformation and is the key mechanism for the shape change in SMAs. The stable lower temperature martensite is in the form of a monoclinic crystal, whereas the stable

high temperature austenite has a body centered cubic crystal structure. Figure 2 represents the crystal structures for the different phases of a typical shape memory alloy.

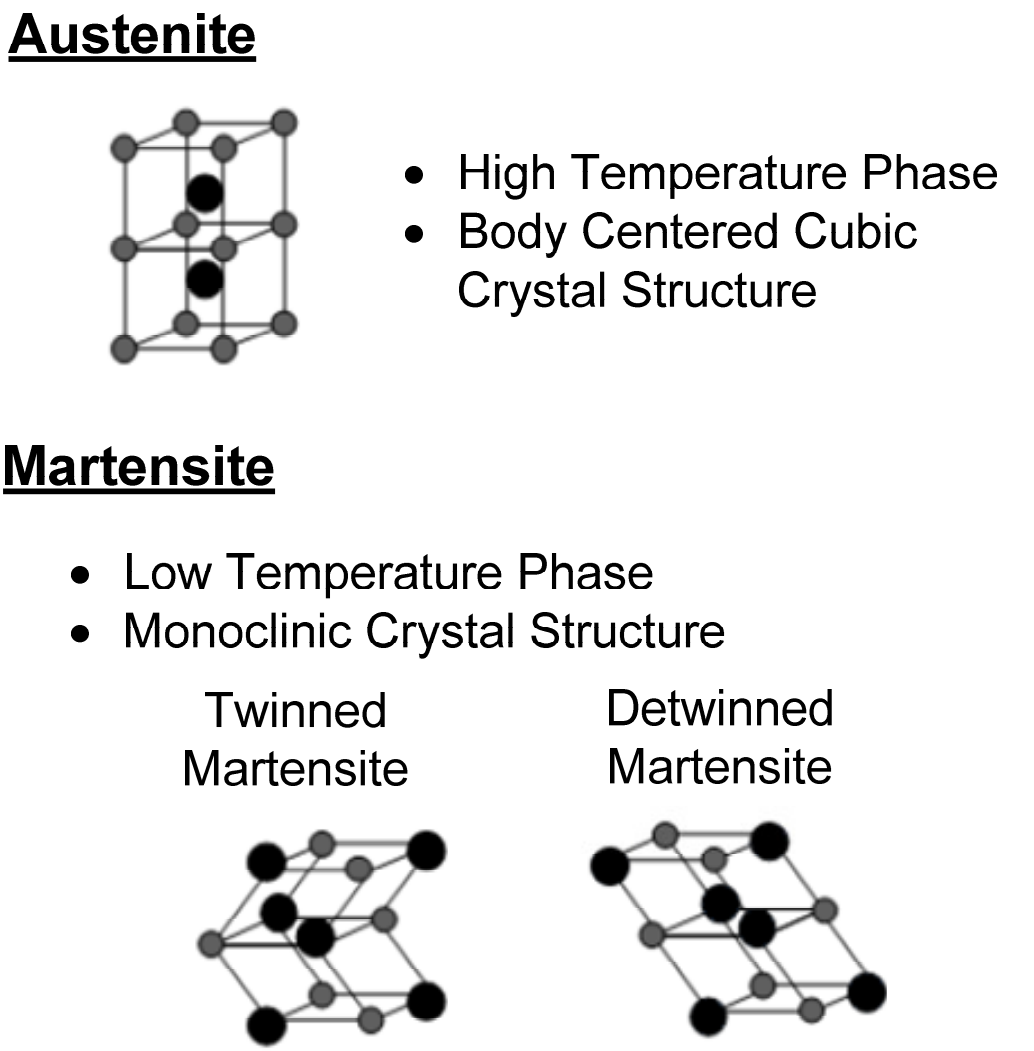

Figure 2: Different phases of a shape memory alloy

Austenite

The body centered cubic, high temperature austenite phase, contains 6 slip planes each having 2 directions (12 slip systems). Applied mechanical loads in the austenite

phase results in either a thermoelastic transformation to the stable martensite phase or slip occurring which results in permanent non-recoverable deformation.

Martensite Twinning & Detwinning

Twinned martensite occurs when the atoms form tilted rows oriented symmetrically across grain boundaries creating a mirror image of each other, otherwise known as twins. The twinned structure allows the internal lattice of individual grains to change while still maintaining the same interface with adjacent grains. Due to the monoclinic structure of the martensite phase having 6 faces and two diagonals, a phase transformation from the parent phase austenite to martensite involves a shearing deformation along the face diagonal of the cubic structure. The stress free transformation to the twinned martensite phase leads to the formation of 24 variants. Twin boundaries are of a relatively low energy state and the application of a stress forces the multiple variants to switch their orientation to one preferential variant, known as detwinning. The orientation of the preferential variant is typically in the direction of the applied stress. The detwinning process results in nearly volume preserving, large macroscopic deformation over a small increase in stress. The deformation can be recovered by heating the SMA to the parent austenitic state. This motion is the cause of the shape memory effect present in SMA materials. The stress-strain relationship for loading in the martensite phase is illustrated in Figure 3.

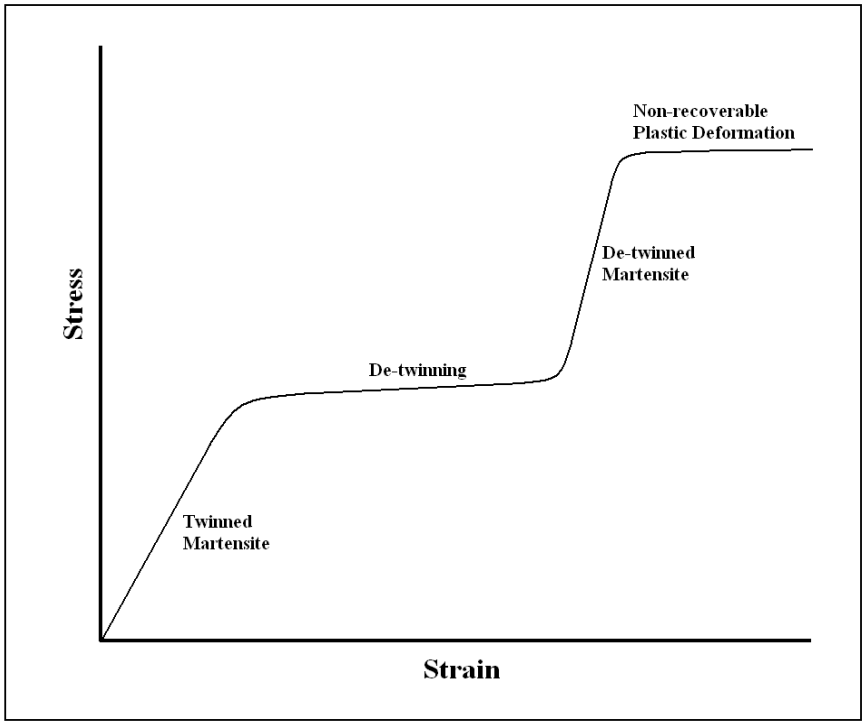

Figure 3: Stress-Strain relationship for martensitic phase loading

At smaller stresses, the material behaves elastically. At a critical detwinning stress, the material starts to detwin and results in a large deformation (4-6% strain) until the structure is entirely detwinned martensite. Once fully detwinned the material again behaves elastically until a yield stress in the material structure is reached and plastic non-recoverable deformation occurs.

Stress-Temperature Phase Diagram

A typical stress versus temperature phase diagram for SMAs is shown in Figure 4. The different phases associated with typical SMAs are twinned martensite, detwinned martensite, and austenite. Full transformation into either the austenite or martensite phase is path independent. Partial transformation into one phase or the other involves

path dependency and the martensitic volume fraction must be tracked until a full transformation is performed, resetting the martensitic volume fraction.

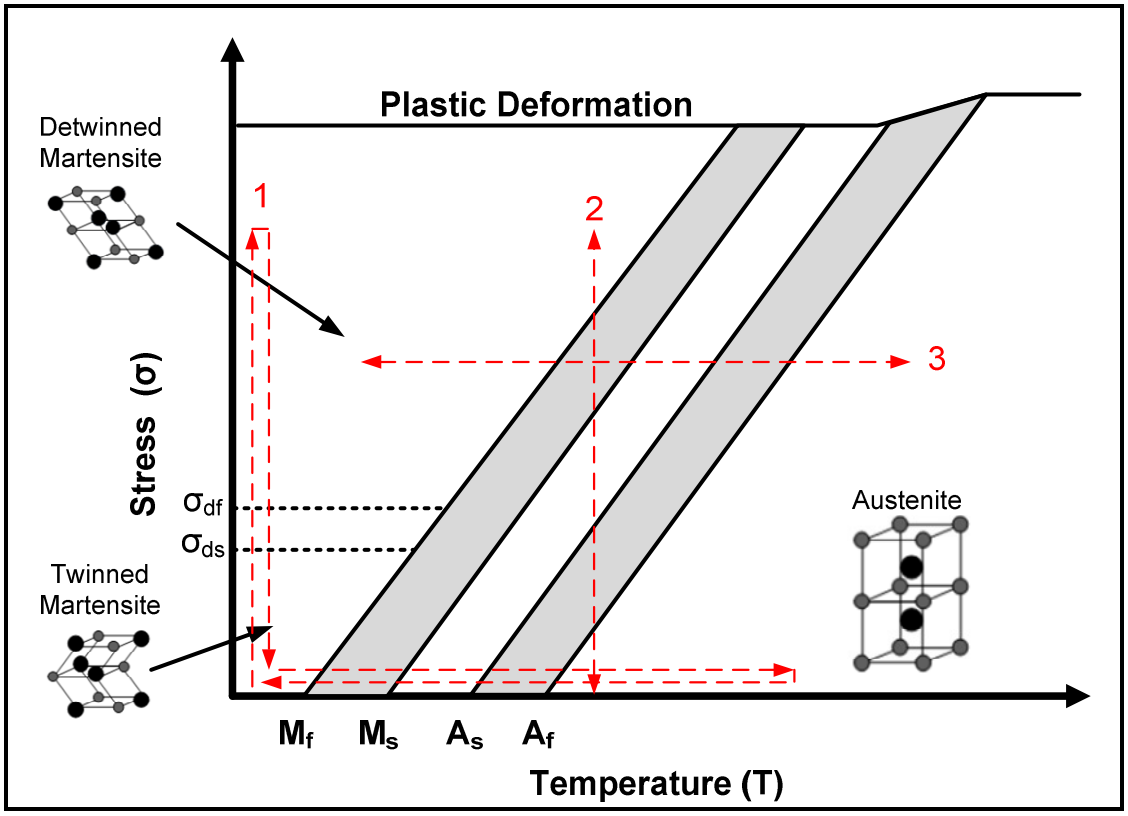

Figure 4: Typical Stress-Temperature phase diagram for NiTi alloys

The four lines outlining the shaded regions represent the martensite start and finish temperatures, M_s and M_f, and austenite start and finish temperatures, A_f and A_s, respectively. As the material is heated from the low temperature martensite state, starting at the austenite start temperature (A_s), transformation from martensite to austenite begins (forward transformation). Once the austenite finish temperature (Af) has been achieved throughout the material, it is considered to be 100 % austenite. The transformation to martensite from the high temperature austenite state occurs in the same manner. Starting

at the martensite start temperature (M_s), transformation from austenite to martensite begins (reverse transformation). Once the martensite finish temperature (M_f) has been achieved throughout the material, it is considered to be 100 % martensite. Notice that the transformation temperatures are a function of the applied stress. For polycrystalline systems, the broadening of the transformation regions occur as one grain transforms and raises the internal stress state on neighboring grains. The increase of internal stress on the neighboring grains requires higher temperature to complete a full transformation.

Three standard loading paths are shown in the stress versus temperature diagram. The first loading path is called the Shape Memory Effect (SME), and temperature is held constant below M_f during loading from a twinned martensite state to detwinned martensite. The load is removed and the material can then be heated above A_f at zero stress to recover deformation, and returns to the twinned martensite state upon cooling. The second loading path is the superelastic or pseudoelastic response, and is performed at a constant temperature above A_f at zero stress. The stress is elevated so a stress induced transformation to martensite is acquired and then unloaded back to zero stress with a transformation to full austenite. The third loading path is considered isobaric thermal cycling. Here stress is held constant and thermal cycling from martensite to austenite and back to martensite is performed to recover deformation from the detwinning of martensite.

Thermomechanical Loading & Training

Shape Memory Effect

The shape memory effect (SME), or loading path #1 in Figure 4, is a phenomenon where plastic strains acquired by an applied stress below A_s recovers by heating to a temperature above A_f [5]. This involves a deformation that causes twinned martensite to shear to a detwinned orientation. A thermally induced transformation to austenite recovers the deformation, and the material returns to the twinned martensite orientation upon cooling. This process is illustrated in Figure 5 and 6. Figure 5 is a visual representation of the process, whereas Figure 6 shows (a) the stress versus strain relationship and (b) the loading path of the process in the Stress-Temperature phase diagram.

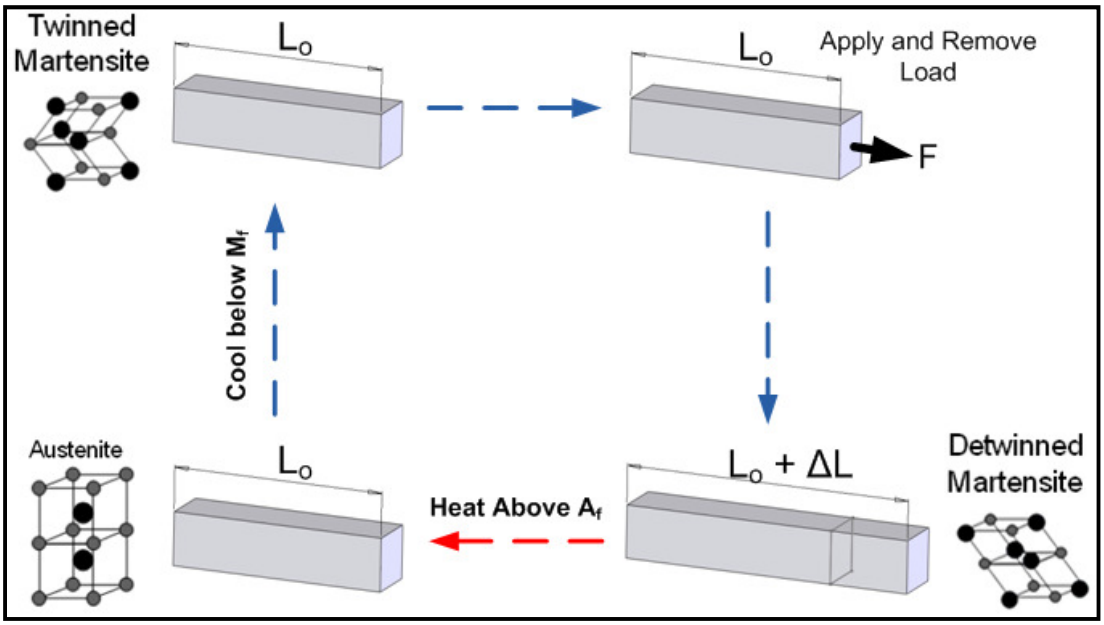

Figure 5: Shape Memory Effect (SME)

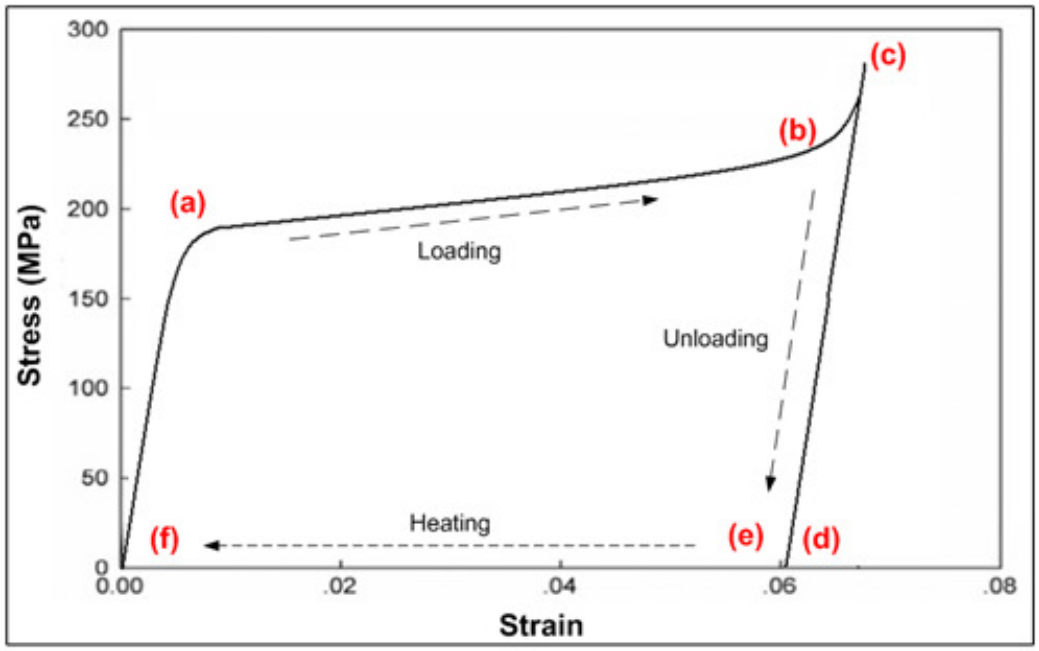

(a)

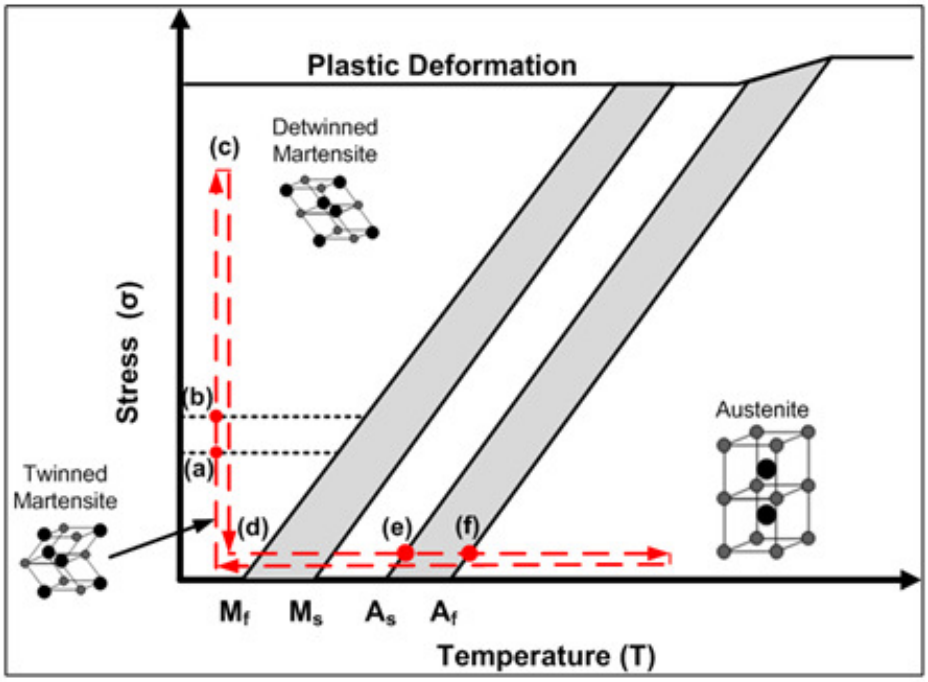

(b)

Figure 6: a.) Stress vs. Strain relationship for SME process and b.) Stress-Temperature phase diagram with loading path and corresponding points of interest

Before training is performed on SMAs, the only geometry which is remembered in the microstructure of the material is the high-temperature austenite shape. Loading below M_f detwins the material, and then upon heating the high-temperature shape that was used during the annealing process will be recovered. During the cooling of the material, there is no geometric change in the shape of the material. This is called one-way shape memory. Two-way shape memory will be discussed later.

Superelasticity

Superelasticity, or loading path #2 in Figure 4, occurs when a specimen in the austenitic phase, at a temperature above A_f, is mechanically loaded such that martensite becomes stable and creates stress-induced martensite. When a critical stress is applied to the material the martensite structure forms allowing the material to acquire a large deformation over a small increase in stress. Upon removing the applied stress the alloy returns to its original shape with no permanent deformation. The stress-strain response, shown in Figure 7, shows the hysteresis during loading and unloading of a shape memory material. Superelastic loading can be performed at higher strain rates, although hysteretic heating from latent heat generation and absorption of the transformations can occur. Literature has shown that non-isothermal high strain rates ($\dot{\varepsilon} = 10^{-3}\ s^{-1}$) in near equiatomic NiTi can lead to temperature increases up to 13°C; whereas, low strain rates ($\dot{\varepsilon} = 10^{-5}\ s^{-1}$) have very small heating increases (1°C)[6].

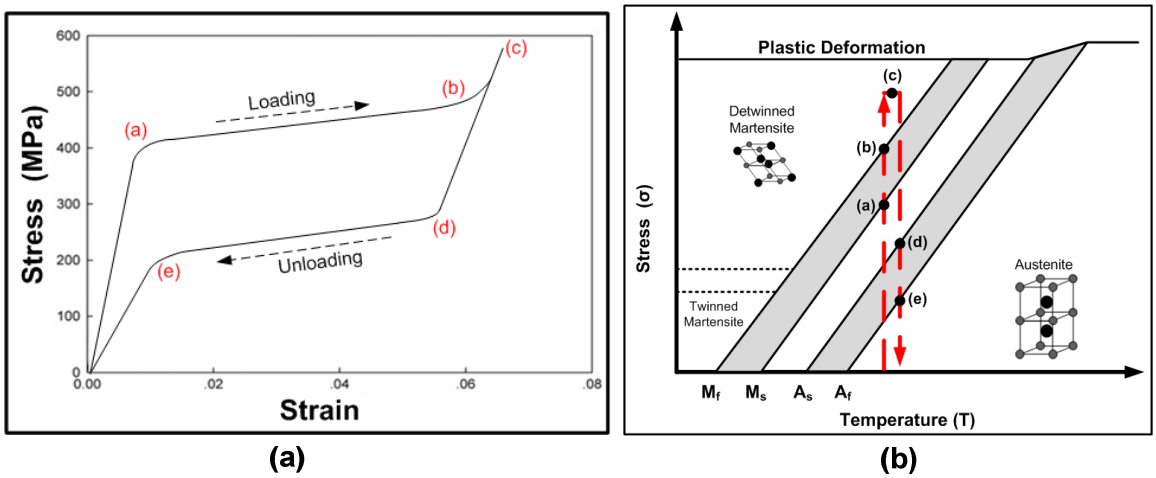

Figure 7: a.) Stress vs. Strain relationship for superelastic loading and b.) Stress-Temperature phase diagram showing loading path and corresponding points of interest

Isobaric Temperature Cycling

Isobaric temperature cycle loading, or loading path #3 in Figure 4, is used primarily for SMA actuators. At constant stress levels, the SMA is thermally actuated to recover strains by heating the material from martensite to austenite. The strain versus temperature diagram for a thermally induced transformation from martensite to austenite upon heating and back again to martensite upon cooling is shown in Figure 8.

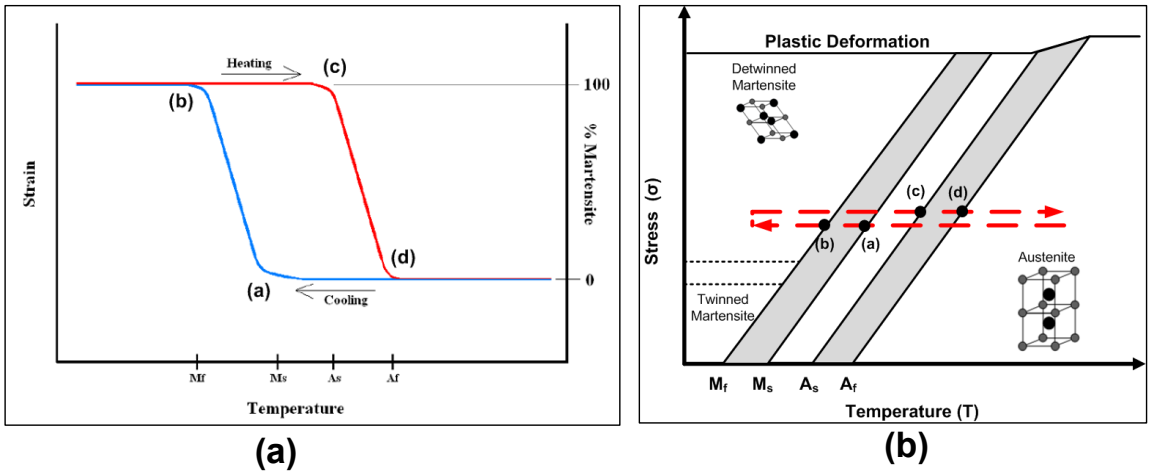

Figure 8: a.) Isobaric temperature cycle and b) Stress-Temperature phase diagram showing loading path and corresponding points of interest

During the heating process the material starts below the A_s temperature and is 100% martensite. Once the A_s temperature has been reached the SMA starts its phase transformation process, recovering deformation until it has reached the A_f temperature and is considered 100% Austenite. During the cooling process the material starts to transform at the M_s temperature and achieves full transformation, returning to 100% martensite, at the M_f temperature.

Thermomechanical Training

One major issue that limits the ability of the material from being used directly as an actuator is the large, non-recoverable strains likely to accrue in the material during each cycle, mechanical or thermal. The generation of plastic strains associated with each cycle is a phenomenon known as Transformation-Induced Plasticity (TRIP). This is associated with both superelastic and isobaric temperature cycles. TRIP is generally significant during initial cycles and stabilizes as the number of cycles increases. Thermomechanically training SMAs at a constant temperature or constant stress eliminates further plastic strain growth. It is important to note if complete phase transformations are not performed during training, path dependence through the phase space is developed. Once trained using full transformation cycles, this history dependence is remembered as full transformations. If partial transformations are performed after training has been completed, one full transformation will reset it to its remembered state from training.

Figure 9 shows the effect of TRIP during superelastic training. The first cycle during training starts at zero stress and zero strain in the austenitic phase. The

temperature remains constant above A_f at zero stress during the entire process. During each loading cycle in the training process, a small amount of non-recoverable plastic strain is accrued before the next cycle is started. The critical stress levels where the stress-induced martensite starts and finishes transformation from austenite lowers during each cycle. Once plastic strain growth has saturated, the material is considered fully trained. More information on superelastic training and deformation can be found in research performed by Miyazaki et al.[7] and Yoon and Yeo[8].

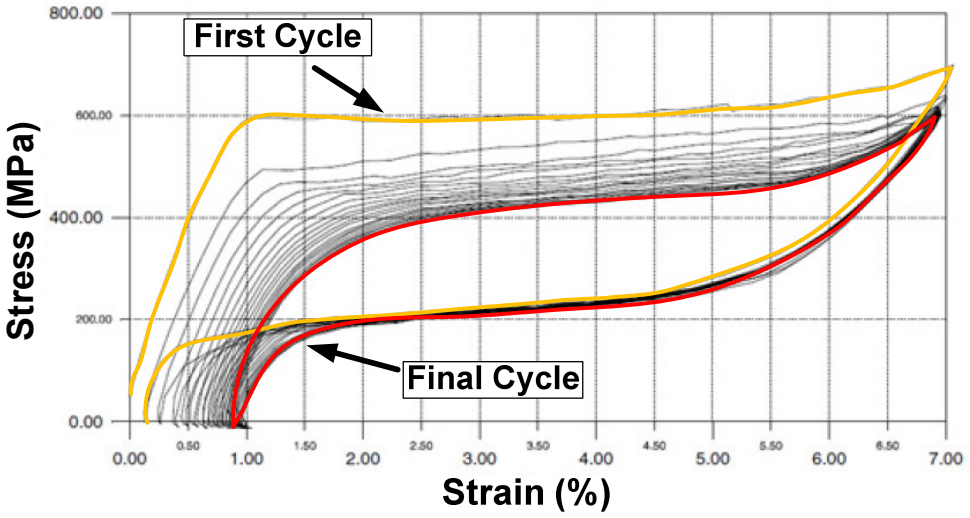

Figure 9: Typical superelastic training

When thermal cycling is performed at a constant stress, a hysteresis curve develops and reaches a steady state strain recovery response. At the point where plastic strain stops growing, or saturates, the SMA has been successfully trained at that specific stress level. Figure 10 shows the effect of constant stress temperature cycle training.

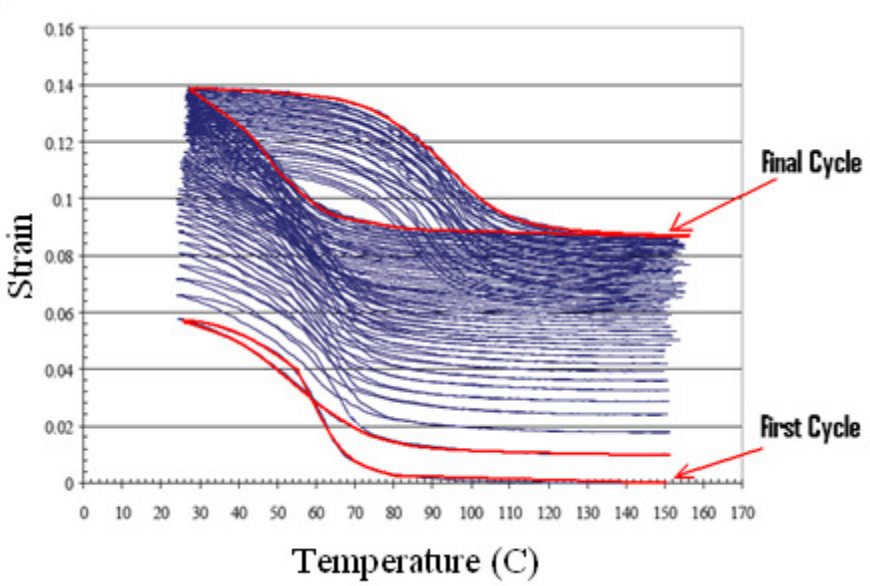

Figure 10: Typical isobaric temperature cycle training of a SMA material

The first cycle in the training process starts at 0.0% strain and 150°C in the fully austenite phase. The cycle temperature is lowered to 25°C which develops approximately 5.8% strain and is now in the fully detwinned martensite state. The first cycle is then completed by returning the temperature to 150°C, the fully austenitic phase. The plastic residual strain that is not recovered on the first cycle is about 1%; therefore, the SMA recovered approximately 4.8% strain in the first cycle. As the temperature is continually cycled during the training process, the recovery strain per cycle starts to reach steady state and plastic strain growth saturates. The final steady state actuation strain or recovery strain at the final cycle is approximately 5.2% strain. The material is then fully trained and can then be used at stress levels up to this training stress without any additional plastic strain growth during thermal actuations. The amount of strain recovered continuously at the training stress level becomes a major actuator design specification.

Two-Way Shape Memory

Due to invoked training methods, shape memory alloys have the ability to remember the high-temperature austenite and low temperature martensite configurations. Unlike the one-way shape memory effect, the SMA has both a high temperature shape and low temperature shape in its memory. This multiple shape memory of both high and low temperature states is called Two-Way Shape Memory (TWSM)[9]. TWSM is only achieved through training or teaching the material. A training regime that involves repeated deformation, transformations, and TRIP produces a deformation microstructure. This structure creates an anisotropic residual stress field favoring the new preferential oriented martensite variants, resulting in a macroscopic shape change between the phase transformations[10]. After training the material at an applied stress, a trained reversible shape change can be achieved at zero stress and both high and low temperature configurations of the microstructure can be utilized[11]. It is important to note that during training, plastic deformation will accumulate upon transformation and create the residual stress field guiding the martensite microstructure to its particular orientation. Although there are not any unique relationships between TWSM and plastic strain growth, plastic strain growth is always associated with training and the development of TWSM[12]. The TWSM established in a trained SMA is ideal for use as an actuator when there is no room for an additional element. One-way shape memory requires an additional element, such as a spring or external force, to return the material to a cold shape upon cooling.

Models

Many constitutive models have been developed to describe the unique thermo-mechanical behavior of SMAs. These models can be grouped into two classes: 1) phenomenological models based on micromechanics of the transformation or macroscopic response of the SMA and 2) thermomechanical models based on thermodynamics. The first class of constitutive models includes the Tanaka model[13, 14] which was the first model proposed for SMAs that utilized the "start" and "finish" phase transformation boundaries. Liang and Rogers[15] and Patoor[16] have proposed other models in this same class. The second group of constitutive models include models by Boyd and Lagoudas[17] and Brinson[18]. Lagoudas and Bo[19] demonstrated that by properly selecting a form of the Gibbs Free Energy, several of the previously developed models mentioned above could be derived.

It has been observed that the maximum transformation strain achieved during a thermal cycle is a function of the applied load, and an advanced constitutive model is required to account for the variance of the transformation strain with the applied load. Bo and Lagoudas[20,21,22] and Lagoudas and Bo[19] have developed a phenomenological constitutive model for polycrystalline SMAs under cyclic loading using a general thermodynamic framework with internal state variables derived through examination of the phase transformation micromechanics. The model is capable of describing cyclic thermomechanical response of SMAs for both stress and thermally induced phase transformations with evolving plastic strains and two-way memory effect with respect to thermal loading cycles.

The model used in this work follows the one given by Bo et al.[23]. Although this model is capable of modeling minor loops (partial transformations), it is the stable major loops (complete transformations) that we are concerned with. The Gibbs Free Energy for this model in 1-D form[23] is given in equation 1 in terms of applied stress (Σ), current temperature (T), and internal state variables of martensitic volume fraction (ξ), transformation strain (E^m), plastic strain (E^p), back stress (α), and drag stress (η):

$$\begin{aligned} G(\Sigma, T, \xi, E^m, E^p, \alpha, \eta) = & -\frac{1}{2\rho} S\Sigma^2 - \frac{1}{\rho}\Sigma\left(E^p + E^m + E^\theta\right) \\ & -\frac{1}{\rho}\int_0^\xi \left(\alpha \frac{\partial E^m}{\partial \tau} + \eta\right) d\tau + c\left[T - T_0 - T\ln\left(\frac{T}{T_0}\right)\right] \\ & -s_0(T - T_0) + G_0^{ch} + \bar{G}^p \end{aligned} \tag{1}$$

In the Gibbs Free Energy model (equation (1)), $\left[-\frac{1}{2\rho} S\Sigma^2 - \frac{1}{\rho}\Sigma\left(E^p + E^m + E^\theta\right)\right]$ represent the Gibbs Elastic Free Energy; $\left[-\frac{1}{\rho}\int_0^\xi \left(\alpha \frac{\partial E^m}{\partial \tau} + \eta\right) d\tau\right]$ is the Mixing Energy induced by the phase transformation; $\left[c\left[T - T_0 - T\ln\left(\frac{T}{T_0}\right)\right] - s_0(T - T_0) + G_0^{ch}\right]$ is the Gibbs Chemical Free Energy; and $[\bar{G}^p]$ is the Elastic Strain Energy induced by plastic strains in the austenite phase. The two variables of concern from the Gibbs Free Energy model are the applied stress and back stress, Σ and α, respectively.

The effective stress, Σ^{eff}, which drives the transformation, is derived from the Gibbs Free Energy, given in equation 1, by taking the derivative of the energy function with respect to the transformation strain, $\Sigma^{eff} = -\frac{\partial G}{\partial E^m} = \Sigma - \alpha_n$. The effective stress

will decay to zero as the transformation completes and ξ (martensite volume fraction) approaches "1", i.e. $\Sigma + \alpha(\xi)|_{\xi=1} = 0$. The result is the following relation[22,23]:

$$\alpha = sign(E^m)\left\{-D_3\left[-\ln\left(1-\frac{H^{cur}}{H}\right)\right]^{\frac{1}{m_1}} + D_2 H^{cur}\xi + D_1\right\} \tag{2}$$

$$\Sigma - sign(E^m)\left\{D_3\left[-\ln\left(1-\frac{H^{cur}}{H}\right)\right]^{\frac{1}{m_1}} - D_2 H^{cur}\xi - D_1\right\}\Bigg|_{\xi=1} = 0 \tag{3}$$

This relation is used in the model to account for the applied stress on the thermally induced transformation strain. It models the experimental data extracted from a series of temperature cycles at various levels of constant applied load for one-way and two-way specimens. For this work, the back stress equation and its material parameters is of concern.

The second term in Equation 3, $D_3\left[-\ln\left(1-\frac{H^{cur}}{H}\right)\right]^{\frac{1}{m_1}}$, enters into the back stress formulation[22] to account for hardening of the transformation from the combination of initial and transformation induced material heterogeneity of the SMA. Three material parameters control the contribution of the material heterogeneity to the back stress: m_1, the back stress shape coefficient, D_3, the heterogeneity back stress, and H, the maximum transformation strain. H^{cur} is the maximum transformation strain for a specific transformation cycle and applied stress, Σ. It can be asserted that all polycrystalline NiTi SMAs will have a similar shaped Σ *vs.* H^{cur} curve for which a single value of the m_1 parameter is required.

The third term in Equation 3, $D_2 H^{cur} \xi$, enters into the back stress formulation[22] to account for the elastic distortion energy associated with the nucleation of martensite inclusions. The nucleation of martensite in the parent austenite induces elastic distortion energy that can be released by further martensite transformation. In this way, a chain reaction, or autocatalytic process, ensues to drive the transformation to completion. This effect is introduced into the model by the autocatalytic parameter, D_2, and is linear with the transformation strain. The autocatalytic process has a small effect on the overall response of the Σ *vs.* H^{cur} curve. This is expected since the governing equation, equation 3, is only evaluated at the end of transformation, ξ=1, and the autocatalytic behavior affects the rate of phase transformation as the transformation from ξ=0 to ξ=1.

Two-way trained SMAs will develop macroscopic strain during the forward transformation with zero applied stress due to the residual stresses created during the training process. The Two-way Drag Stress, D_1, represents these residual stresses. For one-way SMAs the value of D_1 is zero, as the material will transform in a self-accommodating fashion if no load is applied[24].

Using the back stress formulation[22] to predict the material parameters m_1, D_1, D_2, D_3, and H, allows comparison of these parameters for standard NiTi alloys and SMA actuator response for thermally induced transformations. The optimized values of the back stress parameters for typical thermomechanical response of a two-way trained equi-atomic NiTi SMA are listed in Table 1.

Table 1: Typical SMA material parameters for Back Stress Formulation[23]

Back Stress Parameters
m_1 = 1.8
D_1 = 250 MPa
D_2 = 1300 MPa
D_3 = 323 MPa
H= 0.057

Heat Treatment, Cold Work, and Manufacturing

Heat Treatment & Cold Work

Annealing of shape memory alloys is used to relieve dislocation densities that have accumulated in the material through various processes of work. The temperature throughout the material must achieve or exceed the recrystallization temperature of the alloy to completely remove all of the defects. For most NiTi alloys, this temperature is around 450-500 ºC [25]. Annealing has the ability to remove previous training in a material and can reset its shape. This method relieves the internal stresses in the material acquired during training or previous work and increases the chance of plastic strain growth through thermal cycling (transformation softening). Annealing prior to training a SMA allows the process to have a consistent starting point prior to putting any work into the material.

Cold-working a SMA has significant effects on the thermomechanical properties of the material. By cold-working the material through methods of drawing, rolling, or cold swaging, residual stresses develop locally in the microstructure. Cold-work in the material creates transformation hardening; where actuation strain through thermal cycling

is lower than a fully annealed material under the same stress level. Although transformation hardening typically lowers the actuation strain, it can virtually eliminate plastic strain growth under critical stress levels[26,27]. Cold worked material that has no plastic strain growth during thermal transformations cannot have a hot and cold memory. This is due to the theory that TRIP deformation is a prerequisite for two-way memory strain as discussed earlier.

Manufacturing Processes

SMAs exhibit high ductility and a high degree of work-hardening during cutting. These effects lead to difficult machining processes and poor quality in the work piece. For turning, results have shown that higher cutting speeds than recommended by literature or by tool producers are favorable to reduce tool wear (Vc = 80-120 m/min). Although tool wear will still exist at these higher cutting speeds, it is much more severe at lower speeds with no lubricant emulsion. Cutting depth for NiTi material should be limited to the cutting edge radius of the tool to avoid high notch wear in the tooling. Another problem observed in turning NiTi is the formation of burrs due to the high ductility of the material. A feed rate of 0.4-0.9 mm/rev in combination with high cutting speeds and larger cutting depths have been shown to reduce tool wear and the formation of burrs significantly, producing a quality work piece with NiTi alloys[28,29]. For large parts, grinding is often used over traditional cutting techniques to avoid high temperatures. Grinding is a much longer process, but due to the heat sensitivity of the material it needs to be kept at temperatures below 100ºC. The Machining Data Handbook published by TechSolve (www. TechSolve.org) details parameters for many

machining configurations such as turning, milling, threading, drilling, grinding, and centerless grinding of NiTi. For smaller parts, laser cutting and electrical discharge machining (EDM) are usually preferred due to the complexity and high tool wear of traditional machining. Electropolishing is often used to fix any surface irregularities and also remove any heat-affected material from the part after laser cutting or EDM[30].

Mechanical methods of joining have always been preferred when joining two NiTi parts together due to difficulties using other methods. Swaging and crimping are used to attach materials and still have the ability to transport electrical current into the material. Due to the ductile nature of SMAs in the martensite phase, these mechanical methods result in high clamping forces. Also, as the material goes to the austenite phase, these clamping forces get even higher due to the recovery of the martensitic deformation. High strength joints are also made by using a SMA as a coupler. A SMA tube connector is expanded mechanically or by cooling it to deformable martensite, inserted over another element, then allowing it to return to austenite to clamp down on the element.

Due to the tough oxide layer accompanying most NiTi alloys (TiO_2), soldering is very difficult. An aggressive flux is needed to remove this layer to promote good wetting. Once the oxide layer is removed, a common Sn-Ag solder can be used to attain satisfactory results. If the material is to be used in medical or biological activities, it is imperative the solder contains no toxic metals such as lead, antimony or cadmium. Indium Corporation of America has specialized flux (Indalloy Flux #2) and solder (Indalloy #121 & #182) with comparative tensile strength for joining NiTi alloys[31].

Welding Nitinol to itself is usually effective if the weld is protected by an inert atmosphere and the heat affected zone is minimized. Laser, TIG, and resistance welding are all processes that have been successful. Weld strength of about 75% of the raw material tensile strength is possible. Welding NiTi to dissimilar metals, especially stainless steel, is especially difficult due to the formation of brittle intermetallic compounds, TiFe and $TiFe_2$. To avoid this problem, an interlayer, such as tantalum (Ta), is used to bridge the two materials[32].

Industry Applications

SMAs have come a long way since their first discovery, with many successful implementations of the material in the engineering field. Due to the high level of stresses and actuation developed in a SMA structure, they can effectively reduce the complexity and size of standard systems that use multiple moving parts. There is significant interest in using SMAs in more engineering fields, but for many of these fields there is still a large knowledge gap to be filled. A large amount of theoretical work has been performed, but a gap between the theory and design implementation must still be bridged. The next few pages will outline a few current uses of SMAs in industry and the principal behind their operation.

Couplings

SMA couplings have been implemented to provide leakproof piping connections in many applications with line pressures of 2000-5000 psi, such as hydraulic systems in fighter jets and naval vessels, and transportation lines in the oil industry. The process for

using SMA couplers is to design the SMA tube to be used as the coupling element between two separate pipes. The coupler is machined so the inside diameter is slightly smaller than the pipes outside diameter. The high transformation temperature is usually much lower than freezing ($A_f \leq -120°C$); therefore, the coupling always remains in the austenite phase during use. In order to apply the coupler, it is mechanically expanded under cryogenic martensite conditions. The pipe ends are inserted and the coupler returns to its original shape. This securely seals and clamps the pipe end making a leakproof metal on metal seal as illustrated in Figure 11.

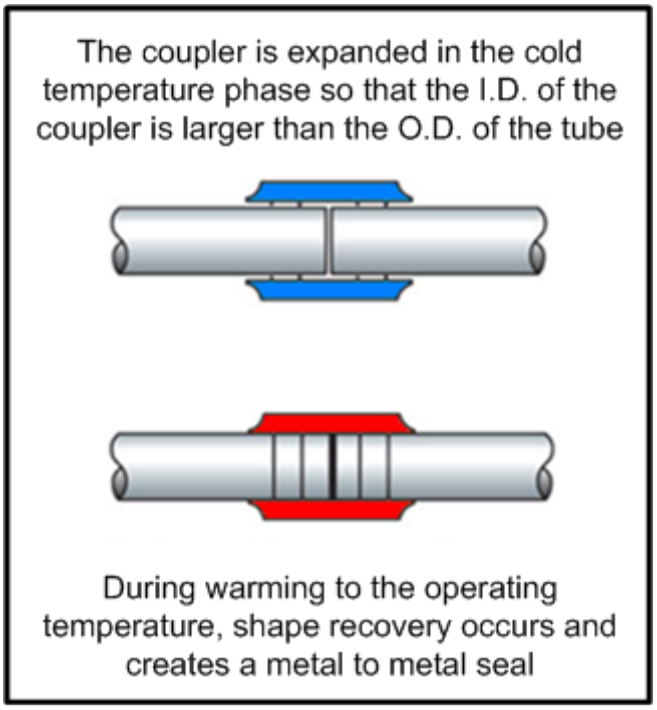

Figure 11: SMA pipe coupling

This same principle is also used as electrical connectors. These are two examples of a constrained recovery. The material is not allowed to fully recover due to the opposing force on the material[33].

Biomedical Devices

SMAs have become extremely useful in the biomedical industry due to the biocompatibility of the material. Most NiTi alloys do not react within the human body and are approved for medical use. Stents and blood clot traps are widely used in the industry due to the deformable nature of the material at the low temperature phase and recovery at the high temperature phase. This implies a stent or blood clot trap can be deformed and packaged in a delivery system such as a catheter in the cold state. As the item is placed in the blood stream, the warm temperature recovery or shape memory effect fully recovers the original shape as a free recovery shown in Figure 12.

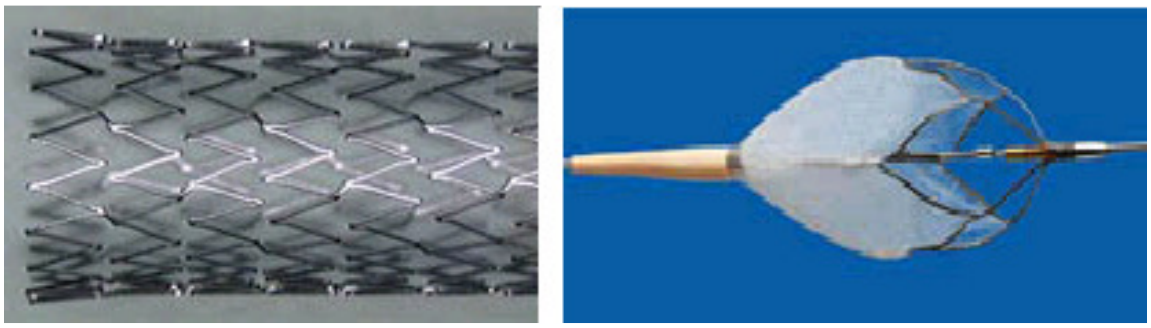

Figure 12: SMA stent (left) & blood clot trap (Right)

Actuators

Actuators require a very high number of stable actuation cycles or long fatigue life. SMA actuators have the unique ability to be incorporated as a smart structure and use their thermal properties transform with the sensed temperature change. One fault to using SMAs as actuators is the frequency at which they can operate, due to the heating and cooling times required. The actuation frequency is significantly lower for larger thermal mass materials such as SMA bars. The smart aspect of SMA actuators lends

itself to a large variety of engineering fields dealing with changing temperature profiles such as flow mixing valves in fluid lines (Figure 13), radiator flow valves in a vehicle, or thermally activated air flow controllers for an air conditioner[34].

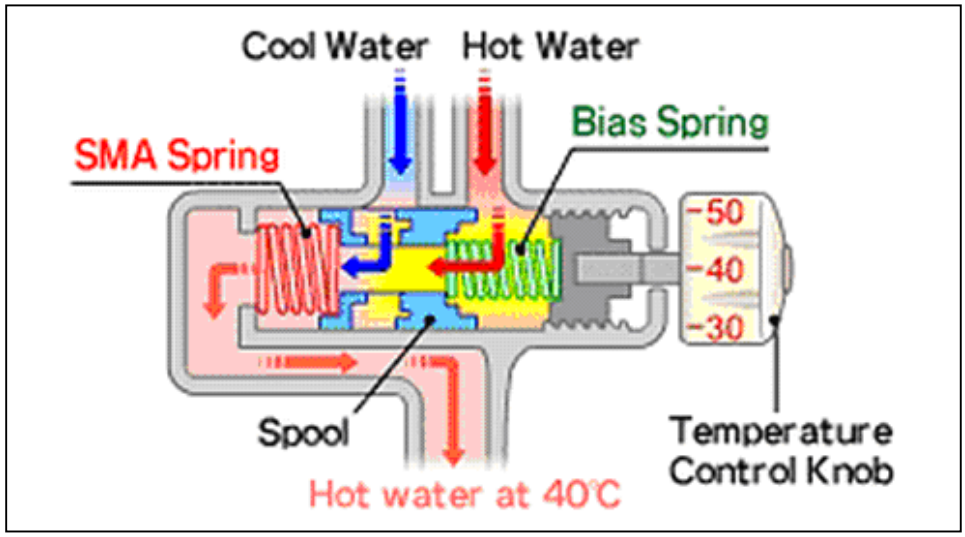

Figure 13: Example of SMA flow mixing valve

The development of using embedded SMAs as actuators has become a considerable interest to aerospace affiliates, i.e. Boeing, Lockheed Martin, and NASA. Though there are many designs currently being tested and developed, Boeing has been working to help solve takeoff and landing noise issues from the jet engines attached to their jumbo airliners. Boeing has incorporated a variable geometry chevron on the bypass end of the turbine engines that adjust with the change of flow temperature associated with altitude. The chevron utilizes SMA beams in conjunction with the elastic effect of the composite structure. One of Boeing's new 787 composite airliners utilizing the QTD2 active SMA chevron is shown in Figure 14. At low speeds & altitude, the SMA beams are actuated inward to allow better mixing of the exhaust gases and greatly

reduce noise produced from the turbine. As the airliner reaches higher altitudes and speeds, the SMA beams are relaxed and the elastic effect of the composite returns the chevron to the flat condition to allow better engine performance[35].

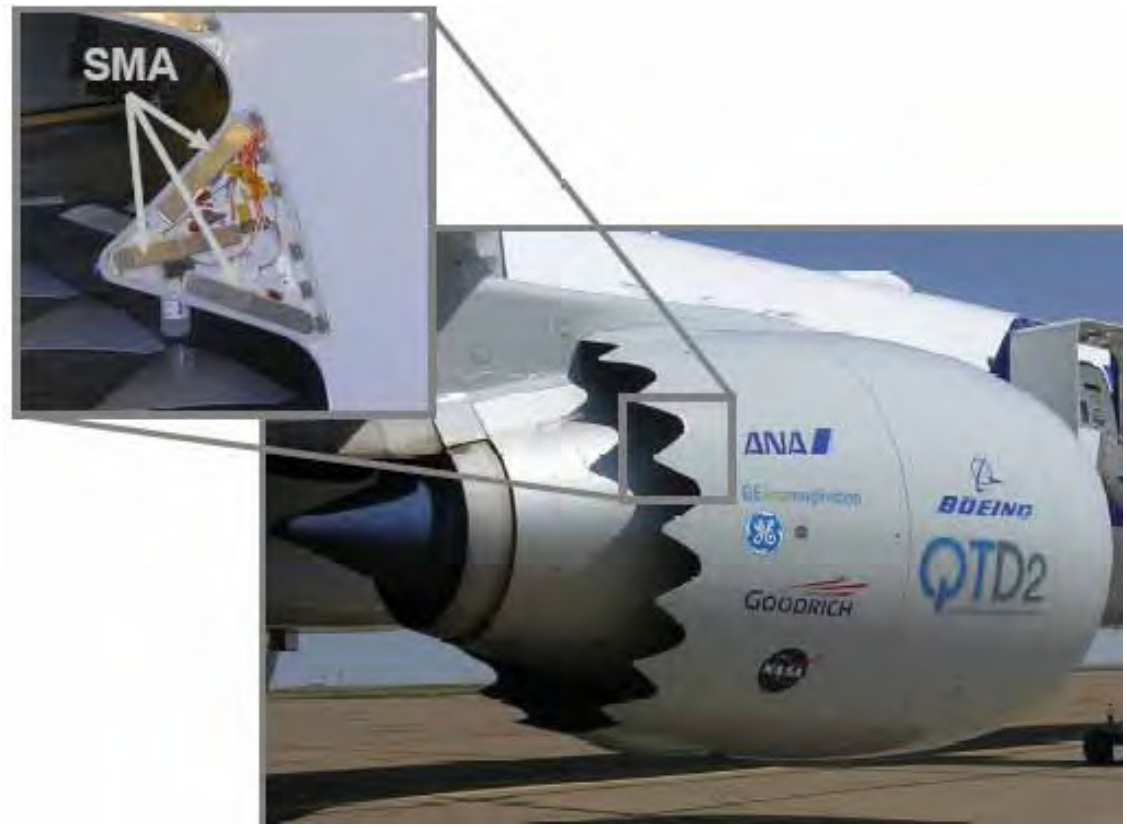

Figure 14: Boeing's active SMA chevron

EXPERIMENTAL PROCEDURE

Experimental Problem Definition

This research was conducted to help increase the knowledge of linear 1-D training of SMAs. Most SMA manufacturers deliver materials to the customer as-straightened (high cold work percentages & low actuation strains) or trained to the customer's desired shape (large actuation strains & high cost). The processing method performed by manufacturers on the material to achieve the trained state is usually proprietary and not discussed in detail. This research will develop a method of actuator training based on any SMA material and the proper steps to take to develop a material characterization for 1-D linear SMA actuators.

Thermomechanical Characterization

Preliminary testing was performed to develop a basis for the material under which the training procedure was then built for each material sample. Thermomechanical characterization of the SMA material involved finding phase transformation temperatures for the determination of the stress-temperature phase diagram.

Differential Thermal Analysis

Differential Thermal Analysis (DTA) measures the temperature change of a sample relative to the temperature of a non-reactive reference sample as the DTA chamber is heated and cooled. This differential measurement is plotted against time or temperature. The baseline of the DTA curve should then exhibit discontinuities at the

transition temperatures and the slope of the curve at any point will depend on the microstructural constitution at that temperature. The measured temperature differences determine endothermic (heat absorbed) or exothermic (heat released) reactions which are used to investigate thermal properties and phase changes of the samples which may be unknown [36].

DTA was conducted on a Linseis L81 vertical bench top research balance (Figure 15). The DTA was controlled through the Linseis design PCI controller / data acquisition card and evaluated using a Linseis Windows package with evaluation tools. An aluminum oxide crucible was used as the sample holder.

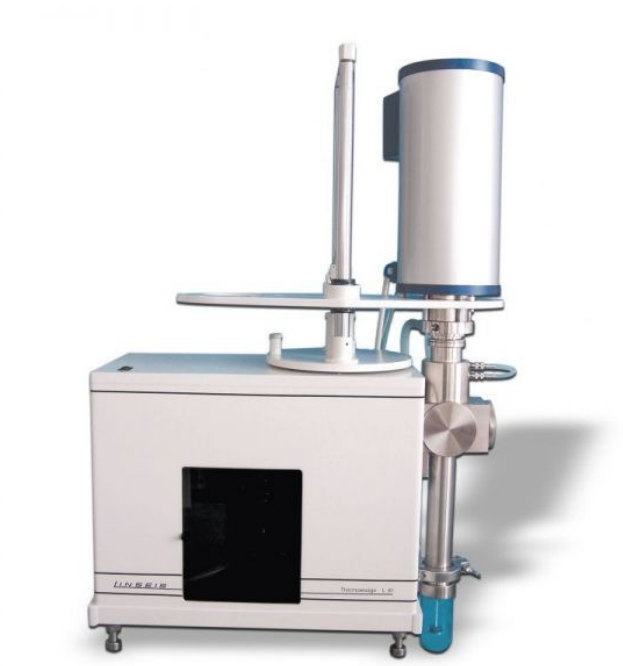

Figure 15: Linseis L81 Research Balance TG/DTA machine

A baseline reference curve was first obtained for the temperature profile tested by placing an equal amount of aluminum oxide powder in the reference and sample

crucibles. The sample crucible was then loaded with a test sample, weighed on a balance and placed in the DTA. The tests were all conducted in an air oxidizing atmosphere chamber vented to atmosphere pressure and cycled from room temperature (20°C) up to a maximum temperature of 250 °C. The Linseis data analysis software was utilized to subtract out the effect of the reference material on the balance as measured in the baseline curve.

Heat Treatments

One sample of each size was trained and characterized in the as-received or as-machined condition and a second sample with identical geometry was tested in the fully annealed condition. The annealing process was carried out using a Lindberg #51442 Materials Furnace controlled by a Lindberg #59344 Controller. All of the fully annealed samples were run at 450ºC for 1 hr. and allowed to cool in room temperature ambient air. An Omega #HH22A handheld digital thermometer equipped with a K type thermocouple was used to verify the annealing temperature in the furnace with the controllers display temperature. To ensure that the wire and ribbon samples were annealed straight and flat, the specimens were held between two flat pieces of steel.

Instron Testing

Larger cross-sectional area samples were mechanically loaded using an Instron 5882 load frame (Figure 16) equipped with an Instron 5800 Controller. The load frame is capable of adjustable loading for tensile loads up to 100 kN.

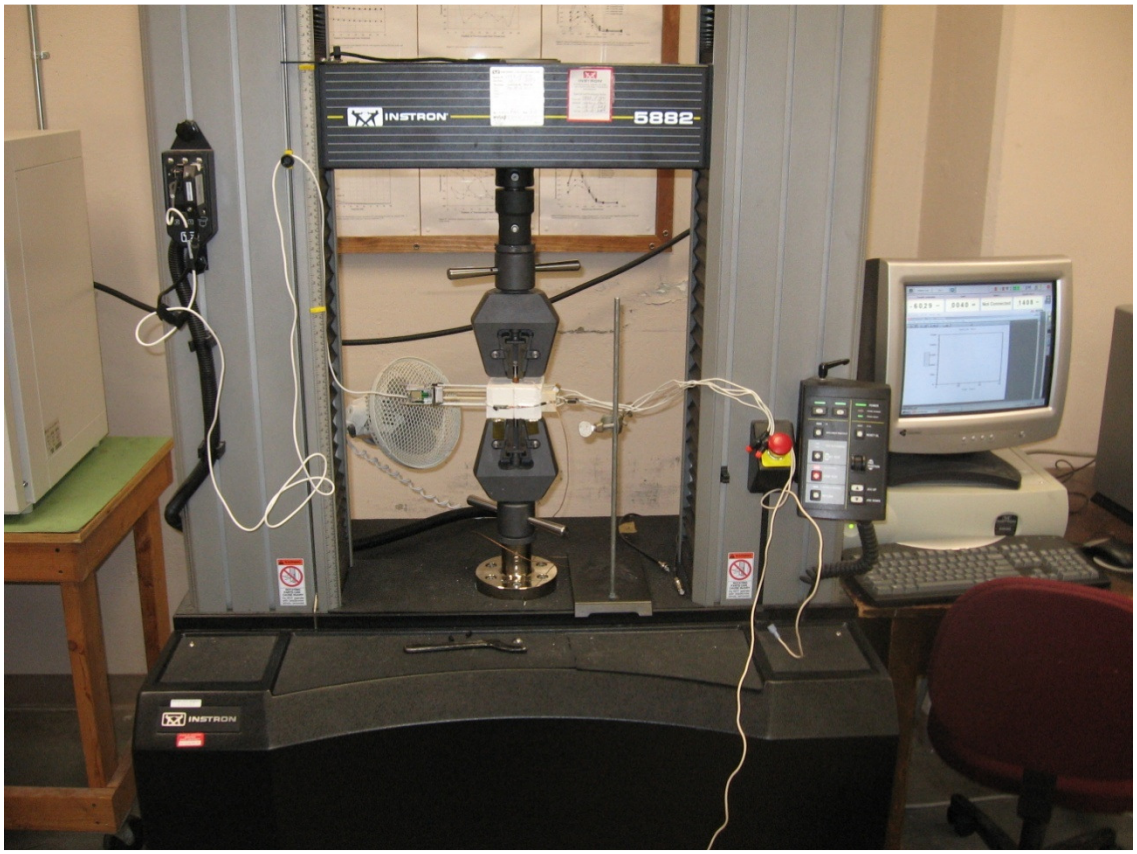

Figure 16: Instron 5882 load frame equipped with custom clamshell furnace

The Instron controller is used in conjunction with Instron's Merlin graphical user interface (GUI) through Windows. Using the Merlin GUI, loading profiles were created to attain particular loads at controlled rates. The loads could be held for constant stress temperature cycles or cyclic loadings up to a set stress level for SME and superelastic testing. An Epsilon #3448-0050-020 high temperature furnace model extensometer acquired accurate strain measurements. The extensometer has a 0.5 in. gage length and ±0.1 in. of travel (±20% strain). The load cell, extensometer, and thermocouple voltage signals were monitored and stored using a National Instruments USB-6221 16-bit, 16 input data acquisition system (DAQ). The Instron was fitted with a custom clamshell

furnace, shown in Figure 17, to control the temperature of the test specimens. The custom built furnace design and drawings are shown in Appendix A.

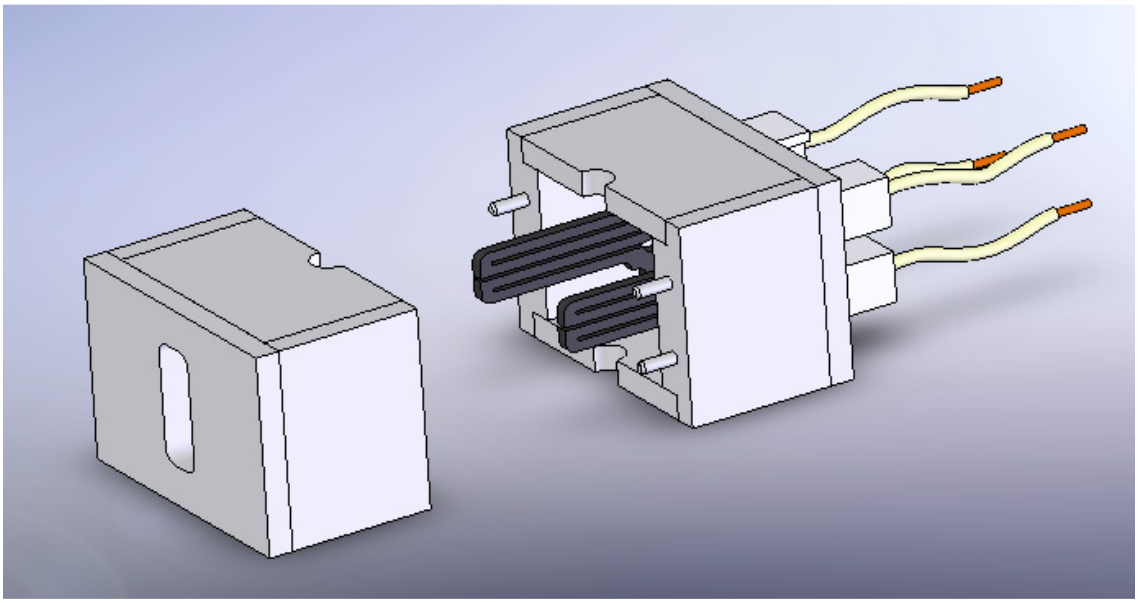

Figure 17: Custom MSU clamshell furnace

Creep Frame Testing

Smaller cross-sectional area samples such as wires and ribbons were mechanically loaded using a static creep frame shown in Figure 18. The frame is equipped with a load cell capable of tensile loads up to 1.5 kN. The sample is held in a vertical position with custom clamps on both ends. The bottom clamp has a threaded J-hook attached to allow weights to hang thus inducing various tensile stresses in the specimen. A hydraulic bottle jack is used to raise and slowly lower the weights onto the lower grip, therefore eliminating shock loading of the sample.

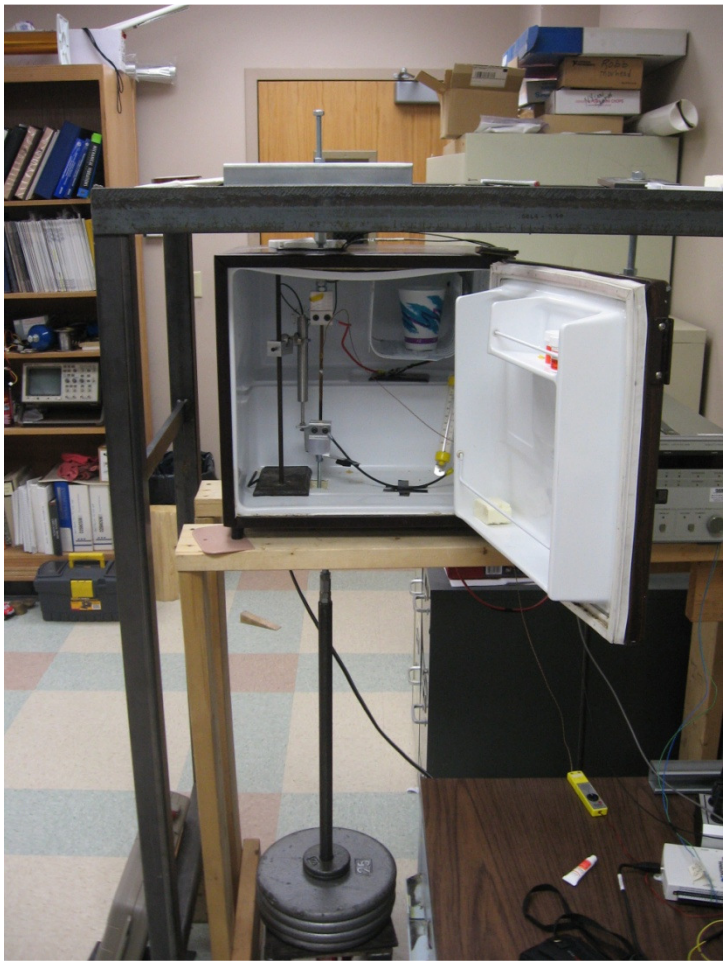

Figure 18: Creep frame and environment chamber for ribbon & wire testing

An LVDT is attached to the bottom clamp for an accurate displacement measurement of the test specimen. The creep frame is also equipped with an insulated environment chamber to allow cooling temperatures down to 5 ºC. The load cell, LVDT, and thermocouple voltage signals are monitored and stored using a National Instruments USB-6212 16-bit, 16 input DAQ.

Temperature Control

The custom clamshell furnace is equipped with two 120V resistive heating elements. The heating elements are powered through an electronic Control Concepts #1652-12-20 electronic power controller. The controller reads an input of 0-5V from the DAQ and outputs 0-100% of full power to the heating elements.

The creep frame testing utilizes a 20V-30A HP Agilent programmable power supply to heat the sample through resistance. Current is run through the sample to uniformly heat it. The programmable power supply is controlled by an analog input of 0-5V to 0-100% of the set output current.

Both the Instron load frame and the creep frame test setups use National Instruments LabView 8.5 to control and monitor the sample temperature during testing. The temperature is read using exposed junction type "K" thermocouples made of fine diameter (0.010") wire to minimize thermal response time of the measurement. An Omega type K miniature electronic ice point cold junction compensator is used between the thermocouple and the DAQ. The signal from the Omega electronic ice point can be converted to temperatures using the standard temperature-mV polynomial for type K thermocouples. Thin copper wire was used to tie the bead of the thermocouple directly to the samples, and a thermally conductive past (Omegatherm 201) was used for electrical insulation and to ensure good thermal conduction with the specimen.

The input to the controller is programmed in LabView to run temperature cycles once the constant stress has been achieved in the sample. The heating and cooling temperature dependent rates were controlled by adjusting ramp rates to the power

controllers depending on the temperature of the sample. Utilizing the programming controls of LabView the temperature can by cycled between a set high and low temperature. Appendix B contains the LabView Control VI designed to control the temperature and collect data during testing.

Test Specimens

A combination of eight test samples were fully trained and compared. Of these eight samples, three different near equiatomic NiTi alloys and four different geometries were utilized (Table 2).

Table 2: Material matrix of test specimens

Sample Identifier	Material	Supplier	Geometry (Size)	Annealed
A1	55 NiTi (49.9 at% Ni ~ 50.1 at% Ti)	NASA-GRC	Round (Dia.=6.36mm)	No
A2	55 NiTi (49.9 at% Ni ~ 50.1 at% Ti)	NASA-GRC	Round (Dia.=6.33mm)	Yes
B1	55 NiTi (49.9 at% Ni ~ 50.1 at% Ti)	NASA-GRC	Round (Dia.=4.60mm)	No
B2	55 NiTi (49.9 at% Ni ~ 50.1 at% Ti)	NASA-GRC	Round (Dia.=4.34mm)	Yes
C1	50.4 at% Ni ~ 49.6 at% Ti	SAES	Rectangular (5.74mm x 0.26mm)	No
C2	50.4 at% Ni ~ 49.6 at% Ti	SAES	Rectangular (5.74mm x 0.26mm)	Yes
D1	49.3 at% Ni ~ 50.7 at% Ti	NDC Corp.	Square (0.72mm x 0.72mm)	No
D2	49.3 at% Ni ~ 50.7 at% Ti	NDC Corp.	Square (0.72mm x 0.72mm)	Yes

The bar material supplied from NASA-GRC (Dia.=10mm) was machined to allow a reduced cross-sectional area and consistent gage length for testing (Figure 19). Two sizes were machined from the stock material. The larger diameter of 6.36mm was

machined at NASA Glenn Research Center (NASA-GRC), and the smaller diameter of 4.60mm was machined at Montana State University (MSU).

Figure 19: Machined bar sample

The wire and ribbon material was left in its as received cross-section and not machined prior to testing. The grips used for testing on the creep frame were rounded on the grip edges to stop large stresses from being induced into the sample as it exited the grips.

The eight different test samples were first thermomechanically trained by running thermal cycles at a specific constant training stress. Once the samples were trained at the training stress level, they were subjected to lower constant stress values and thermally cycled to acquire a characterization of the materials transformation strains and phase transformation temperatures. The test matrix used for the training stress and the constant stress thermal cycle tests that followed the training run for each test sample is illustrated in Table 3. The data from each sample was collected and will be compared in the next section.

Table 3: Testing matrix for each sample

Sample Identifier	Training Stress	Constant Stress Intervals (MPa)
A1	300 MPa	250, 200, 150, 100, 50, 0
A2	300 MPa	250, 200, 150, 100, 50, 0
B1	300 MPa	250, 200, 150, 100, 50, 0
B2	300 MPa	250, 200, 150, 100, 50, 0
C1	350 MPa	300, 250, 200, 150, 100, 50
C2	350 MPa	300, 250, 200, 150, 100, 50
D1	350 MPa	300, 250, 200, 150, 100, 50
D2	350 MPa	300, 250, 200, 150, 100, 50

EXPERIMENTAL RESULTS

Differential Thermal Analysis

DTA testing was performed on three samples from the NASA-GRC 55NiTi to evaluate the heat treating process and zero stress transformation temperatures. Three samples were machined down to a nominal size of 4mm dia. by 4mm long that would fit into the crucible for the DTA. One sample was tested in the as-machined condition and the other two samples were annealed for 30 minutes at 450º and 800ºC. The three temperature cycles for each sample are shown in Figure 20-22.

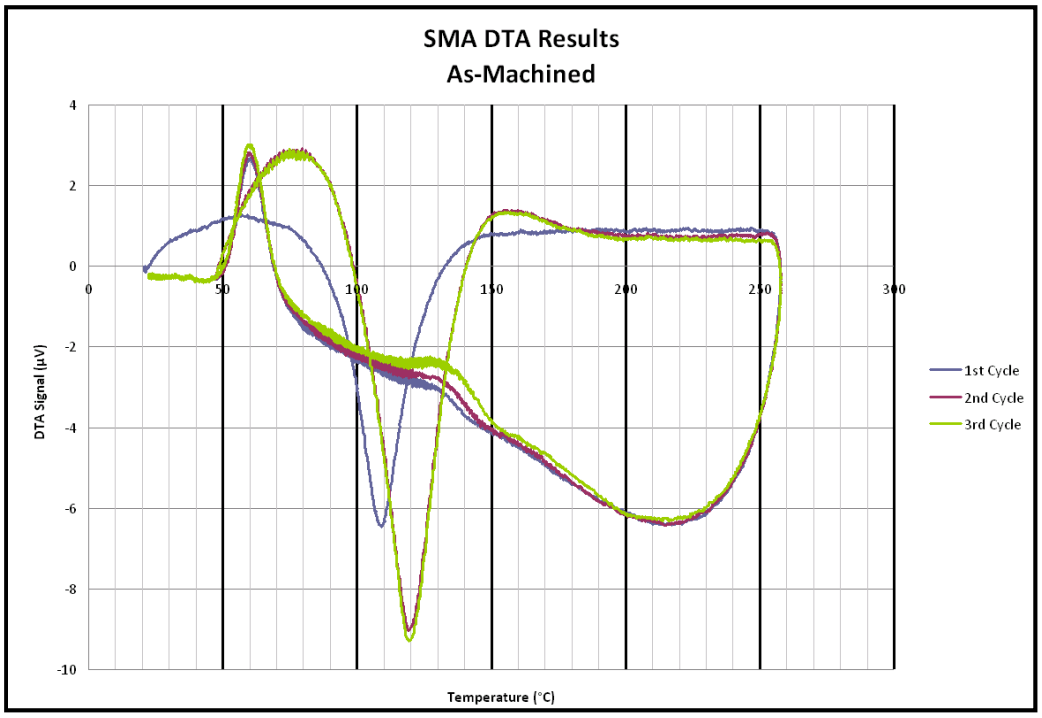

Figure 20: Differential Thermal Analysis (DTA) results for 55-NiTi as-machined

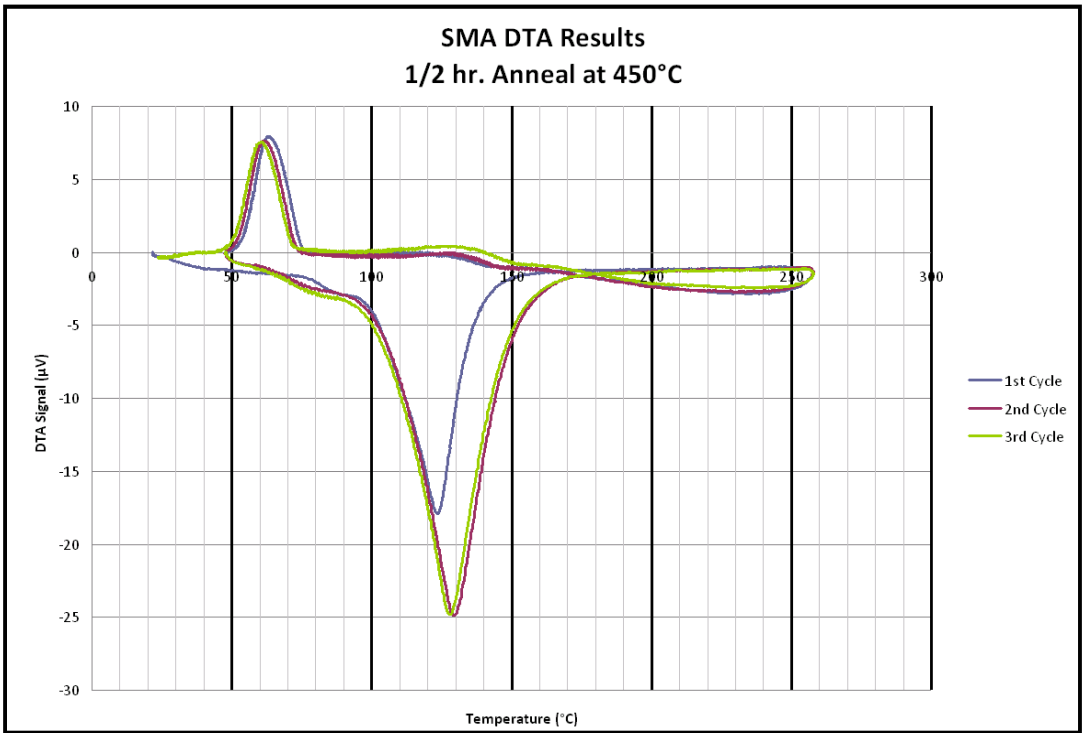

Figure 21: DTA results for 55-NiTi annealed at 450ºC

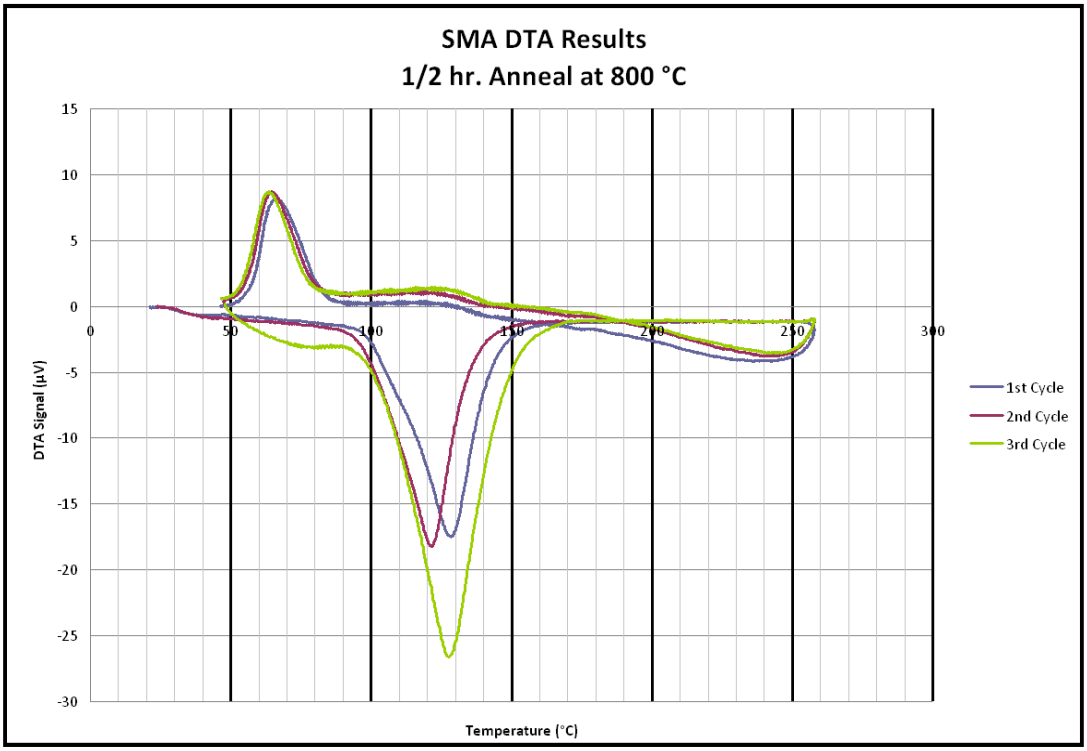

Figure 22: DTA results for 55-NiTi annealed at 800ºC

The DTA results were plotted with all three samples for the first temperature cycle (Figure 23) and the third temperature cycle (Figure 24) to compare the differences between the different heat treatments.

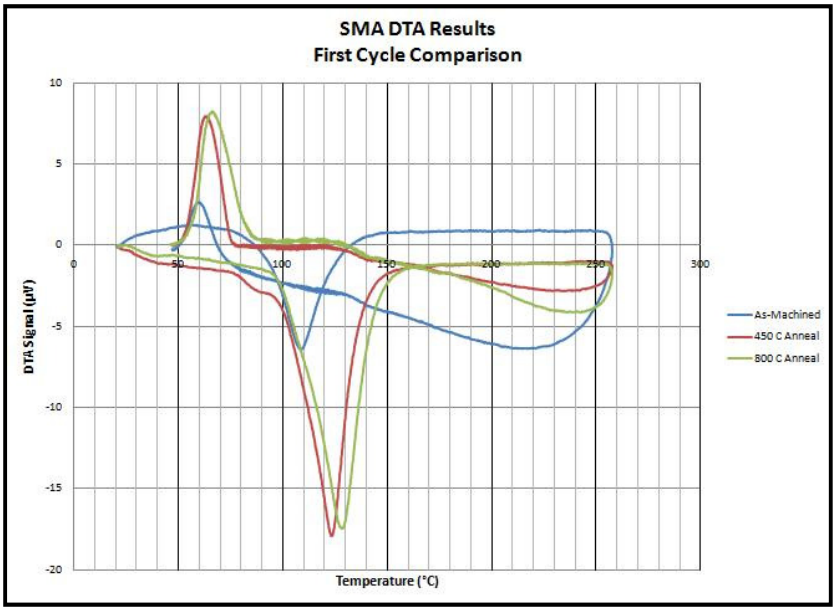

Figure 23: First cycle DTA results for all three samples

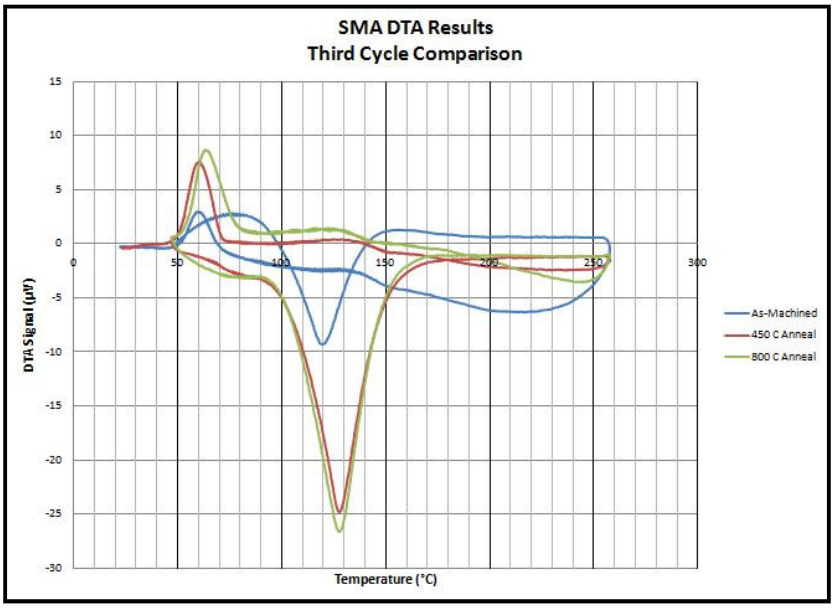

Figure 24: Third cycle DTA results for all three samples

Shape Memory Effect Loading

Shape memory effect loading (path #1, Figure 4) was performed on a 55NiTi bar sample annealed at 800ºC for ½ hour. The sample had a reduced cross-sectional diameter of 6.60 mm. This test was loaded and unloaded at room temperature at a rate of 0.15mm/min to determine the critical stresses where detwinning occurs, and then heated above the austenite finish temperature at zero load to recover deformation. Figure 25 exhibits the loading path and recovery due to heating the sample under zero stress.

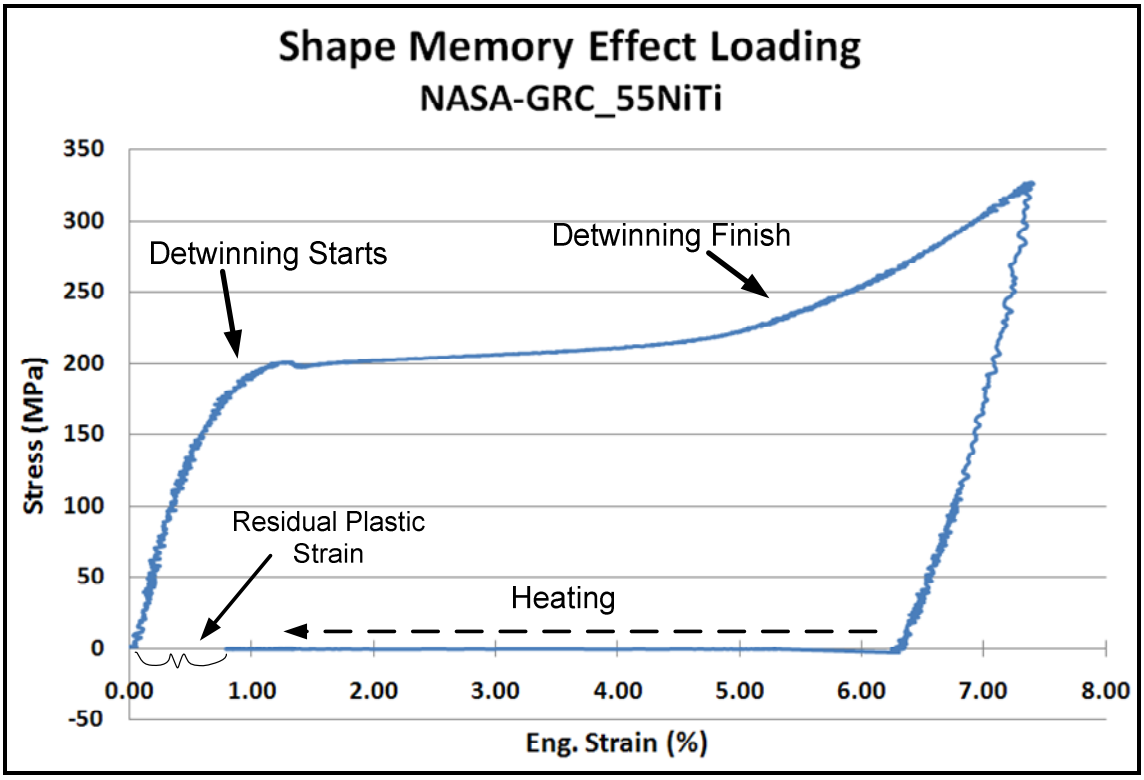

Figure 25: SME Loading on 55NiTi Bar Sample.

Superelastic Loading

The same bar sample that was used in the SME test (annealed at 800ºC for ½ hr.) was loaded in the austenite state at 200ºC (approximately 50°C above A_f). The superelastic test was run at a constant rate of 0.15 mm/min up to a stress of 650 MPa to avoid hysteretic heating or high strain rate effects. The load was then removed at the same constant rate to a stress free state (0 MPa). The superelastic loading test results are shown in Figure 26.

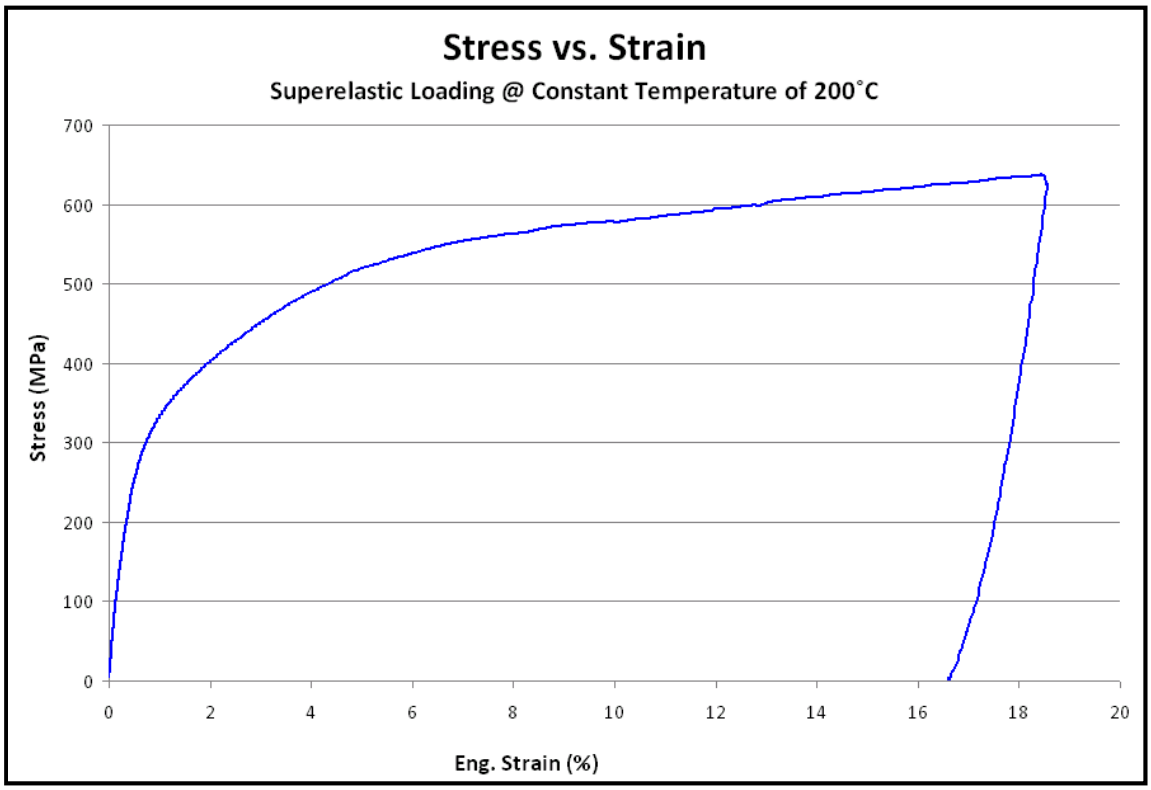

Figure 26: Superelastic loading at 200ºC.

Constant Stress Thermal Cycles

Before the SMA samples can be characterized for actuator usage, they must first be fully trained at the desired training stress. Once the plastic strain growth saturates during the training of the sample, the stress is reduced to begin characterizing the actuation strain versus stress level for each sample.

Training

The training process was carried out on the Instron tensile testing load frame for specimens designated A1, A2, B1, & B2. The 55 NiTi bar samples had very large plastic strain growth during the training process. Due to the thermal mass of the bar specimens, heating and cooling times were greatly increased.

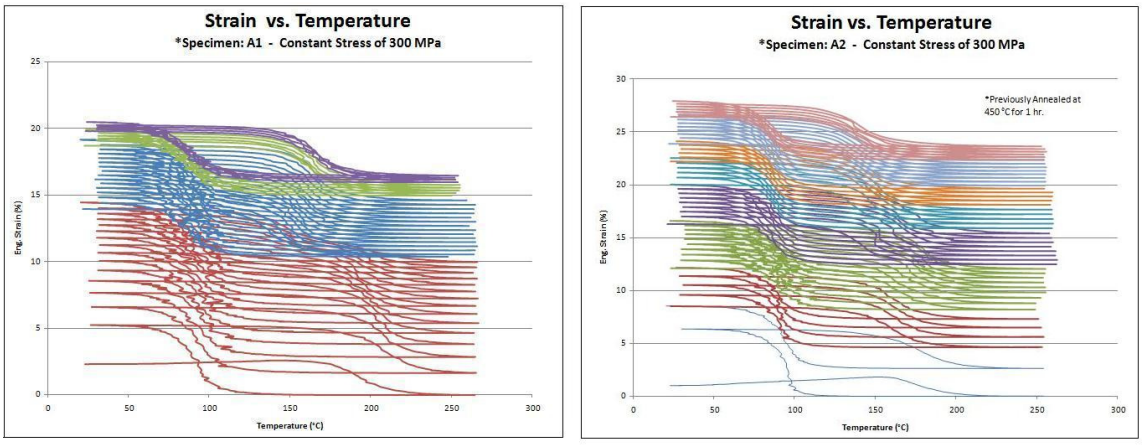

a.) b.)

Figure 27: Constant stress thermal cycle training at 300 MPa; a.) Specimen A1 (As-recieved 55NiTi bar) b.) Specimen A2 (55NiTi bar, Annealed at 450ºC for 1 hr.)

The length of time and large plastic strain growth involved during training required multiple testing runs and recalculating the load to maintain a constant stress in the sample. The different training runs are shown by different colors in Figures 27 & 28.

Figure 29 shows the plastic strain growth during the training for the four large cross-section specimens.

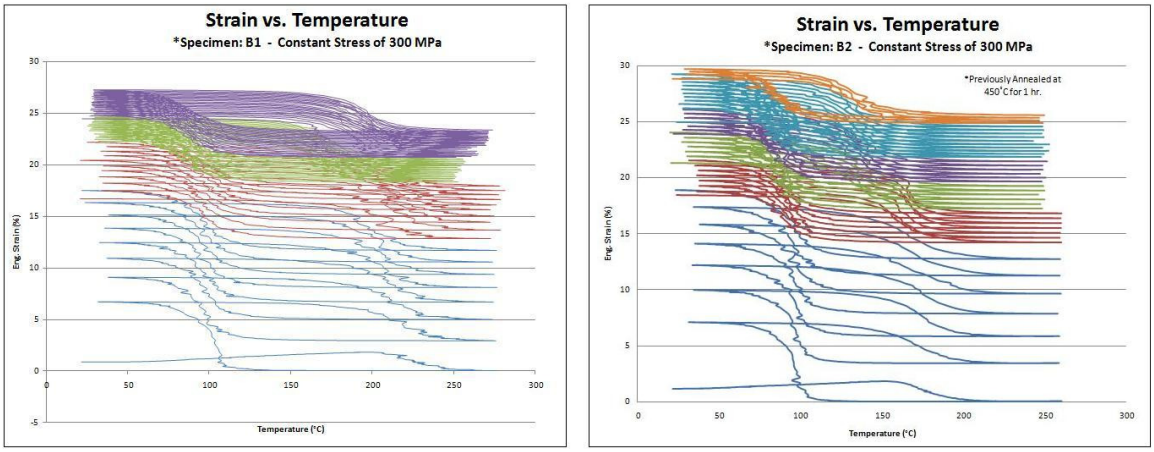

a.) b.)

Figure 28: Constant stress thermal cycle training at 300 MPa; a.) Specimen B1 (As-recieved 55NiTi bar) b.) Specimen B2 (55NiTi bar, Annealed at 450ºC for 1 hr.)

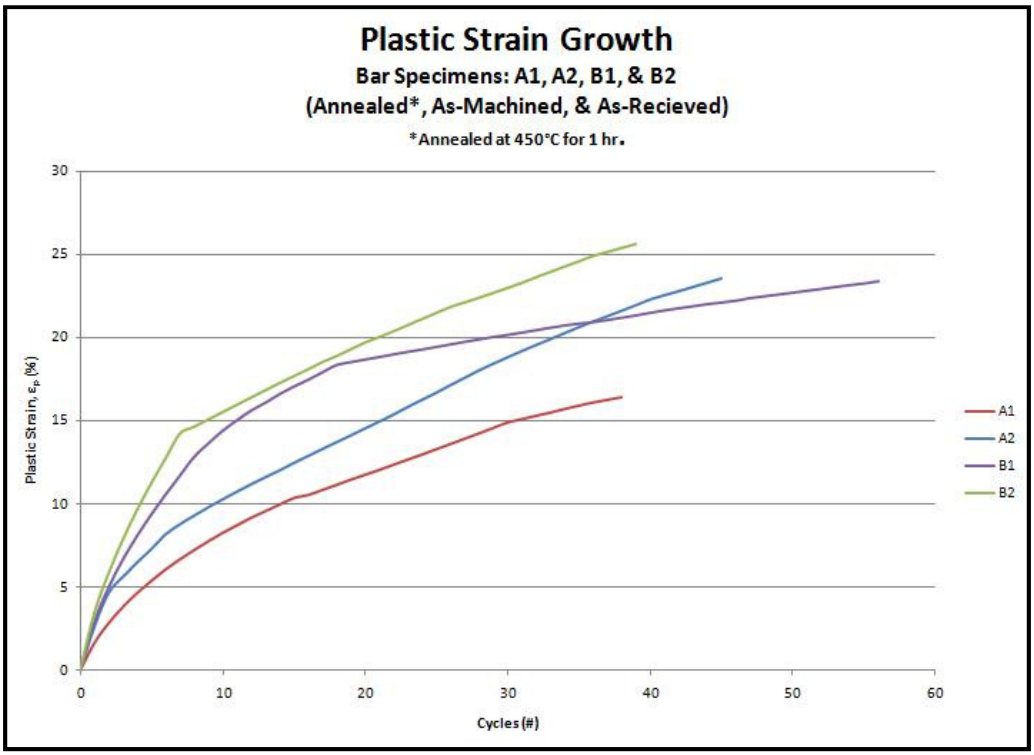

Figure 29: Plastic strain growth for all bar samples

The ribbon and wire specimens, designated C1, C2, D1, & D2, were tested on the constant stress creep frame. After the training stress was applied to the specimen the temperature cycles were started. Once TRIP had saturated or neared saturation, the temperature cycles were stopped, and training was considered complete. The as-received ribbon and wire specimens acquired no plastic strain growth during the training process. This will be discussed in more detail later. The results of the training runs for the ribbon and wire specimens are illustrated in Figures 30 & 31. Figure 32 shows the plastic strain growth during the training for the annealed wire and ribbon specimens.

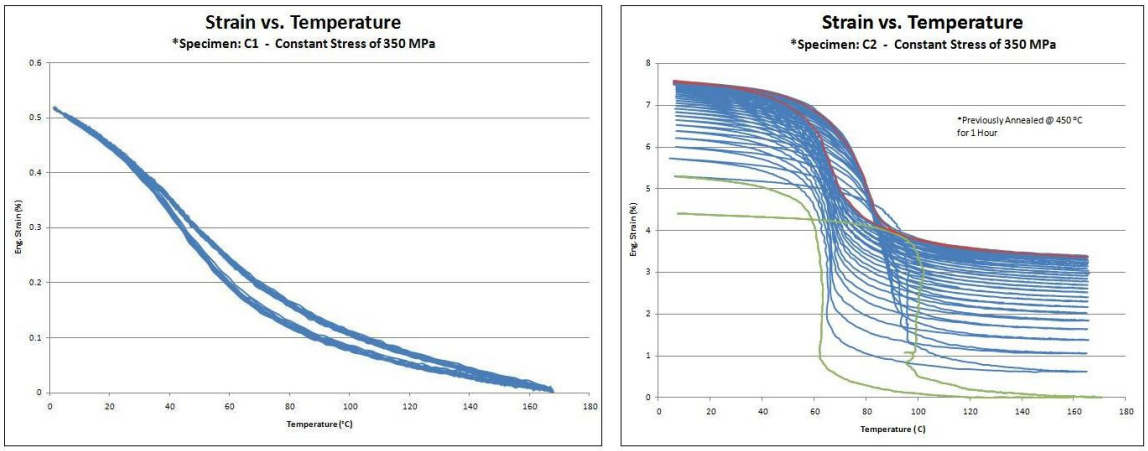

a.) b.)

Figure 30: Constant stress thermal cycle training at 350 MPa; a.) Specimen C1 (As-recieved NiTi ribbon) b.) Specimen C2 (NiTi ribbon, Annealed at 450ºC for 1 hr.)

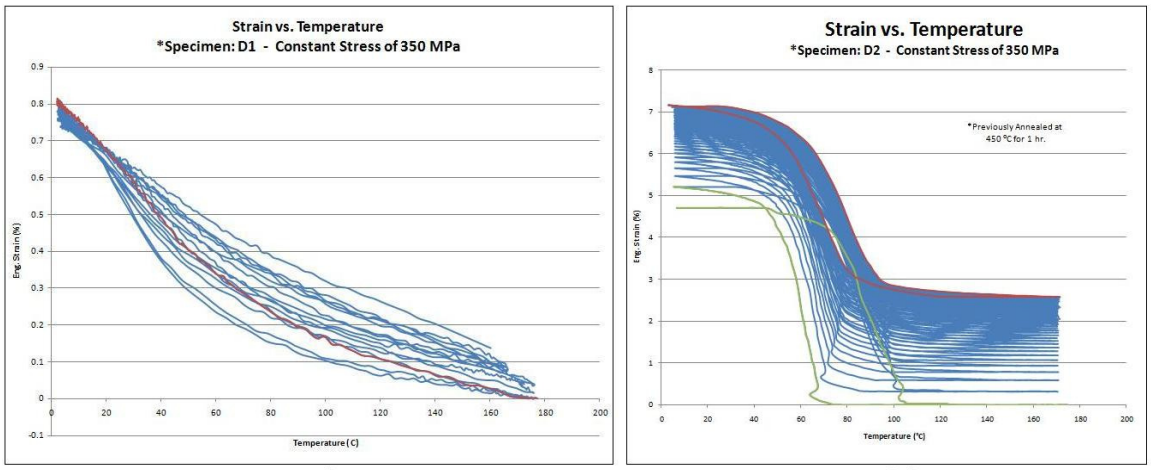

a.) b.)

Figure 31: Constant stress thermal cycle training at 350 MPa; a.) Specimen D1 (As-recieved NiTi Wire) b.) Specimen D2 (NiTi Wire, Annealed at 450ºC for 1 hr.)

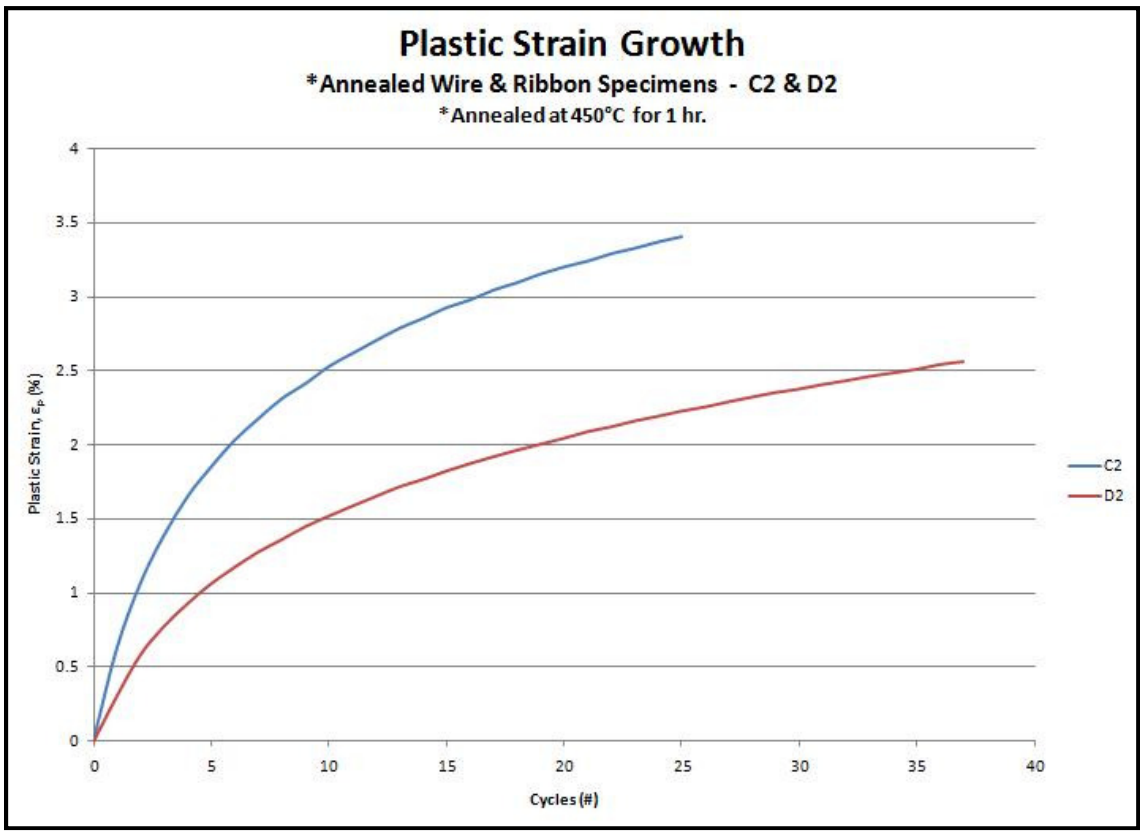

Figure 32: Plastic strain growth for annealed wire & ribbon samples

Actuation Strains

Once a specimen reached a fully-trained state, the load was reduced below the training stress in 50 MPa increments. At each incremental step, the stress was held constant, and 3-5 thermal cycles were run to acquire the actuation strain through full transformation of the material. The results of the actuation strain testing for the A1 bar specimen are shown in Figures 33 & 34.

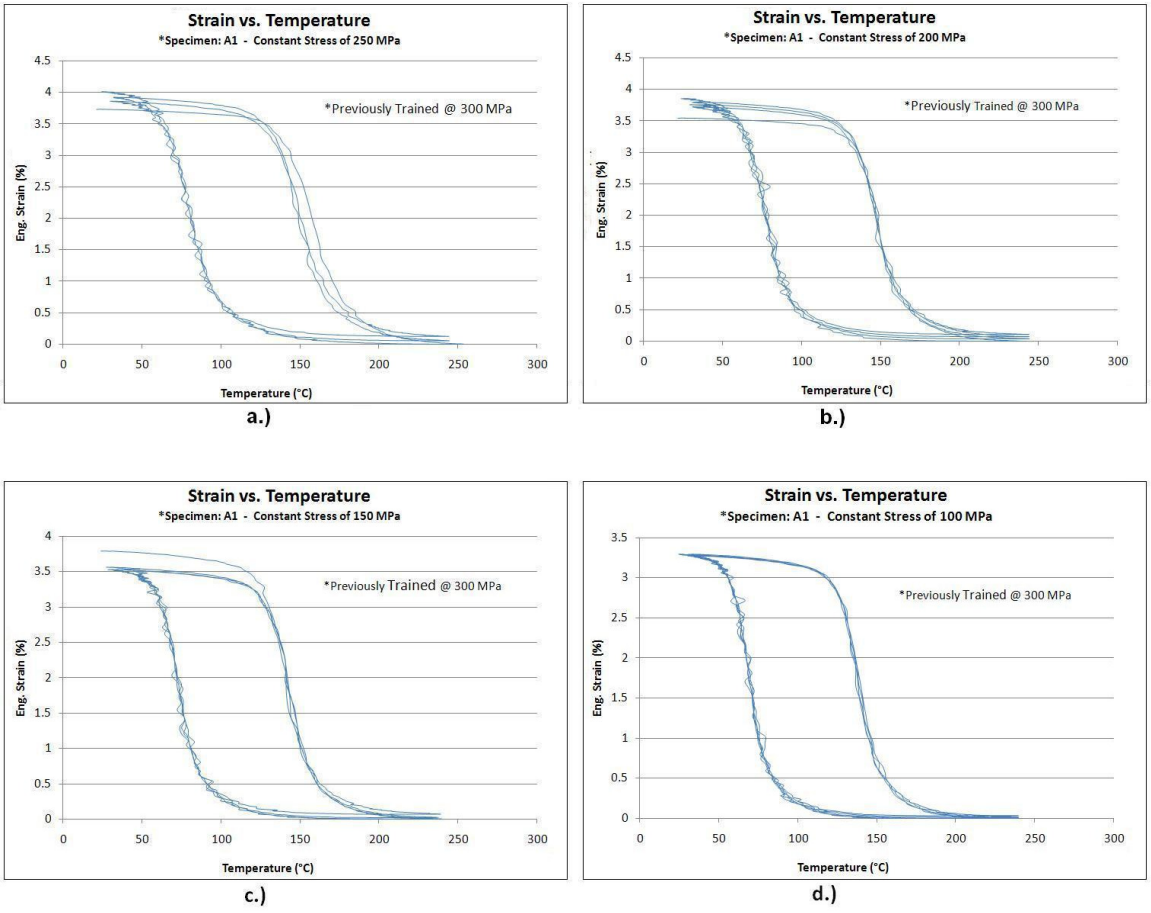

Figure 33: Actuation Strains for Sample A1; Temperature cycles at constant stress of:
a.) 250 MPa b.) 200 MPa c.) 150 MPa d.) 100 MPa

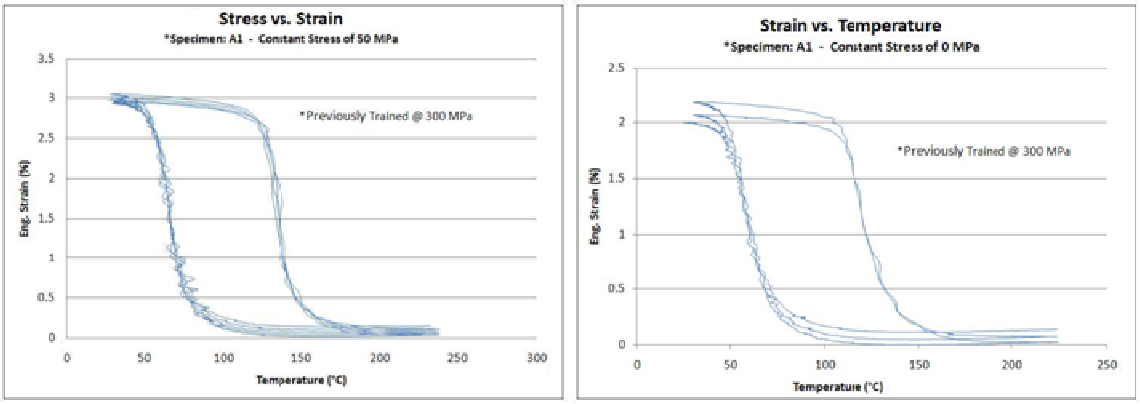

a.) b.)

Figure 34: Actuation Strains for Sample A1; Temperature cycles at constant stress of: a.) 50 MPa b.) 0 MPa

The strain vs. temperature figures showing the actuation strains for specimens A2, B1, B2, C1, C2, D1, & D2 are shown in Appendix C. The actuation strain at each applied stress level for the constant stress temperature cycling on all the samples is shown in Table #4 and in Figure 35.

Table 4: Actuation Strains (%) for each sample

Test Sample:	Material:	350 (MPa)	300 (MPa)	250 (MPa)	200 (MPa)	150 (MPa)	100 (MPa)	50 (MPa)	0 (MPa)
A1	55 NiTi	-	3.8465	3.7865	3.6886	3.5280	3.2730	2.9136	2.0988
A2	55 NiTi	-	4.0321	3.9470	3.8120	3.6596	3.4367	3.0086	2.1930
B1	55 NiTi	-	3.9135	4.0607	3.8786	3.5585	3.0290	2.4909	1.4308
B2	55 NiTi	-	4.1237	4.0942	3.9972	3.8306	3.5017	3.0547	1.8216
C1	55.49%Ni ~Ti Balance	0.5050	0.4506	0.3460	0.2950	0.2636	0.2100	0.1850	-
C2	55.49%Ni ~Ti Balance	4.1897	3.9800	3.8400	3.6100	3.4400	3.1000	2.4040	-
D1	54.4%Ni ~Ti Balance	0.8150	0.7921	0.7157	0.6100	0.5513	0.3826	0.3195	-
D2	54.4%Ni ~Ti Balance	4.5573	4.2814	4.2008	4.0419	3.8595	3.4117	1.7470	-

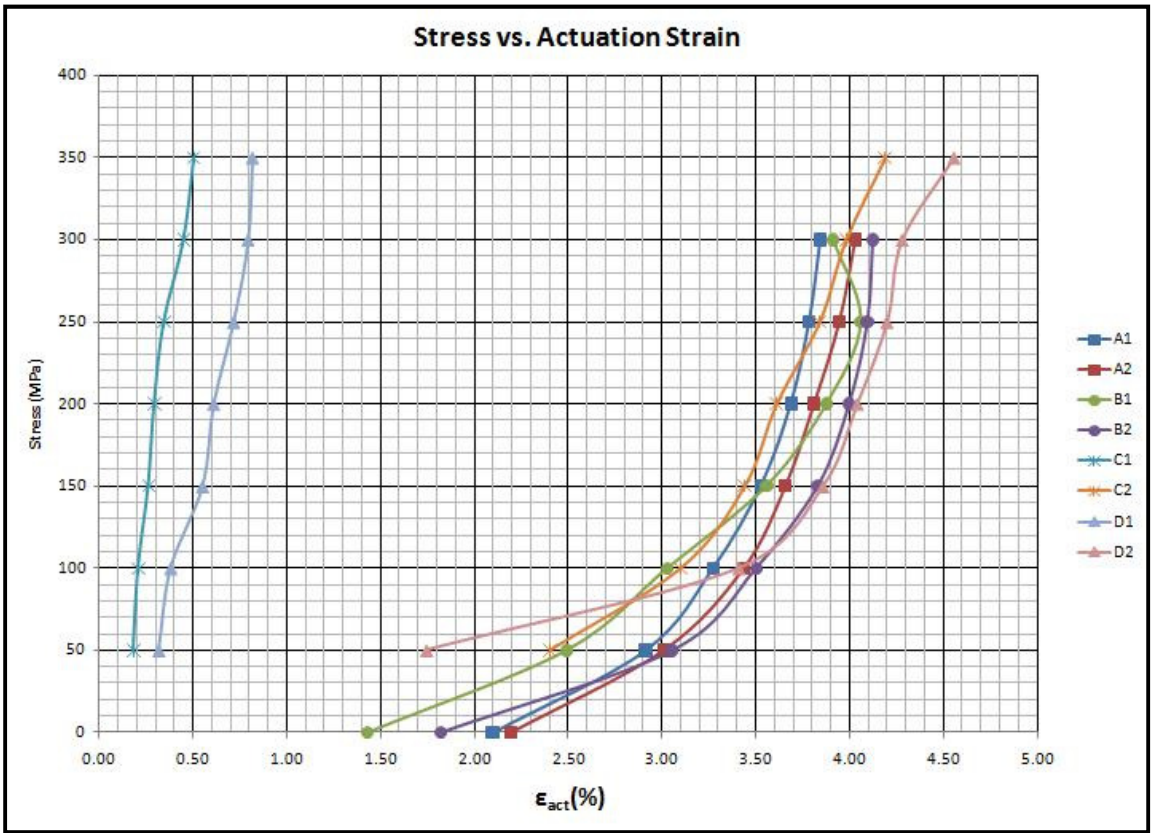

Figure 35: Applied Stress vs. Actuation Strain for all samples

Transformation Temperatures

From each constant stress thermal cycle test, the approximate transformation temperatures at that stress level were determined by the intersection of linear fits between the martensite, austenite, and transformation regions. This data characterizes the phase transformation temperatures for the samples at any stress level at or below the training stress. Figure 36 and 37 show the transformation temperature differences between the as-received, or as-machined, and fully annealed states for the two different size bar samples. The results of the transformation temperatures for each stress level for the fully annealed ribbon and wire specimens are illustrated in Figure 38.

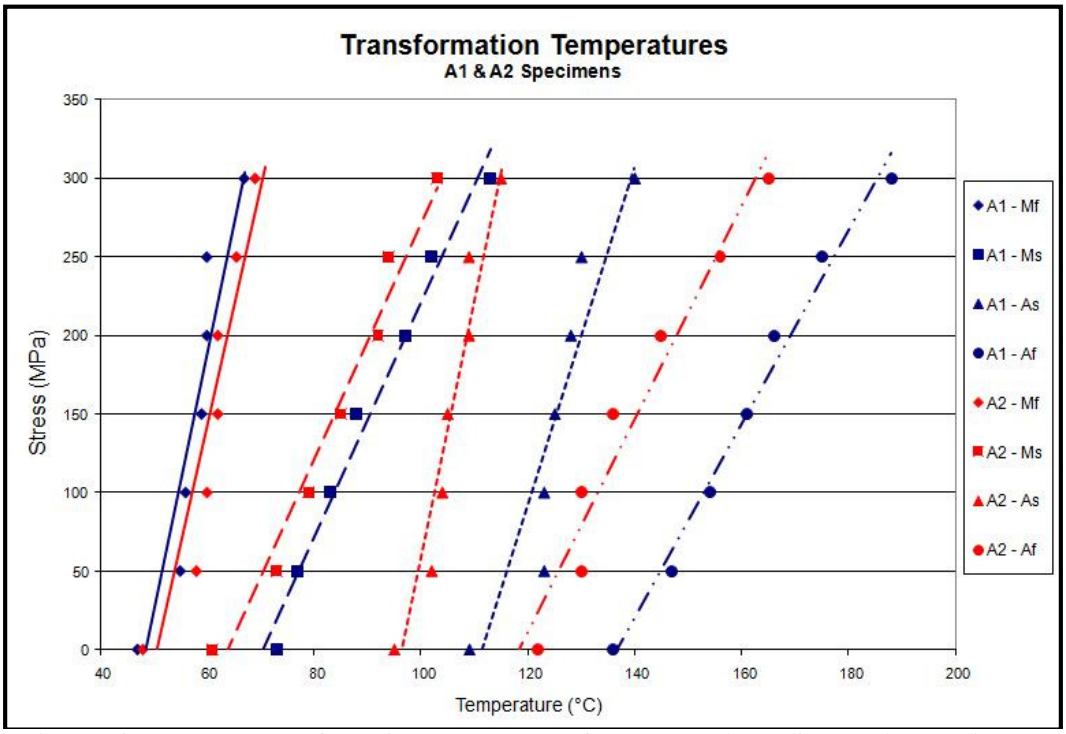

Figure 36: Stress vs. Transformation Temperatures for A1 & A2 large diameter bar specimens.

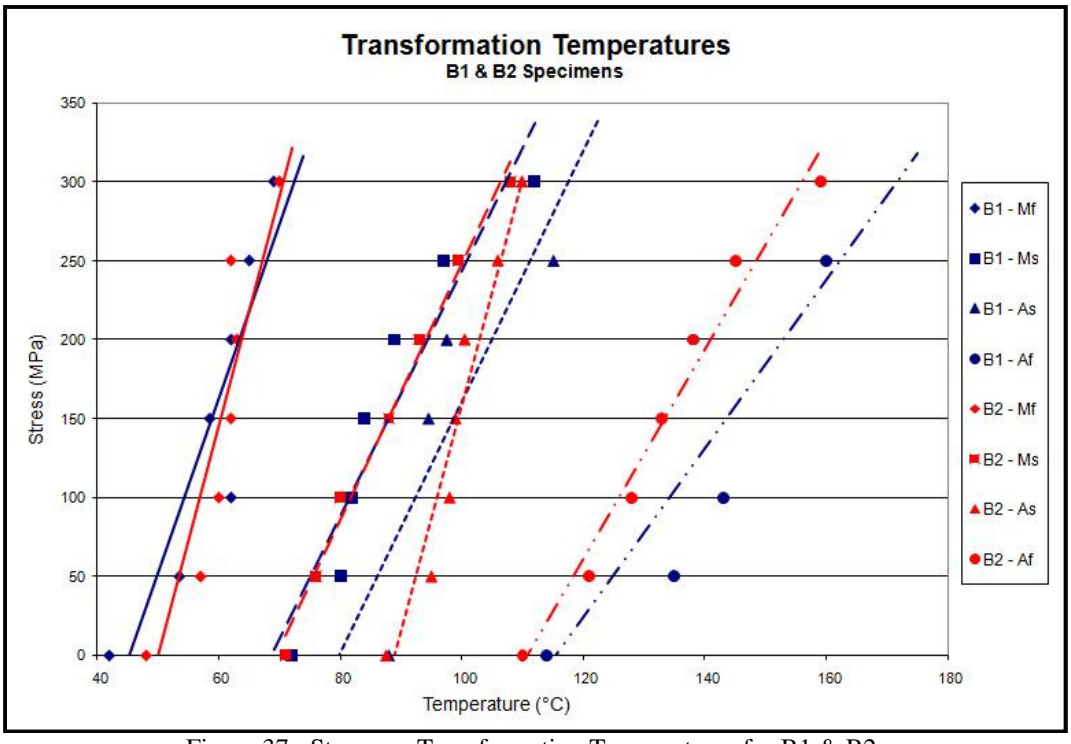

Figure 37: Stress vs. Transformation Temperatures for B1 & B2.

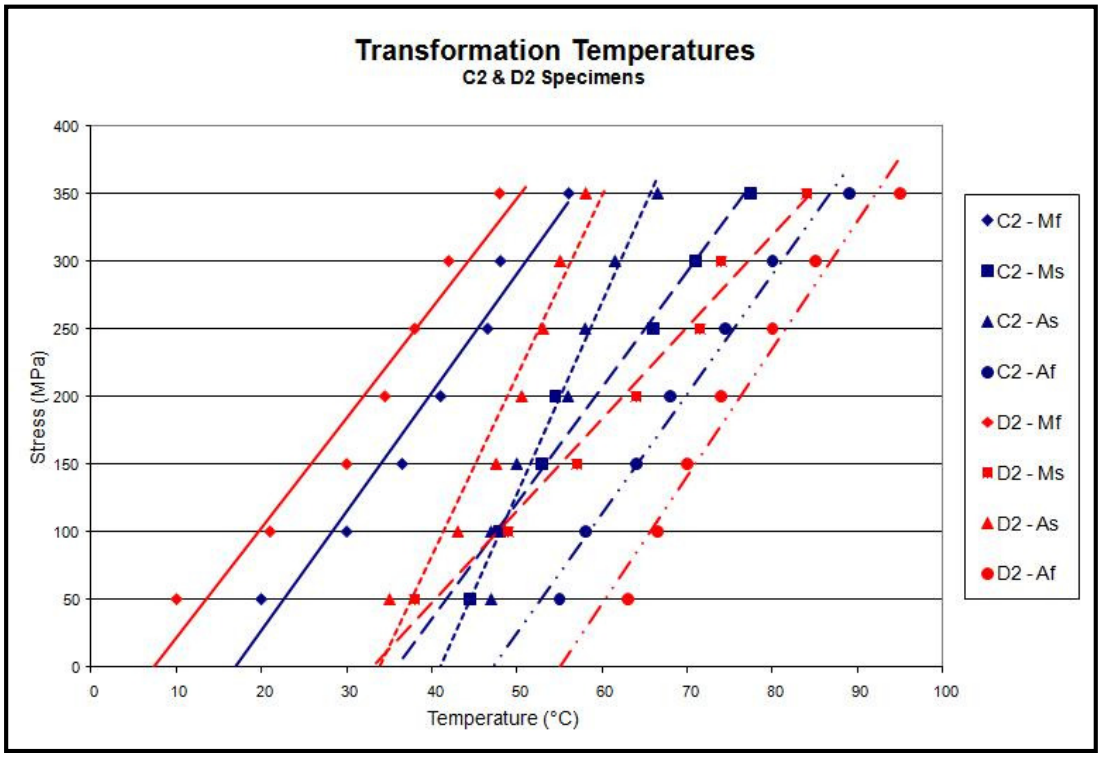

Figure 38: Stress vs. Transformation Temperatures for C2 & D2.

Modeling Results

Utilizing SigmaPlot analysis software, the model in equation (3) was fitted to the actuation strain versus applied stress level data for the samples exhibiting two-way shape memory after training. The highly worked ribbon and wire samples C1 & D1, respectively, showed little actuation strain (0.05-0.08%) when subjected to the maximum stress level during training. Although the back stress formulation can be used to model the parameters for one-way shape memory materials, the actuation strains are not significant enough to accurately fit to the parameters in the model. The data for the samples exhibiting TWSM in Figure 35 and Table #4 was fitted in the fully constrained condition with parameters m_1 and D_2 held constant at 1.8 and 0 MPa, respectively. The variable parameters, D_1, D_3, and H, for the samples are listed in Table 5.

Table 5: SMA material parameters for back stress formulation

Sample	D_1 (MPa)	D_3 (MPa)	H
A1	179.567	197.62	0.0385
A2	191.385	209.7	0.0403
B1	121.2477	191.296	0.0421
B2	128.935	162.95	0.0414
C2	195.82	256.86	0.0413
D2	64.094	143.793	0.043
Averages:	146.84	193.70	0.0411

*m_1 and D_2 parameters held constant at 1.8 and 0, respectively.

The parameters for each set of sample test data is plotted against the collected data for samples A1 & A2, B1 & B2, and C2 & D2, in Figures 39, 40, and 41 respectively. Figure 42 shows the average values for the parameters from Table 5 plotted against all of the test data exhibiting TWSM.

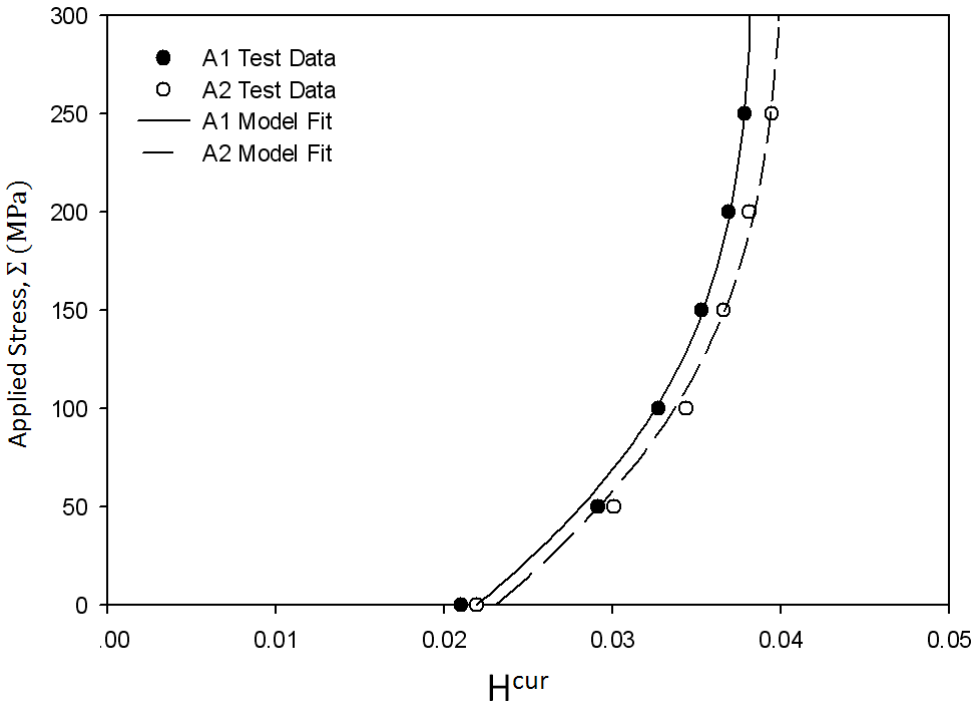

Figure 39: Back Stress modeling for large diameter bar samples A1 & A2

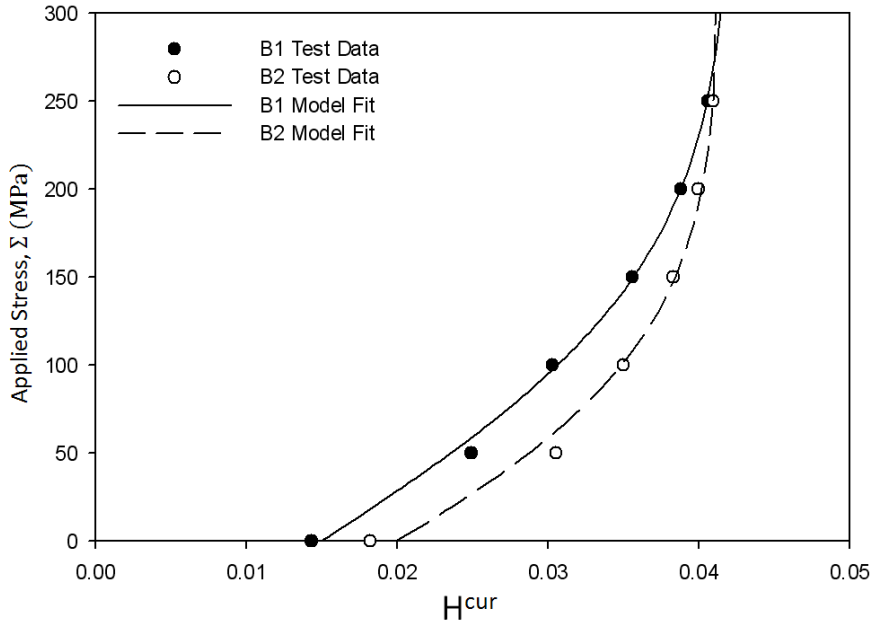

Figure 40: Back Stress modeling for small diameter bar samples B1 & B2

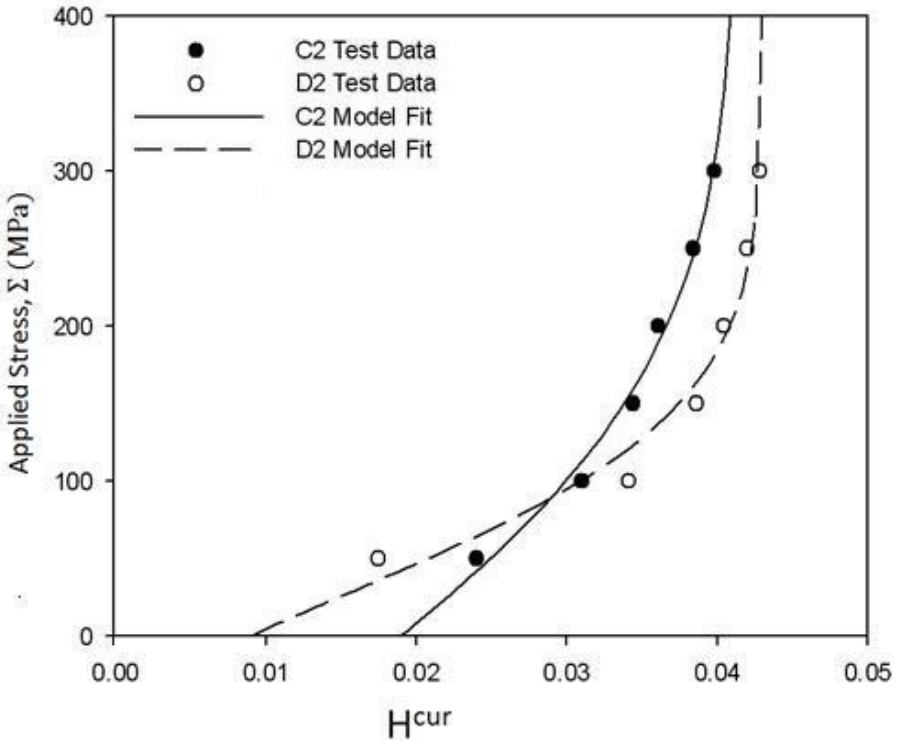

Figure 41: Back Stress modeling for annealed ribbon and wire samples C2 & D2

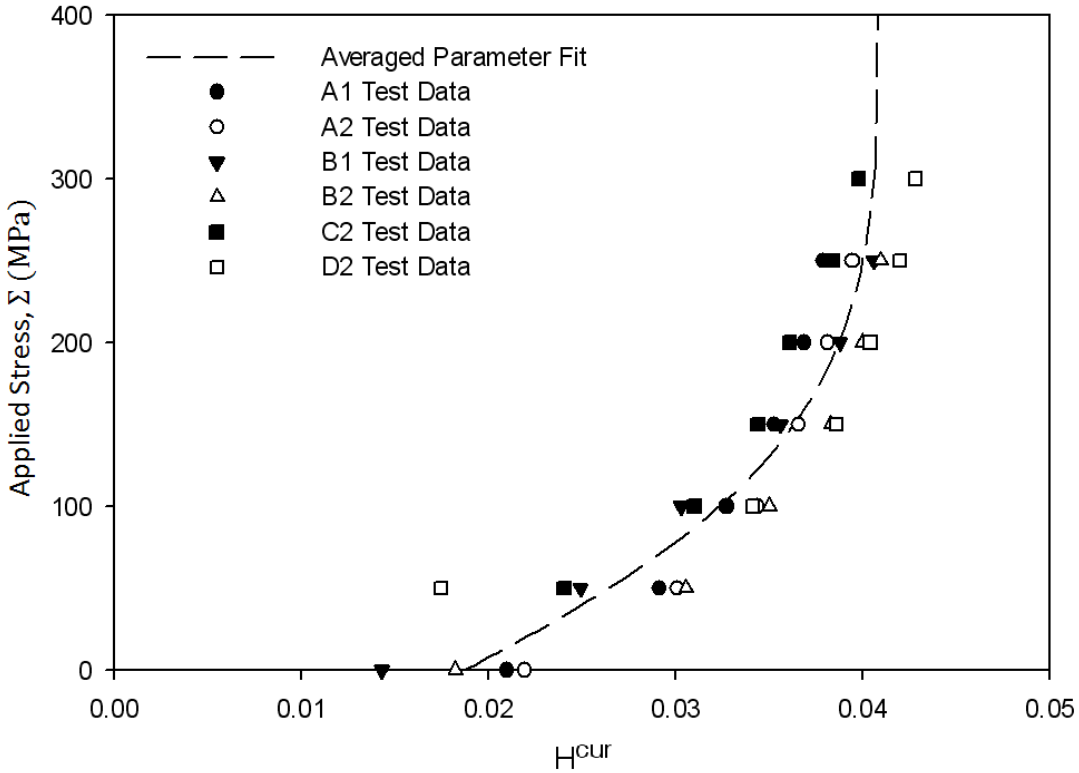

Figure 42: Averaged Back Stress model parameters plotted against all TWSM samples.

DISCUSSION

The purpose of this research is to establish a training method to be used for linear SMA actuators. This method is developed using three different NiTi alloys of four different sizes to show independence of alloy, size, and process. Of these variables, each material and size combination was tested in the as-received, or as-machined, state and a fully annealed state. In this section we report the findings from the research and the method used to get from an as-received (unknown history) SMA material to a trained linear SMA actuator.

Initial Characterization

Differential Thermal Analysis

The bar material that was acquired from NASA Glenn Research Center had been received with very little material information or data sheets. In order to determine a starting place for the material, a series of DTA tests were run to find the transformation temperatures at a zero load state. The method of intersecting tangents was used to determine the onset and offset temperature of the phase transformations. The material was first machined down to a nominal size (4mm dia. x 4mm long) that could be placed into the test crucible. Three samples were tested in the as-machined, 450ºC - ½ hr. annealed, & 800ºC - ½ hr. annealed states, respectively.

The endothermic (martensite to austenite) and exothermic (austensite to martensite) energies, or latent heat of transformation, are shown by the area under the curve peak for each heating and cooling cycle during the DTA tests. The DTA results in

the previous section shows the latent heat of transformation significantly increases in both the first and third cycles with annealing treatments at or above the recrystallization temperature. The results show that the peak martensite and austenite transformation temperatures and DTA signal increase with the result of annealing the sample (Tables 6 & 7). The internal stresses generated from machining or work hardening NiTi alloys locks in and restricts martensite variants from transforming to austenite. The locked in martensitic structure limits transformations from martensite to austenite, therefore lowering the latent heat of transformation. As annealing temperatures at or above the recrystallization temperature relieves the internal stresses, latent heat of transformation increases with the amount of material that can fully transform. The grain size and growth during the annealing process was not considered and thought to be in the range of typical metallic grain sizes of 0.5-10μm. Processes producing ultrafine grain and nanograin sizes in NiTi has been performed by Kockar et.al[37] and Waitz et.al[38]. Literature has shown that grains less than 60nm exhibit no thermal or stress induced transformation to martensite[39,40].

Table 6: 1st Cycle transformation temperatures & DTA signal

1st Cycle Results	Martensite Temperatures (°C)			DTA Signal	Austenite Temperatures (°C)			DTA Signal
Sample	M_f	M_p	M_s	μV	A_s	A_p	A_f	μV
As-Machined	50	60	70	2.69	94.5	110	133	-6.471
450°C Annealed	52	65	75	7.9	95	123	140	-17.93
800°C Annealed	54	66.4	85	8.22	96	129	148	-14.481

Table 7: 3rd Cycle transformation temperatures & DTA signal

3rd Cycle Results	Martensite Temperatures (°C)			DTA Signal	Austenite Temperatures (°C)			DTA Signal
Sample	M_f	M_p	M_s	μV	A_s	A_p	A_f	μV
As-Machined	51	60	70	3.01	95	119	145	-9.29
450°C Annealed	50	60.5	72	7.58	100	128	154	-24.825
800°C Annealed	50	63.5	79	8.7	98	127.5	155	-26.62

Shape Memory Effect Loading

SME loading was performed on the 55 NiTi bars (Figure 25) in order to establish the critical stresses where martensite detwinning starts and finishes. This test was done on a 6.60 mm diameter bar specimen that had been annealed for ½ hour at 800°C. The test results show that detwinning in the material starts at approximately 200 MPa and finishes at approximately 225 MPa. The small rise in stress, where detwinning starts and finishes, is where the majority of strain growth occurred (4%). The test also gives the martensite elastic modulus of approximately 27 GPa upon loading before detwinning occurs and during unloading to zero stress.

Superelastic Loading

Loading above the austenite transformation temperature showed significant permanent plastic deformation. This test was performed at a constant rate of 0.15 mm/min and temperature of 200°C. The results showed significant plastic strain growth (approximately 17.3%) between stress values of 350 to 650 MPa (Figure 26). Unlike typical superelastic testing with SMAs, upon unloading the sample, no hysteresis or recovery was present. This test showed that a critical austenite yield stress for the 55 NiTi was reached around 350 MPa. This test also showed that at a temperature of 200°C, no stress-induced transformation from austenite to martensite was achieved during loading before permanent plastic strain developed.

Actuator Training & Characterization

In order to develop a general axial training routine for typical SMA actuators, an assortment of materials and sizes were used. This allowed for a broad range of transformation temperatures and unknown processing history in the materials. The training process in this work considered three different near equiatomic NiTi alloys and four different sizes. The alloy assortment consisted of 55NiTi (49.9 at% Ni 50.1 at% Ti) bar material from NASA-GRC, and two alloys from recognized SMA manufacturers, (50.4 at% Ni ~ 49.6 at% Ti) ribbon from SAES Smart Materials, and (49.3 at% Ni ~ 50.7 at% Ti) wire from NDC Corporation. The constraints and results will be discussed further throughout this section.

Fixed Values & Constraints

During testing, particular constraints were used to ensure consistent results. Of the four different material sizes used, two samples of each size were created. One sample was tested in the as-received or as-machined condition. The second sample of each size was tested in the fully annealed state. This annealing process was held constant throughout all of the heat treated samples. These samples were placed into the materials furnace at a temperature of 450°C for 1 hr. and then removed to cool in room temperature ambient air. The annealing temperature of 450°C was selected based on the initial DTA results (Figure 23 & 24). This process relieved internal stresses in the material induced by either machining or working hardening.

The training stress for the bar samples was selected based on the results of the superelastic and SME testing shown earlier. It was found that martensite is in the fully

detwinned state above 225 MPa and room temperature (below M_f). Above 350 MPa in the austenitic state (200°C), permanent plastic strain ultimately leading to non-uniform deformation occurred, i.e. necking. From these results, a training stress of 300 MPa was selected and samples were then cycled to saturate TRIP. Once training was complete, the stress levels were stepped down to zero stess in 50 MPa increments and thermal-induced transformations at each stress increment were performed to achieve seven applied stress versus actuation strain data points for each bar sample.

For the wire and ribbon samples, a training stress of 350 MPa was used because of the absence of severe necking. Due to the challenge of testing the wire and ribbon under zero-load, a minimum load of 50 MPa was used instead of 0 MPa. After the samples were fully trained at the training stress and plastic strain growth was saturated, the stress levels were then stepped down to 50 MPa in 50 MPa increments and thermal-induced transformations at each stress increment were ran to achieve seven applied stress versus actuation strain data points for each ribbon and wire sample.

As-Received vs. Annealed

The results of the training process show the fully annealed bar samples (A2 & B2) experience a slightly larger plastic strain growth of about 5% during training (see Figure 29) than the as-received or as-machined samples of the same size (A1 & B1). The wire and ribbon samples show the material in the as-received condition contained high levels of cold-worked based on the little to no plastic strain growth during the training process and also the loss of hysteresis during temperature cycling.

The annealed bar samples (A2 & B2) experienced larger actuation strains (A2 vs. A1: 0.09%-0.19%; B2 vs. B1: 0.03%-0.56%) than the as-received or as-machined bar samples (A1 & B1) at each stress level (see Figure 35). The results of the actuation strains were significantly larger between annealed and as-received ribbon and wire specimens due to the large amount of cold-work induced in the as-received samples. The annealed samples (C2 & D2) experienced larger actuation strains (C2 vs. C1: 2.22%-3.68%; D2 vs. D1: 1.43%-3.74%) than the as-received samples (C1 & D1) at each stress level (see Figure 34).

Transformation temperatures for both bar samples show that the fully annealed state varies slightly from the as-received state for the martensite transformation temperatures. The austenite finish temperature for both specimens was lower for the fully annealed samples. The large diameter bar samples experienced the largest difference for both austenite start and finish temperatures. The austenite finish temperatures observed for the fully annealed large diameter bar sample (A2) was approximately 20°C lower than that observed by the as-received sample. The austenite start temperature for the A2 sample was approximately 15°C lower at small stress levels and 25°C lower at the training stress. These differences are not as significant for the smaller diameter bar samples B1 & B2. This result could show that additional internal stress states were developed during the machining process before the samples arrived at MSU to be tested. Again, the A1 & A2 samples were machined at NASA-GRC, whereas B1 & B2 samples were machined at MSU. The transformation temperature comparison for the ribbon and wire samples was unable to be made due to the loss of hysteresis in the

highly cold-worked samples C1 & D1. Without hysteresis, the approximate transformation temperatures are not distinguishable in the transformation stain versus temperature data.

Size Effects

From the results, it is shown that even for the large size differences that were tested, the actuation strain versus stress levels follow a very similar trend (except the as-received ribbon and wire samples C1 & D1) (see Figure 35). The actuation strains in this trend average 2.60% at 50 MPa and 4.03% at 300 MPa. The as-received ribbon and wire specimens have actuation strains significantly smaller than this trend due to the assumption of large amounts of cold work induced in the samples to stop plastic strain growth during use.

A considerable size effect occurred during the training process, where permanent plastic strain growth during training was considerably larger for the bar samples than the smaller cross-section samples (ribbon & wire). The plastic strain accrued during training was approximately 2.60% for the annealed wire sample and 3.40% for the annealed ribbon sample. For the larger cross-section bar samples, the plastic strain accrued during training was 16.4%, 23.6%, 23.4%, & 25.6% for samples A1, A2, B1, & B2 respectively. The large plastic strain growth of the bar samples required load adjustments throughout testing to compensate for the uniform reduction in cross-sectional area.

Model Numbers

The results of the Back Stress model presented in Table 5, fits a set of parameters for multiple NiTi alloys and sizes that exhibited TWSM. Although the variation for parameters D_1 and D_3 is large (±35% from the average), the maximum transformation strain parameter, H, varies slightly by a range of ±6% from the average. The model parameter values do not show any significant increase or decrease related to the size or alloy of each tested material. The severely cold worked ribbon & wire samples did not provide significant transformations strains to achieve an accurate one-way shape memory fit from the model. This leads to the parameters in the Back Stress Formulation being independent of size and alloy effects, and dependent on the training stress for alloys exhibiting a permanent plastic strain growth or TRIP greater than 2% during training.

Training Methods

This research identifies a thermomechanical training method for SMA 1-D axial actuators. The method outlines the steps taken to train & characterize a shape memory alloy with unknown history. The first steps taken for the bar samples were to machine the material to the sizes desired and find the transformation temperatures using DTA testing. These temperatures were known from the manufacturer for the ribbon and wire samples and the sizes of the materials were suitable for direct testing. The results show that annealing the sample before training relieved any internal stresses and produced higher two-way actuation strains for all samples.

Once the sample is fully annealed, a maximum stress is chosen for training based on the design requirements for the SMA; however, this training stress must be less than the yield stress for both the martensite and austenite phases. The material is then loaded in tension to the training stress level and held constant while thermal cycles are performed. Thermal cycles must complete full forward and reverse transformations from martensite to austenite. Once the plastic strain growth, or TRIP, saturates, the material has reached a fully trained state and the transformation strain for the training stress level can be evaluated. With the SMA in a fully trained state, it can be characterized at stress levels below the training stress and thermally cycled to achieve a full actuation strain characterization. It is important to note that the fully trained material now has history dependence, and thermally cycling the material above the training stress will produce additional unwanted TRIP.

The method developed in this work is illustrated in dark blue in Figure 43. This figure also illustrates that work-hardening the SMA material may also be a possible option, but two-way shape memory and maximum transformation strain is usually reduced during this process[26]. The developed method is specific to 1-D axial SMA actuators, utilizing thermally induced phase transformations.

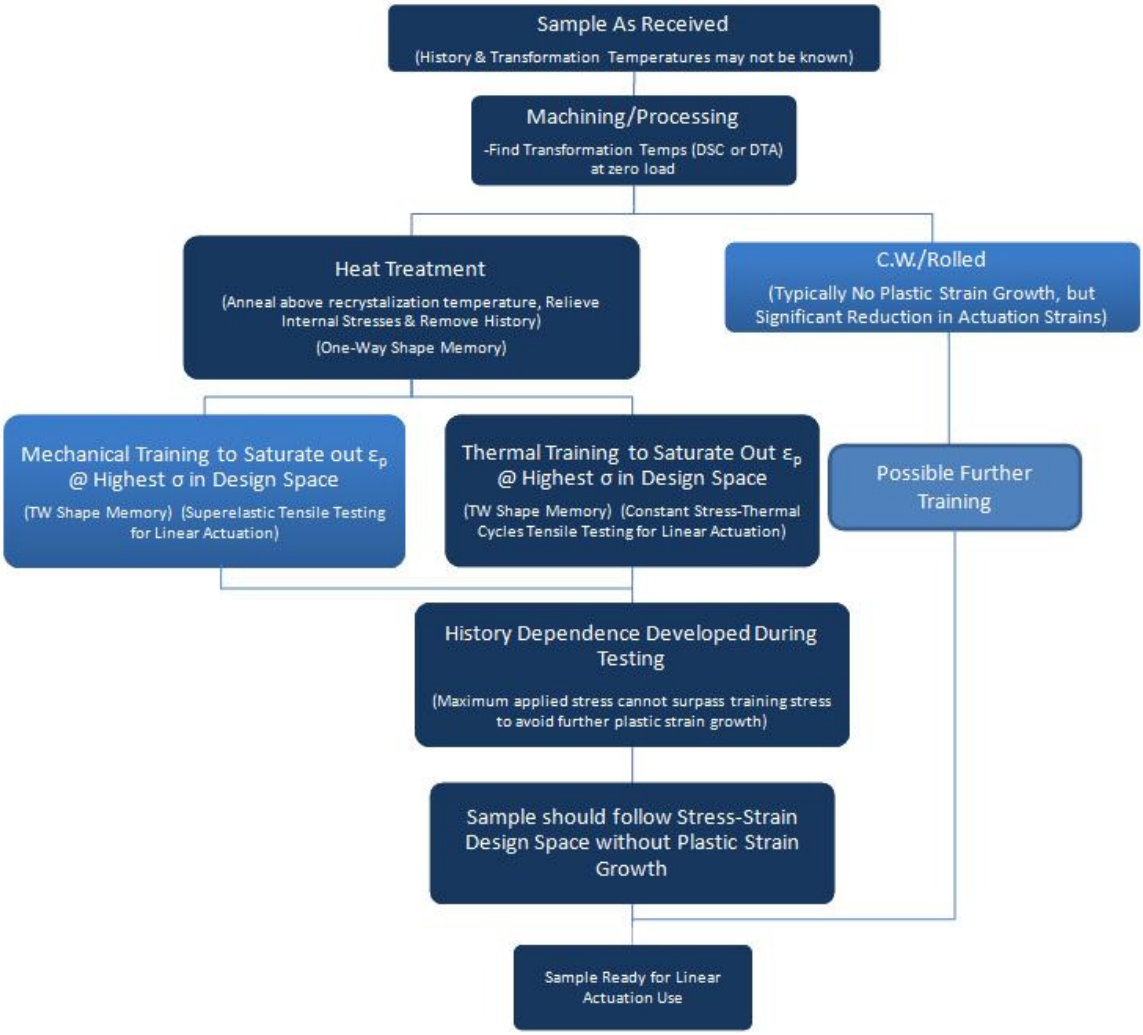

Figure 43: Training flowchart for 1-D SMA actuators;
Dark blue path is the method developed in this work for training.

CONCLUSION

This research has developed and evaluated a training process for 1-D linear SMA actuators. Although all testing was performed on NiTi materials, the process was developed to be used on any common SMA material. Initial thermal testing (DTA) and thermomechanical loading (SME & Superelastic) was performed on the 55 NiTi bar material supplied by NASA-GRC. These initial test were used to determine certain unknowns in the bar material. For this work, thermal analysis was performed using DTA to identify an annealing temperature and unknown transformation temperatures; although, this is not required if the equipment is not readily available. Annealing temperatures are typically above 400°C and transformation temperatures can be found during the training process.

The heat treatment process performed ensured that each annealed sample started its training process in a fully annealed state with no initial internal stresses. It was found that fully annealing the material prior to training, increased the actuation strain at all stress levels equal to or less than the training stress.

It was determined that the size of the materials being tested did not affect overall actuation strains of a fully trained material, but did have a significant effect on the overall plastic strain growth developed during the training process. The larger cross-section bar samples experienced significantly greater plastic strain growth during training compared to the smaller ribbon and wire samples.

Once plastic strain growth has saturated during the training process, the material will not grow plastic strains at or below that stress level unless an additional heat

treatment process is enacted; thus creating a design space of maximum stress and temperature. The mechanical and thermal constraints on the fully trained sample are: 1) the maximum allowable design stress cannot exceed the training stress, and 2) the maximum allowable temperature cannot exceed the annealing or recrystallization temperature. Once the training method has been fully completed and the actuator design space characterized, results should be consistent as training is repeated for additional actuators.

The model evaluation earlier showed the back stress parameters, D_1, D_3, & H, are independent of the alloy composition and size of material. This evaluation also shows the maximum transformation strain, H, is dependent on the training stress for TWSM materials where TRIP greater than 2% is observed. From the averaged material parameters, the back stress formulation can be used to effectively model applied stress, Σ, versus transformation strain, H^{cur}, for typical SMAs fully trained around 300-350 MPa and exhibiting TWSM.

FUTURE WORK

Currently MSU is working with new SMA bars manufactured by NASA-GRC to further orient this training method to higher transformation temperatures. This research will help characterize a training method with the existence of viscoplastic effects of high temperature creep. Training is also difficult due to the austenite transformation temperatures approaching the materials annealing temperature. As internal stresses are developing in the material to guide the two-way transformation, an annealing process is also being imposed on the sample during thermal cycles which relieves some of those stresses.

MSU is also working to develop a training method for bending in SMA actuators. Plastic strain growth and the asymmetry of tension and compression loading create issues that must be evaluated before a training process for bending is developed. Compression loading in SMAs develops a different hysteresis loop than in tension loading and strain hardening and dislocations occur early in cyclic testing.

Further research into the effect of superelastic loading to saturate plastic strain growth is needed. Superelastic training can usually be performed in less time than isobaric thermal cycle training due to the frequency of loading cycles, especially for large cross-sectional area materials. The design space of stress-induced training has not yet been related to the design space of isobaric temperature cycle training, i.e, a stress-induced training method has not been evaluated for use as a training method for isobaric temperature cycling.

REFERENCES CITED

1. Otsuka, K.; Wayman, C. M., *Shape Memory Materials*. 1 ed.; Cambridge University Press: Cambridge, 1999.

2. Tobushi, H.; Ohashi, Y.; Saida, H.; Hori, T.; Shirai, S., Recovery Stress and Recovery Strain of TiNi Shape Memory Alloy - (Cyclic Properties Under Constant Residual Strain and Constant Maximum Stress. *Jsme International Journal Series I-Solid Mechanics Strength of Materials* **1992,** *35* (1), 84-90.

3. Wang, F. E.; Buehler, W. J.; Pickart, S. J., Crystal Structure and a Unique Martensite Transition of TiNi. *Journal of Applied Physics* **1965,** *36* (10), 3232.

4. Kauffman, G.; Mayo, I., The Story of Nitinol: The Serendipitous Discovery of the Memory Metal and Its Applications. *The Chemical Educator* **1996,** *2* (2), 1-21.

5. Otsuka, K.; Ren, X. B., Recent Developments in the Research of Shape Memory Alloys. *Intermetallics* **1999,** *7* (5), 511-528.

6. Grabe, C.; Bruhns, O. T., On the Viscous and Strain Rate Dependent Behavior of Polycrystalline NiTi. *International Journal of Solids and Structures* **2008,** *45* (7-8), 1876-1895.

7. Miyazaki, S.; Imai, T.; Igo, Y.; Otsuka, K., Effect of Cyclic Deformation on the Pseudoelasticity Characteristics of Ti-Ni Alloys. *Metall Trans A* **1986,** *17 A* (1), 115-120.

8. Yoon, S. H.; Yeo, D. J., Experimental Investigation of Thermo-mechanical Behaviors in Ni-Ti Shape Memory Alloy. *Journal of Intelligent Material Systems and Structures* **2008,** *19* (3), 283-289.

9. Luo, H. Y.; Abel, E. W., A Comparison of Methods for the Training of NiTi Two-way Shape Memory Alloy. *Smart Materials & Structures* **2007,** *16* (6), 2543-2549.

10. Falvo, A.; Furgiuele, F.; Maletta, C., Hysteresis Modeling of Two-way Shape Memory Effect in NiTi Alloys. *Meccanica* **2008,** *43* (2), 165-172.

11. Liu, Y. N.; Liu, Y.; Van Humbeeck, J., Two-way Shape Memory Effect Developed by Martensite Deformation in NiTi. *Acta Materialia* **1998,** *47* (1), 199-209.

12. Liu, Y.; McCormick, P. G., Factors Influencing the Development of Two-way Shape Memory in NiTi. *Acta metallurica* **1990,** *38* (7).

13. Tanaka, K., A Thermomechanical Sketch of Shape Memory Effect - One Dimensional Tensile Behavior. *Res Mechanica* **1986,** *18* (3), 251-263.

14. Tanaka, K., A Phenomenological Description on Thermomechanical Behavior of Shape Memory Alloys *Journal of Pressure Vessel Technology* **1990,** *112* (ASME), 158-163.

15. Liang, C.; Rogers, C. A., One-dimensional Thermomechanical Constitutive Relations for Shape Memory Materials. *Journal of Intelligent Material Systems and Structures* **1990,** *1*, 207-234.

16. Patoor, E.; Eberhardt, A.; Berveiller, M., Micromechanical Modelling of Superelasticity in Shape Memory Alloys. *Journal De Physique Iv* **1996,** *6* (C1), 277-292.

17. Boyd, J. G.; Lagoudas, D. C., A thermodynamical Constitute Model for Shape Memory Materials .1. The Monolithic Shape Memory Alloy. *International Journal of Plasticity* **1996,** *12* (6), 805-842.

18. Brinson, L. C., One Dimensional Constitutive Behavior of Shape Memory Alloys. *Journal of Intelligent Material Systems and Structures* **1993,** *4*, 229-242.

19. Lagoudas, D. C.; Bo, Z. H., Thermomechanical Modeling of Poly-crystalline SMAs under Cyclic Loading, Part II: Material Characterization and Experimental Results for a Stable Transformation Cycle. *International Journal of Engineering Science* **1999,** *37* (9), 1141-1173.

20. Bo, Z. H.; Lagoudas, D. C., Thermomechanical Modeling of Polycrystalline SMAs under Cyclic Loading, Part III: Evolution of Plastic Strains and Two-way Shape Memory Effect. *International Journal of Engineering Science* **1999,** *37* (9), 1175-1203.

21. Bo, Z. H.; Lagoudas, D. C., Thermomechanical Modeling of Polycrystalline SMAs under Cyclic Loading, Part IV: Modeling of Minor Hysteresis Loops. *International Journal of Engineering Science* **1999,** *37* (9), 1205-1249.

22. Bo, Z. H.; Lagoudas, D. C., Thermomechanical Modeling of Polycrystalline SMAs under Cyclic Loading, Part I: Theoretical Derivations. *International Journal of Engineering Science* **1999,** *37* (9), 1089-1140.

23. Bo, Z. H.; Lagoudas, D. C.; Miller, D., Material Characterization of SMA Actuators under Nonproportional Thermomechanical Loading. *Journal of Engineering Materials and Technology-Transactions of the Asme* **1999,** *121* (1), 75-85.

24. Miller, D. Thermomechanical Characterization of Plastic Deformation and Transformation Fatigue in Shape Memory Alloys. Texas A&M University, 2000.

25. Jackson, C.; Wagner, H.; Wasilewski, R., 55-NITINOL - The Alloy with a Memory: Its Physical Metallurgy, Properties, and Application. NASA, Ed. Battelle Memorial Institute: Washington DC, 1972.

26. Miller, D. A.; Lagoudas, D. C., Influence of Cold Work and Heat Treatment on the Shape Memory Effect and Plastic Strain Development of NiTi. *Materials Science and Engineering a-Structural Materials Properties Microstructure and Processing* **2001,** *308* (1-2), 161-175.

27. Filip, P.; Mazanec, K., Influence of Work-hardening and Heat Treatment on the Substructure and Deformation-behavior of TiNi Shape-memory Alloys. *Scripta Metallurgica Et Materialia* **1995,** *32* (9), 1375-1380.

28. Weinert, K.; Petzoldt, V., Machining of NiTi based Shape Memory Alloys. *Materials Science and Engineering a-Structural Materials Properties Microstructure and Processing* **2004,** *378* (1-2), 180-184.

29. Weinert, K.; Petzoldt, V.; Kotter, D., Turning and Drilling of NiTi Shape Memory Alloys. *Cirp Annals-Manufacturing Technology* **2004,** *53* (1), 65-68.

30. Theisen, W.; Schuermann, A., Electro Discharge Machining of Nickel-Titanium Shape Memory Alloys. *Materials Science and Engineering a-Structural Materials Properties Microstructure and Processing* **2004,** *378* (1-2), 200-204.

31. IndiumCorp Soldering NiTi. http://www.indium.com/ (accessed Jan. 10, 2010).

32. Wu, M. In *Fabrication of Nitinol Materials and Components*, International Conference on Shape Memory & Superelastic Technologies, Kunming, China, Memry Corp.: Kunming, China, 2001; pp 285-292.

33. AeroFit SMA CryoFit Couplers & Fittings. http://www.aerofit.com/sma_Couplings.html.

34. Wilkes, K. E.; Liaw, P. K., The Fatigue Behavior of Shape-memory Alloys. *Jom-Journal of the Minerals Metals & Materials Society* **2000,** *52* (10), 45-51.

35. Hartl, D. J.; Lagoudas, D. C., Aerospace Applications of Shape Memory Alloys. *Proceedings of the Institution of Mechanical Engineers Part G-Journal of Aerospace Engineering* **2007,** *221* (G4), 535-552.

36. Bhadeshia, H. K. D. H. Thermal Analysis Techniques. http://www.msm.cam.ac.uk/phase-trans/2002/Thermal1.pdf.

37. Kockar, B.; Karaman, I.; Kim, J. I.; Chumlyakov, Y. J.; Sharp, J.; Yu, C. J., Thermomechanical Cyclic Response of an Ultrafine-grained NiTi Shape Memory Alloy. *Acta Materialia* **2008,** *56* (14), 3630-3646.

38. Waitz, T.; Antretter, T.; Fischer, F. D.; Simha, N. K.; Karnthaler, H. P., Size Effects on the Martensitic Phase Transformation of NiTi Nanograins. *Journal of the Mechanics and Physics of Solids* **2007,** *55* (2), 419-444.

39. Waitz, T.; Kazykhanov, V.; Karnthaler, H. P., Martensitic Phase Transformations in Nanocrystalline NiTi studied by TEM. *Acta Materialia* **2004,** *52* (1), 137-147.

40. Waitz, T., The Self-accommodated Morphology of Martensite in Nanocrystalline NiTi Shape Memory Alloys. *Acta Materialia* **2005,** *53* (8), 2273-2283.

APPENDICES

APPENDIX A

CLAMSHELL HEATER DESIGN & DRAWINGS

The following figures in this section (Figures 44-19) contain the part drawings and assembly drawings for the custom MSU clamshell furnace used for thermomechanical testing on the large cross-sectional area bar samples. The material used in the construction of the furnace was Zircar refractory ceramic and ceramic adhesive paste. The furnace had an open window on one side to allow a quartz rod extensometer to be used to monitor strain while testing. The heating elements were Norton #271W silicon carbide hot surface igniters.

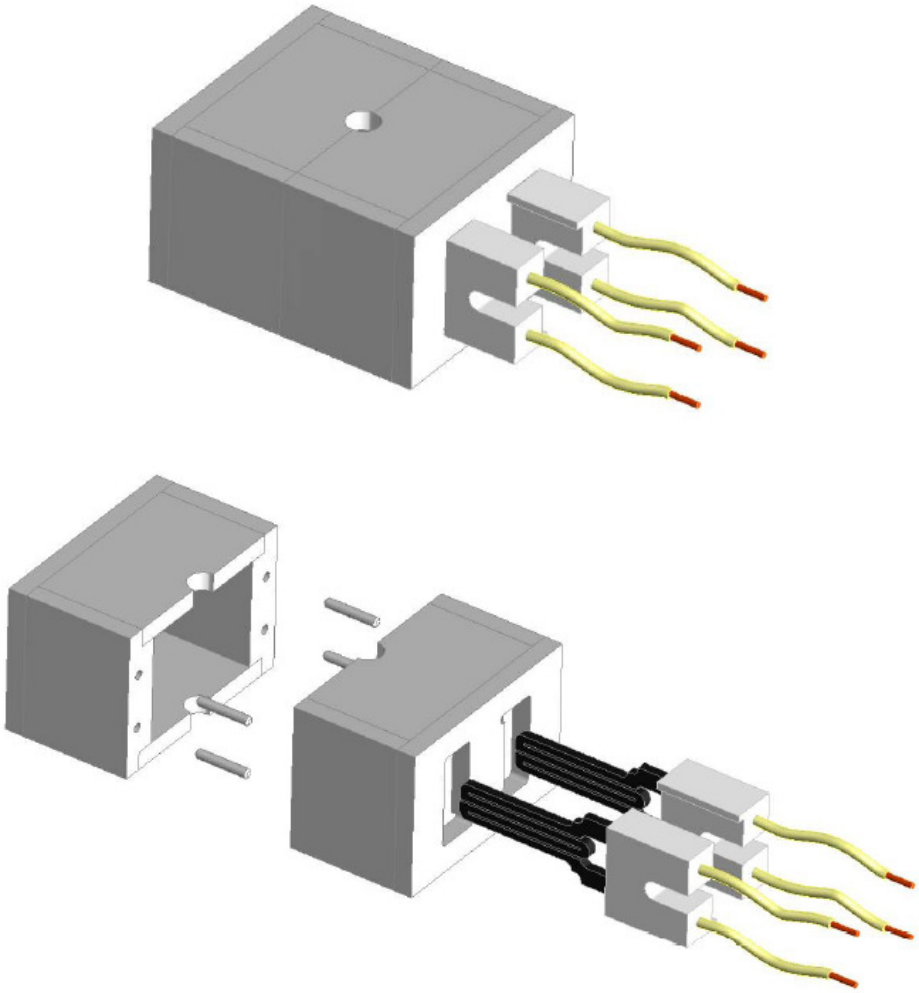

Figure 44: Custom clamshell heater model in collapsed and exploded views.

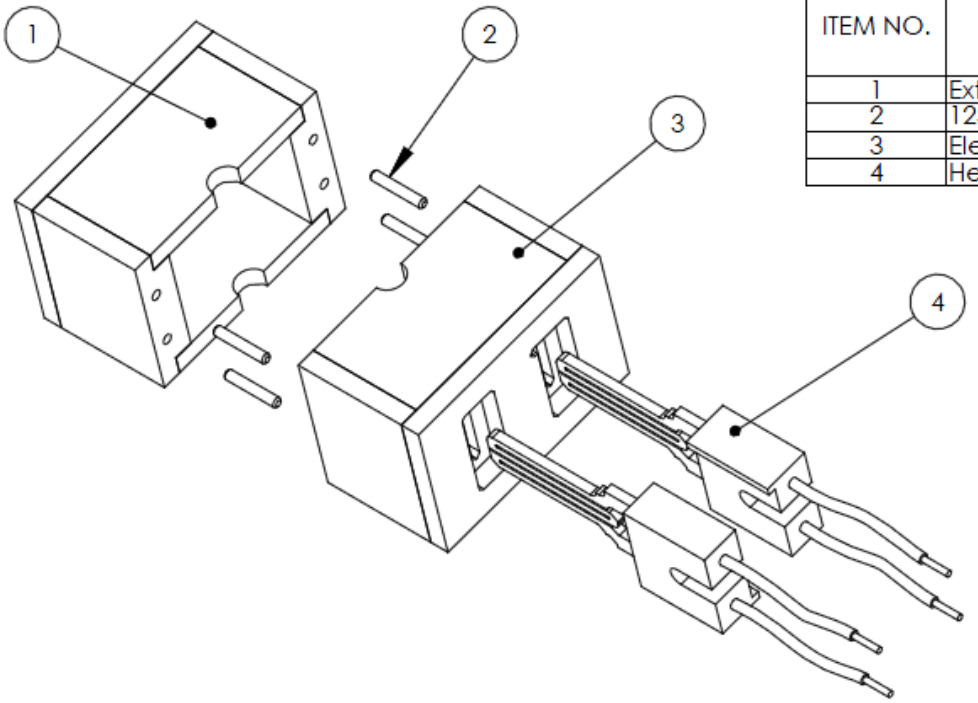

ITEM NO.	PART NUMBER	QTY.
1	Extensometer Side	1
2	125x75 dowel pin	4
3	Element Side	1
4	Heater Element	2

UNLESS OTHERWISE SPECIFIED:		NAME	DATE
DIMENSIONS ARE IN INCHES TOLERANCES: .X +- .1 .XX +- .01 .XXX +- .005	DRAWN	MPB	10/10/09
	CHECKED		
	ENG APPR.		
	MFG APPR.		
	Q.A.		
INTERPRET GEOMETRIC TOLERANCING PER:	COMMENTS:		
MATERIAL			
FINISH			
DO NOT SCALE DRAWING			

TITLE:

Heater Assembly with Heating Elements

SIZE	DWG. NO.	REV
A	Full Assembly	
SCALE: 1:5	WEIGHT:	SHEET 1 OF 1

5 4 3 2 1

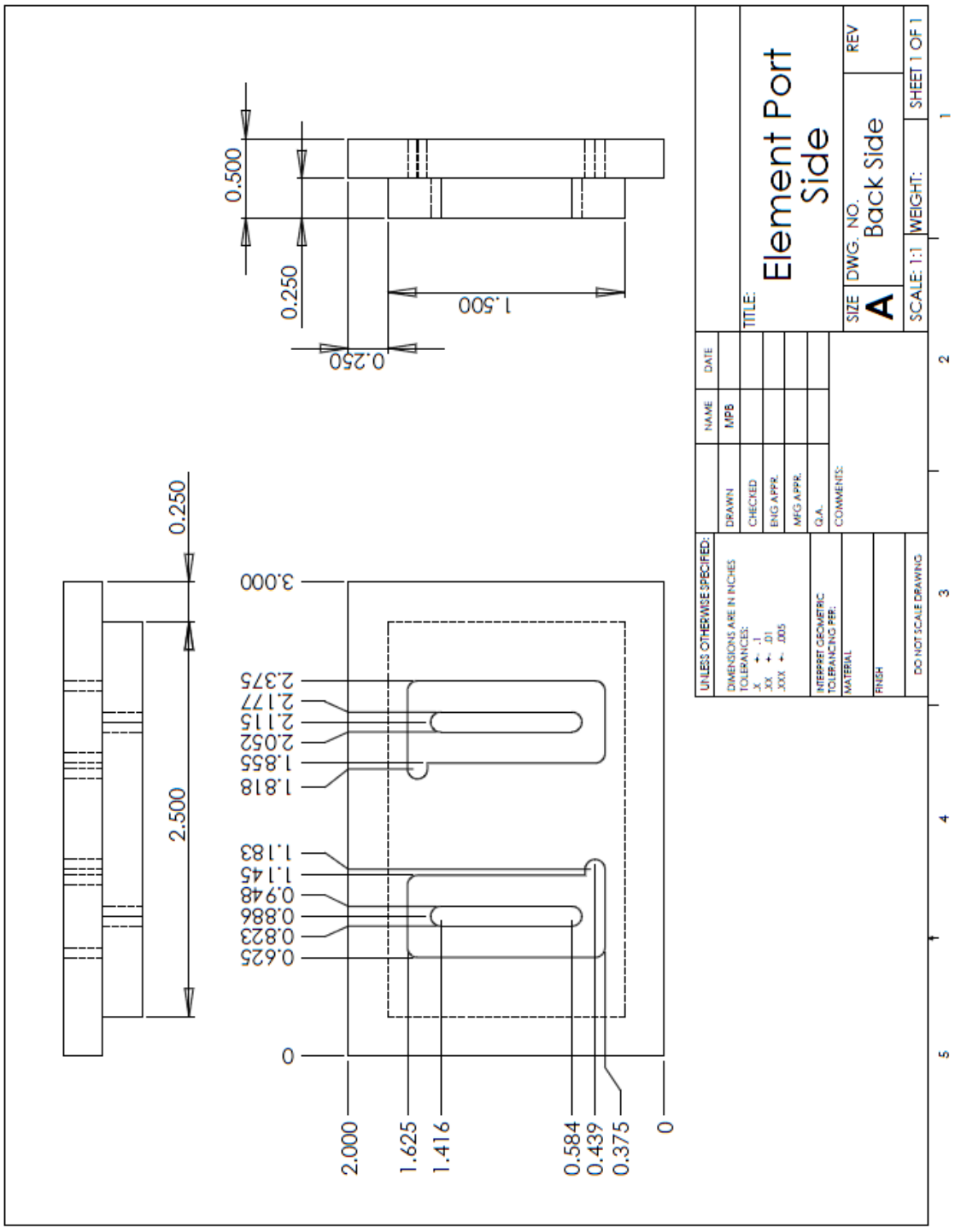
0.500
0.250
1.500
0.250
0.250
2.500
3.000
2.375
2.177
2.115
2.052
1.855
1.818
1.183
1.145
0.948
0.886
0.823
0.625
0
2.000
1.625
1.416
0.584
0.439
0.375
0
UNLESS OTHERWISE SPECIFIED:
DIMENSIONS ARE IN INCHES
TOLERANCES:
.X +- .1
.XX +- .01
.XXX +- .005
INTERPRET GEOMETRIC TOLERANCING PER:
MATERIAL
FINISH
DO NOT SCALE DRAWING
NAME
DATE
DRAWN
MPB
CHECKED
ENG APPR.
MFG APPR.
Q.A.
COMMENTS:
TITLE:
Element Port Side
SIZE
A
DWG. NO.
Back Side
REV
SCALE: 1:1
WEIGHT:
SHEET 1 OF 1

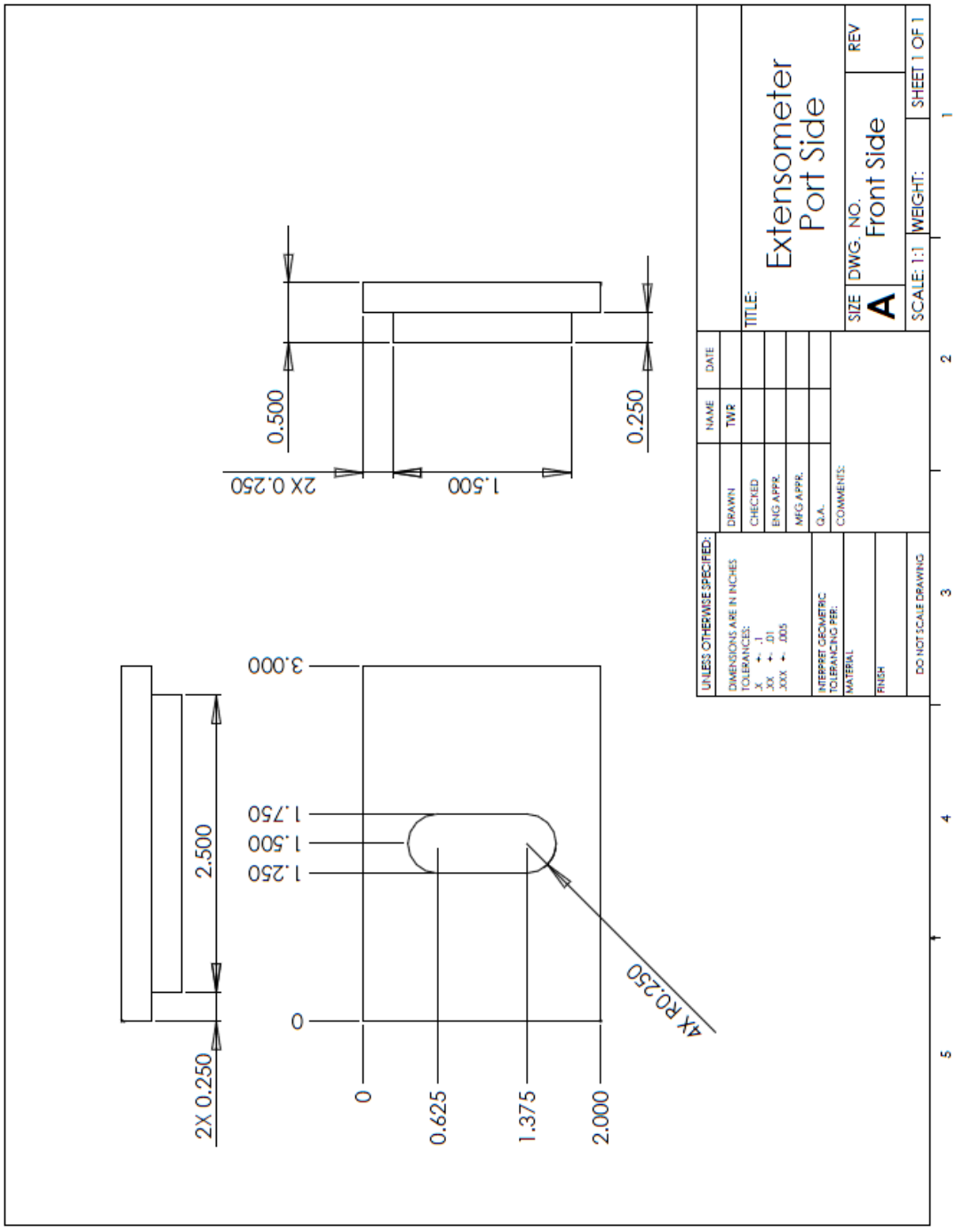
0.500
0.250
2X 0.250
1.500
3.000
1.750
1.500
1.250
2.500
0
4X R0.250
2X 0.250
0
0.625
1.375
2.000
UNLESS OTHERWISE SPECIFIED:
DIMENSIONS ARE IN INCHES
TOLERANCES:
X ± .1
XX ± .01
XXX ± .005
INTERPRET GEOMETRIC TOLERANCING PER:
MATERIAL
FINISH
DO NOT SCALE DRAWING
NAME
DATE
DRAWN
TWR
CHECKED
ENG APPR.
MFG APPR.
Q.A.
COMMENTS:
TITLE:
Extensometer
Port Side
SIZE
A
DWG. NO.
Front Side
REV
SCALE: 1:1
WEIGHT:
SHEET 1 OF 1

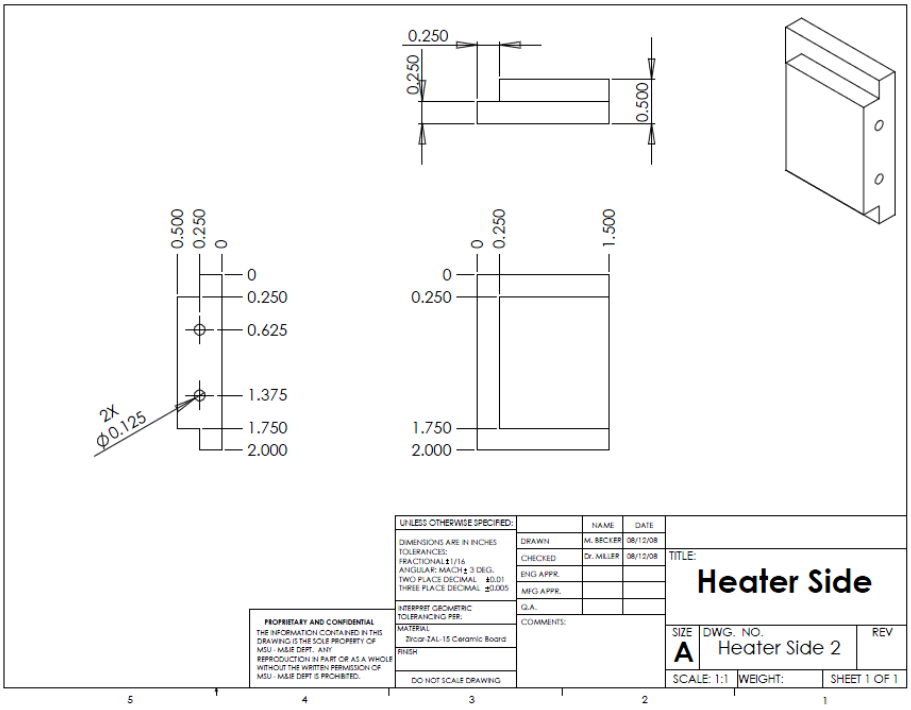

Figure 48: Heater side panel drawing.

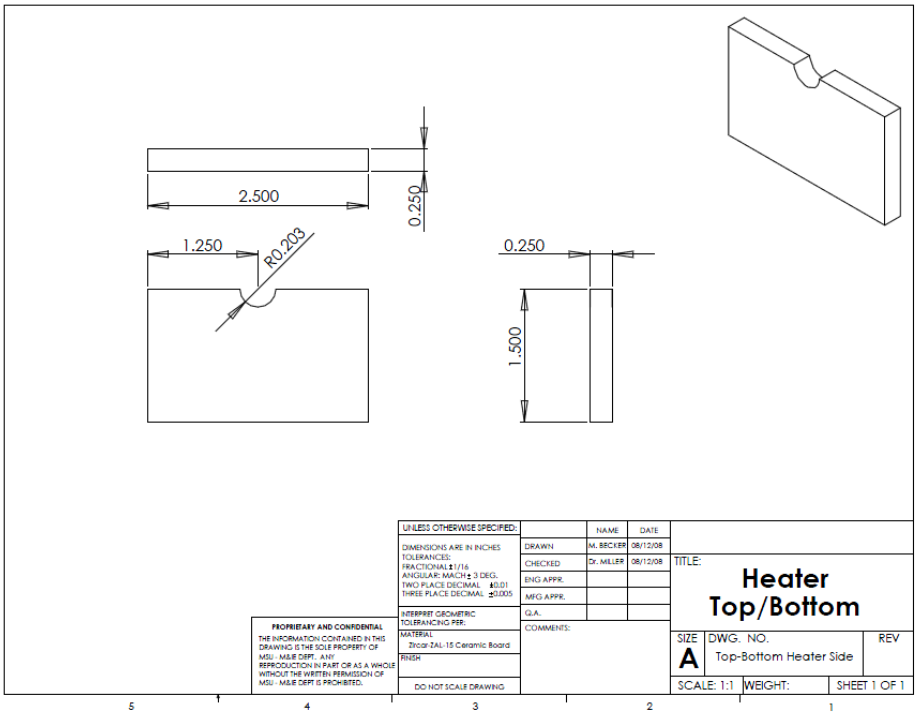

Figure 49: Heater top/bottom side drawing.

APPENDIX B

LABVIEW CONTROL & DATA ACQUISITION

Due to the difficulties of thermomechanical testing, a separate computer equipped with LabView control and data acquisition software was used to control the heating and cooling cycles of the furnace. The LabView front panel shown in Figure 50, and block diagrams for Thermal Cycles On and Off shown in Figure 51 and 52, respectively, were used to monitor and control the furnace temperature and also record time, temperature, load, and displacement.

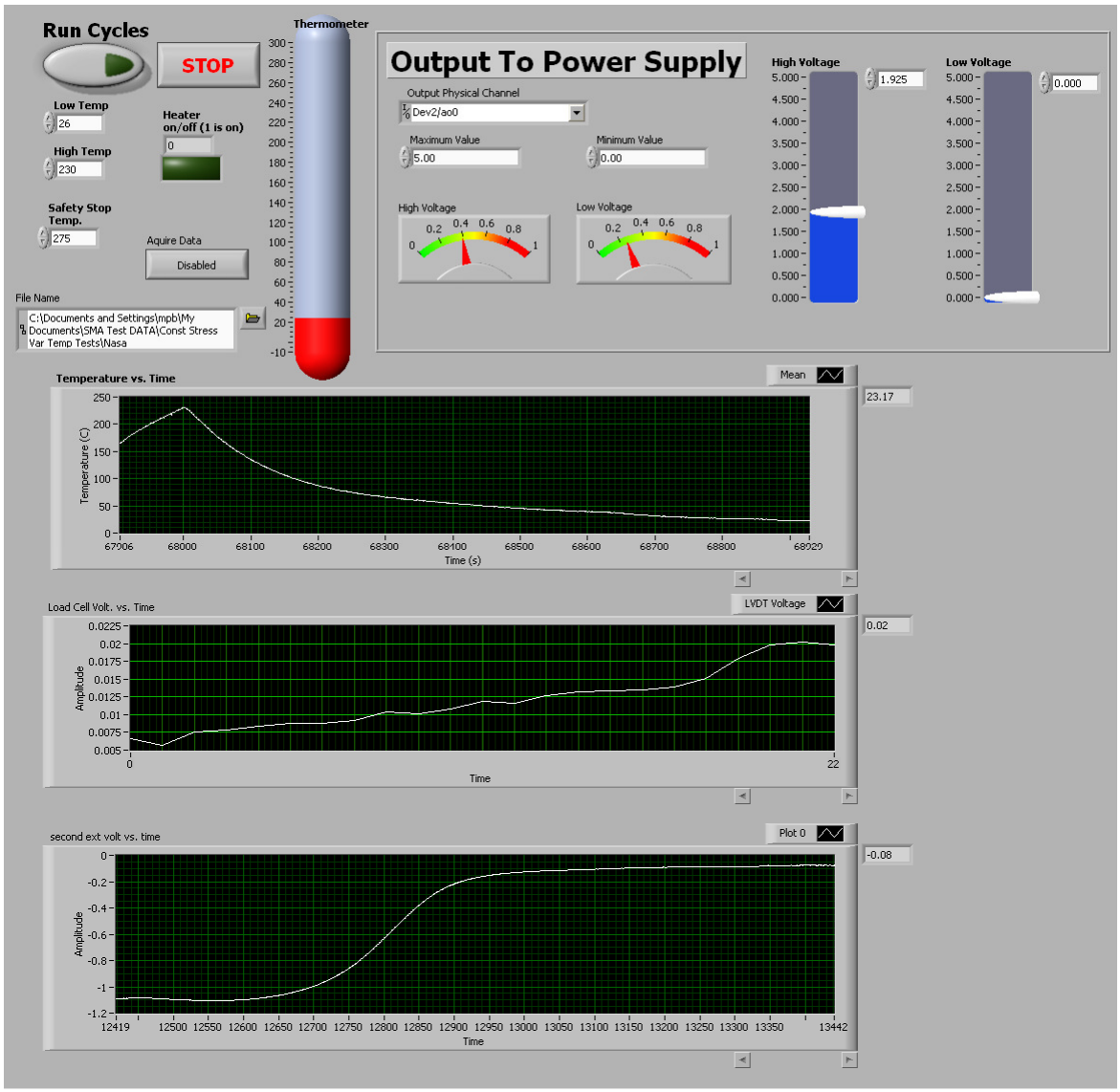

Figure 50: LabView Front Panel Temperature and Test Control.

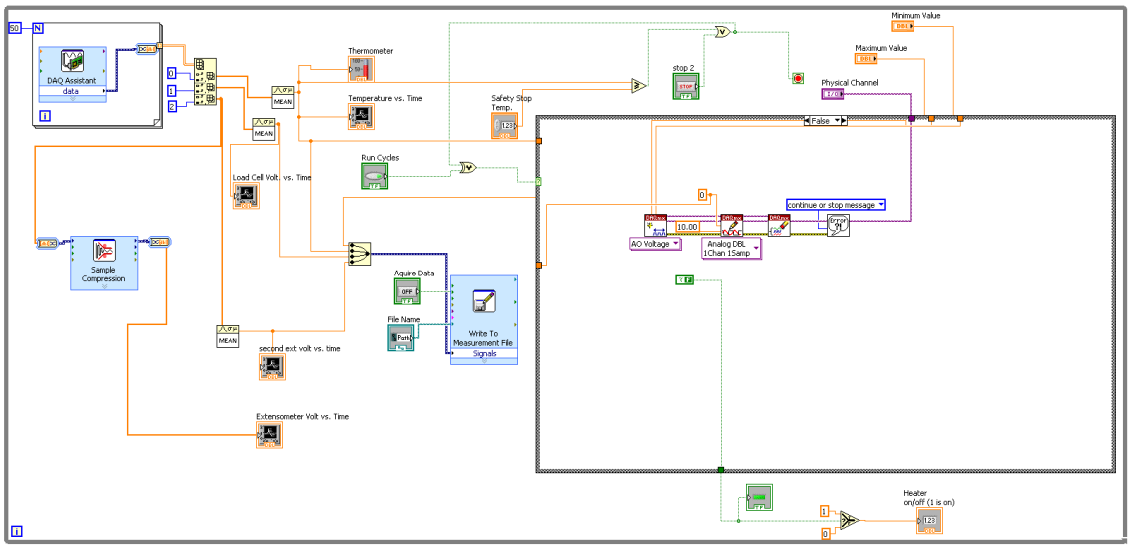

Figure 51: LabView Temperature Cycles (OFF) Control Diagram.

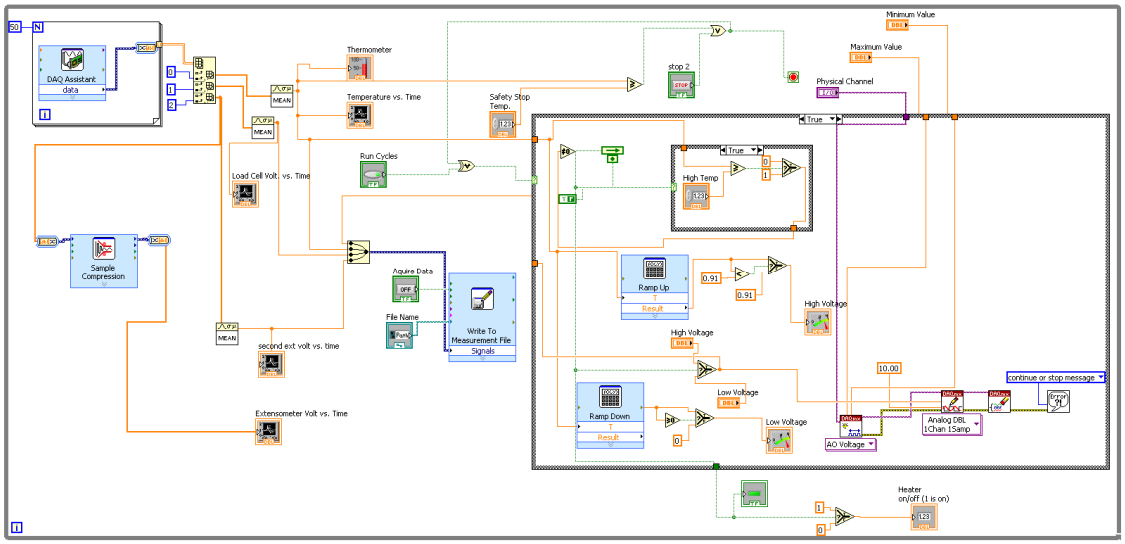

Figure 52: LabView Temperature Cycles (ON) Control Diagram

The load is controlled separately by either the Instron controller, or manually by the application of stress to the creep frame. For both load frames, displacement is measured by an LVDT either internally (Instron) or externally (Creep Frame). Both of these signals are brought into the DAQ using differential voltage signals and linear scaling to the proper units.

APPENDIX C

ACTUATION STRAIN FIGURES

Specimen A2

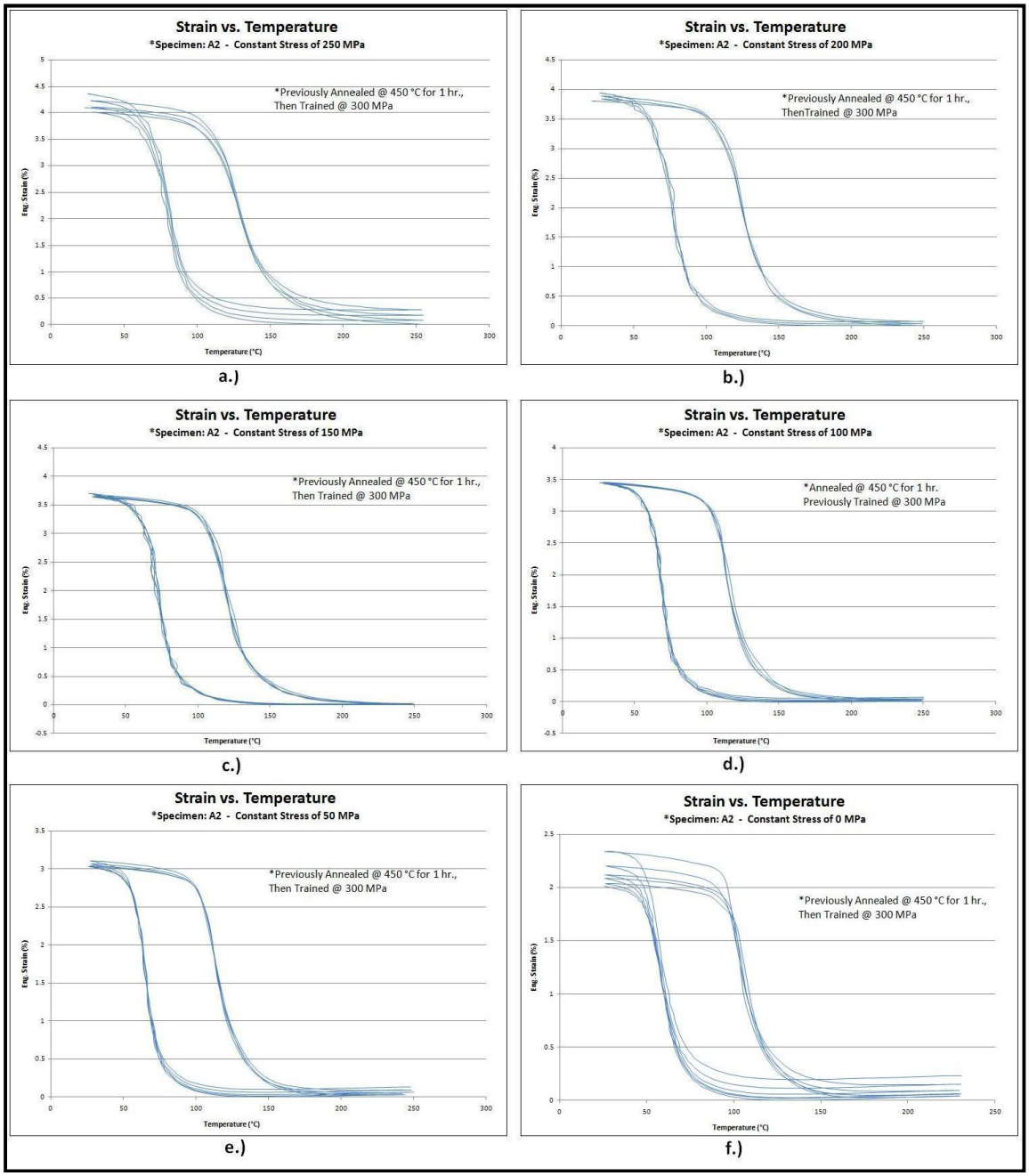

Figure 53: Actuation Strains for Sample A2; Temperature cycles at constant stress of: a.) 250 MPa b.) 200 MPa c.) 150 MPa d.) 100 MPa e.) 50 MPa f.) 0 MPa.

Specimen B1

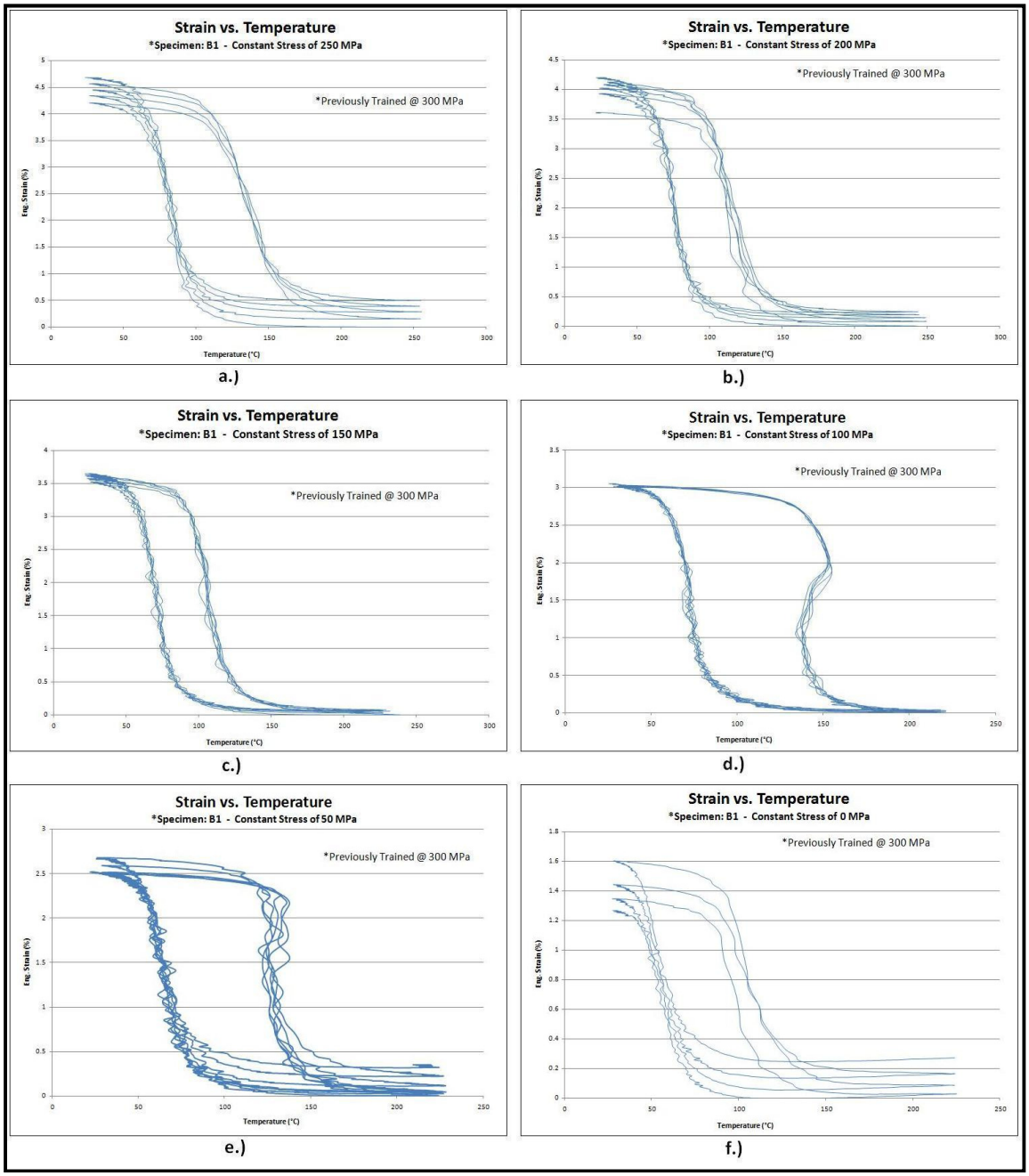

Figure 54: Actuation Strains for Sample B1; Temperature cycles at constant stress of: a.) 250 MPa b.) 200 MPa c.) 150 MPa d.) 100 MPa e.) 50 MPa f.) 0 MPa.

Specimen B2

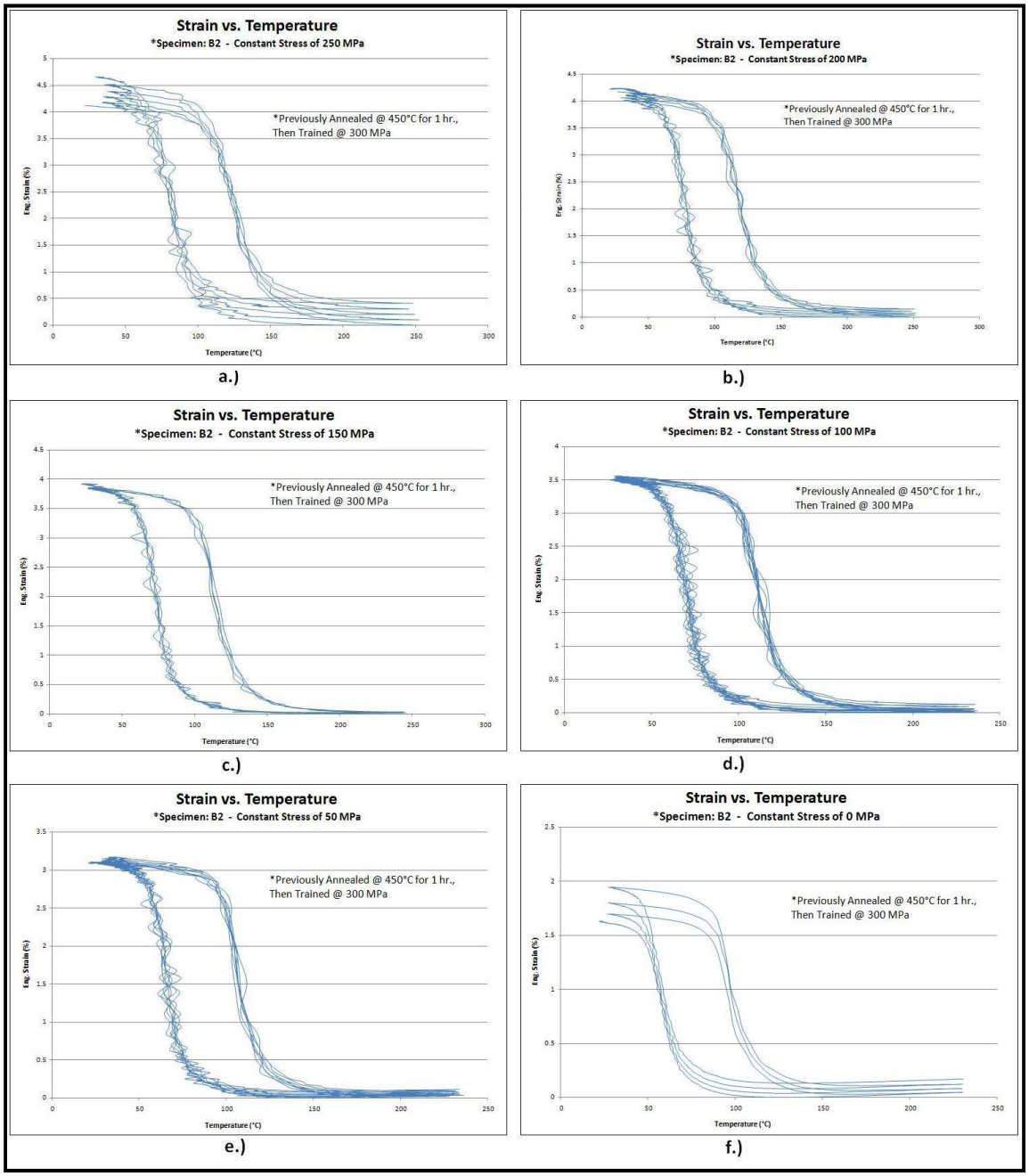

Figure 55: Actuation Strains for Sample B2; Temperature cycles at constant stress of: a.) 250 MPa b.) 200 MPa c.) 150 MPa d.) 100 MPa e.) 50 MPa f.) 0 MPa.

Specimen C1

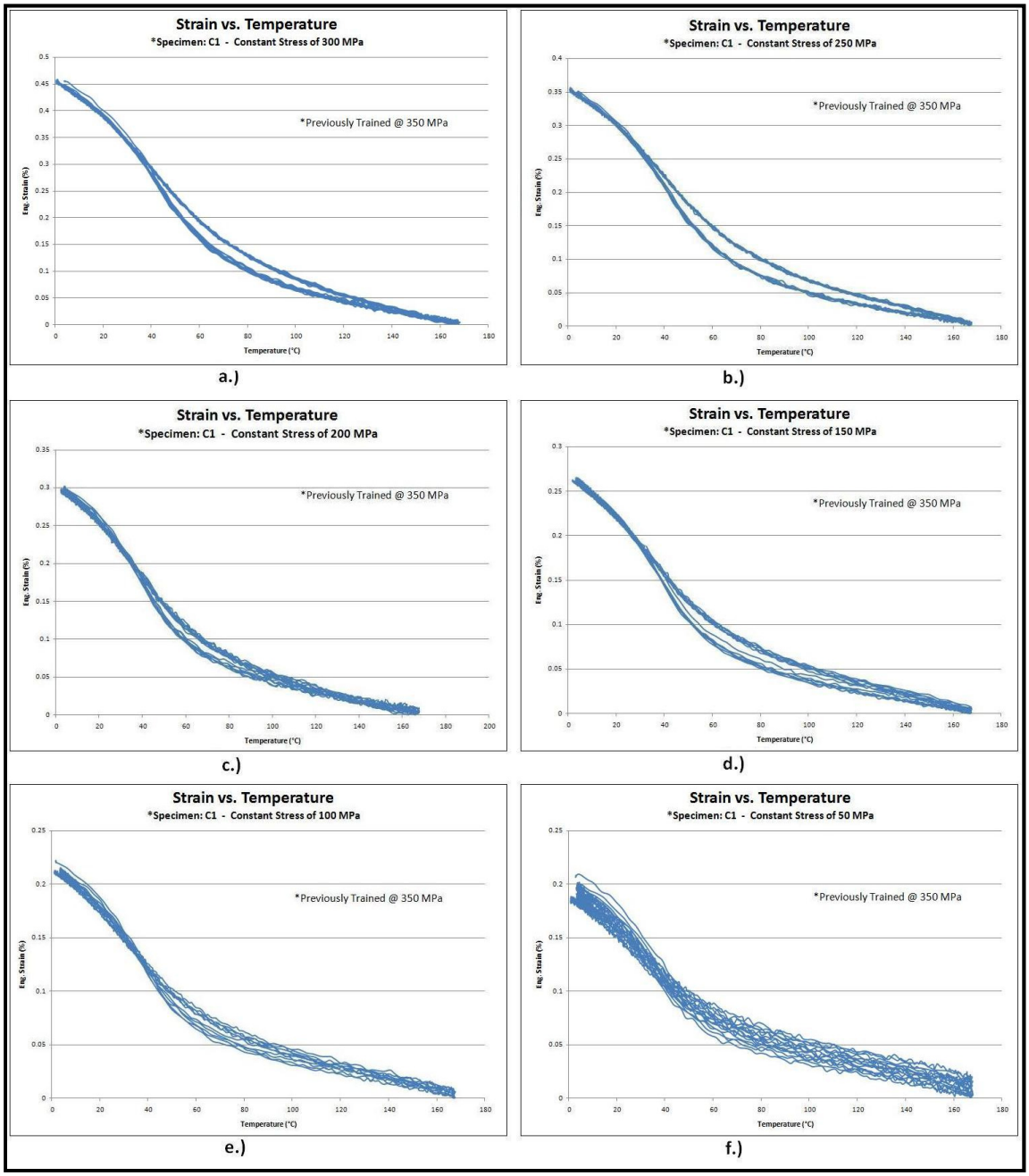

Figure 56: Actuation Strains for Sample C1; Temperature cycles at constant stress of: a.) 300 MPa b.) 250 MPa c.) 200 MPa d.) 150 MPa e.) 100 MPa f.) 50 MPa.

Specimen C2

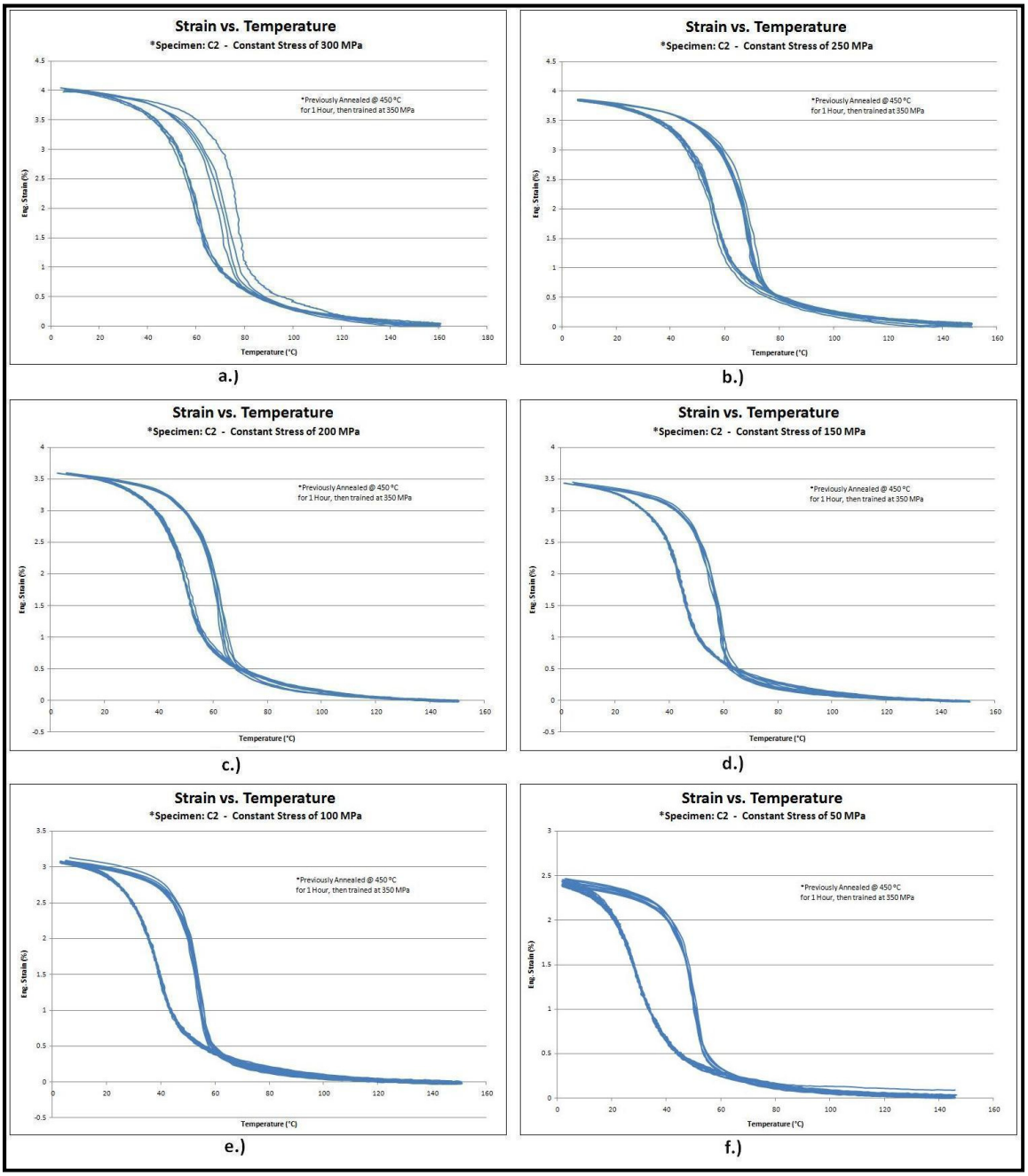

Figure 57: Actuation Strains for Sample C2; Temperature cycles at constant stress of: a.) 300 MPa b.) 250 MPa c.) 200 MPa d.) 150 MPa e.) 100 MPa f.) 50 MPa.

Specimen D1

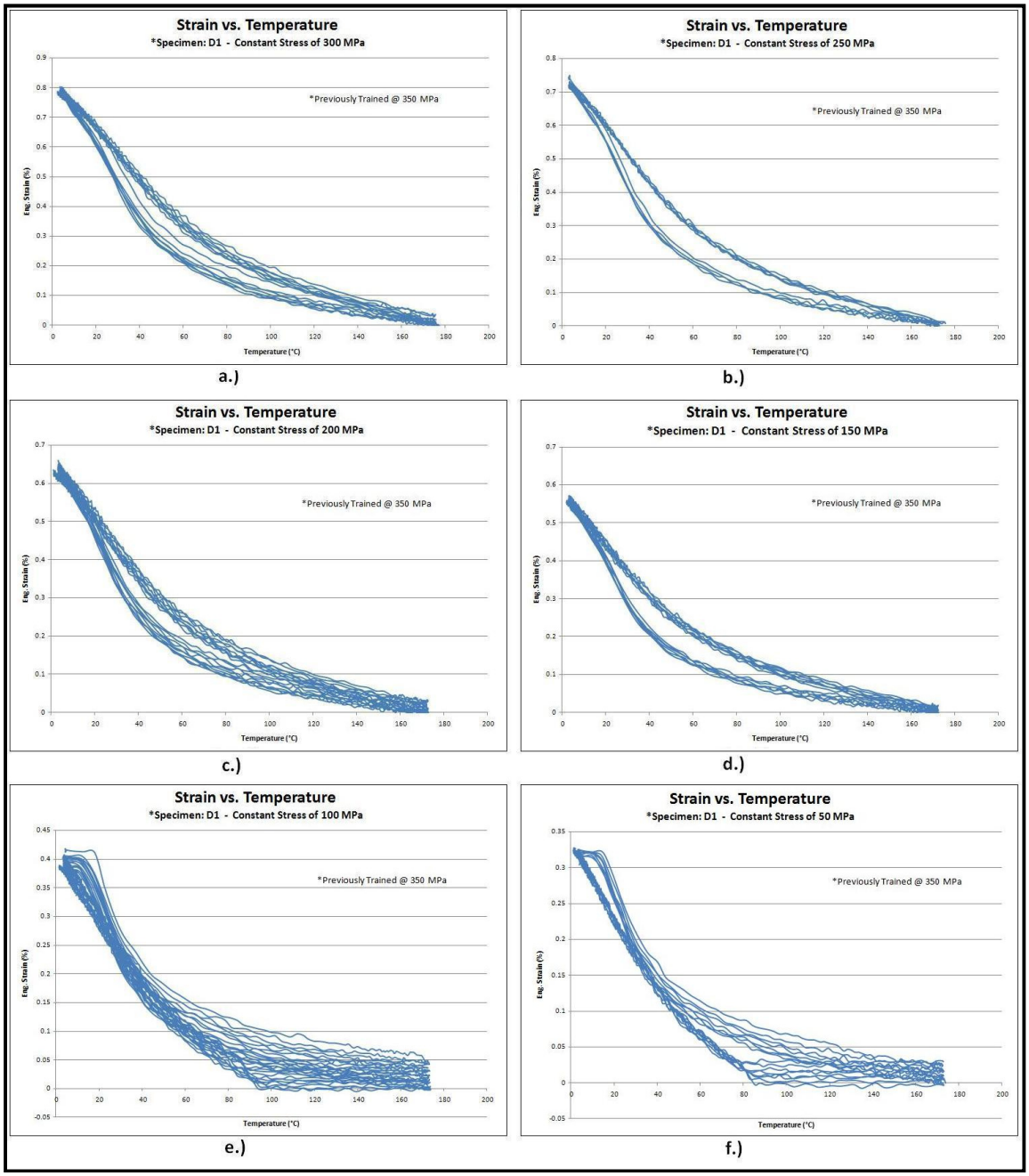

Figure 58: Actuation Strains for Sample D1; Temperature cycles at constant stress of: a.) 300 MPa b.) 250 MPa c.) 200 MPa d.) 150 MPa e.) 100 MPa f.) 50 MPa.

Specimen D2

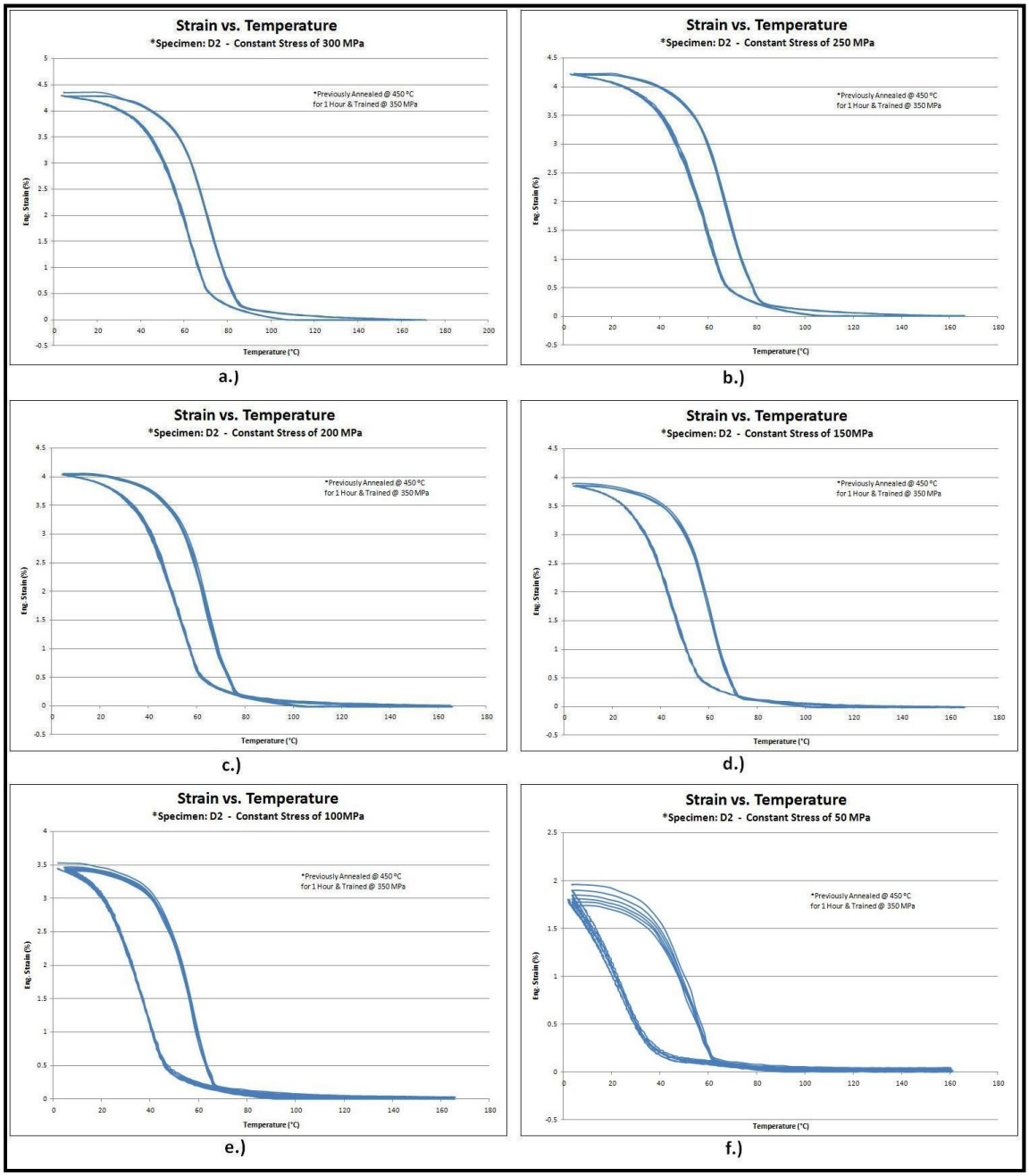

Figure 59: Actuation Strains for Sample D2; Temperature cycles at constant stress of: a.) 300 MPa b.) 250 MPa c.) 200 MPa d.) 150 MPa e.) 100 MPa f.) 50 MPa.